Volume 52, Number 1, 2026.

Mobility & Vehicle Mechanics

International Journal for Vehicle Mechanics, Engines and Transportation Systems

ISSN 1450 - 5304

UDC 621 + 629(05)=802.0

UNIVERSITY OF KRAGUJEVAC, FACULTY OF ENGINEERING

March, 2025.

M V M **M**obility **V**ehicle **M**echanics

Editor: Prof. dr ***Jovanka Lukić***

MVM *Editorial Board*
University of Kragujevac
Faculty of Engineering
Sestre Janjić 6, 34000 Kragujevac, Serbia
Tel.: +381/34/335990; Fax: + 381/34/333192

For Publisher: Prof. dr Slobodan Savić, dean, University of Kragujevac, Faculty of Engineering

Publishing of this Journal is financially supported from:
Ministry of Education, Science and Technological Development, Republic Serbia

Mobility & **M**otorna

Vehicle **V**ozila i

Mechanics **M**otori

Volume 52
Number 1
2026.

Mobility & **V**ehicle **M**echanics

Volume 52
Number 1
2026.

Motorna **V**ozila i **M**otori

MOBILITY & VEHICLE MECHANICS

https://doi.org/10.24874/mvm.2026.52.01.01
UDC: 621.43:662.769.2:620.92

HYDROGEN AND INTERNAL COMBUSTION ENGINES – STATUS, PERSPECTIVES AND CHALLENGES IN PROVIDING HIGH EFFICIENCY AND CO_2 FREE POWERTRAIN FOR FUTURE

Nenad Miljić [1], Slobodan J. Popović [2]*

Received in August 2024 *Accepted in October 2024*
REVIEW ARTICLE

ABSTRACT: Hydrogen as a fuel for internal combustion engines (ICEs) presents a promising pathway towards achieving high-efficiency, carbon-free powertrains for future mobility. This paper explores the current status, potential, and challenges associated with hydrogen-powered internal combustion engines. Hydrogen combustion offers substantial reductions in CO_2 emissions, but challenges persist, including NOx emissions, combustion stability, and the development of a comprehensive hydrogen infrastructure. The analysis delves into hydrogen's unique combustion properties, which differ from traditional fuels and require advanced engine designs and innovative combustion strategies to optimise efficiency. Additionally, the paper evaluates the environmental implications, emphasising the role hydrogen ICEs could play in achieving the ambitious targets of the Paris Agreement and the European Green Deal. Although hydrogen ICEs present a promising alternative, their success depends on overcoming significant technological and economic barriers, as well as aligning with evolving regulatory frameworks. The research concludes that despite the perception of ICEs becoming obsolete in Europe by 2035, hydrogen ICEs remain a viable powertrain solution, particularly for heavy-duty vehicles (HDVs), where they may outcompete fuel cells due to lower production costs and superior performance. This positions hydrogen ICEs as a critical component in global decarbonisation efforts.

KEY WORDS: *Hydrogen internal combustion engine (H_2 ICE), Carbon-neutral powertrains, H_2 ICE efficiency, H_2 ICE technology*

[1]*Nenad Miljić, University of Belgrade Faculty of Mechanical Engineering Department of Internal Combustion Engines, Kraljice Marije 16 11000 Belgrade Serbia, nmiljic@mas.bg.ac.rs, https://orcid.org/0000-0003-3564-0203, (*Corresponding author)*
[2] *Slobodan Popović, University of Belgrade Faculty of Mechanical Engineering Department of Internal Combustion Engines, Kraljice Marije 16 11000 Belgrade Serbia, spopovic@mas.bg.ac.rs, https://orcid.org/0000-0002-6332-9589*

MOTORI SA UNUTRAŠNJIM SAGREVANJEM NA VODONIK – STANJE, PERSPEKTIVE I IZAZOVI U OBEZBEĐENJU VISOKOEFIKASNOG POGONA BUDUĆNOSTI BEZ CO_2

REZIME: Vodonik kao gorivo za motore sa unutrašnjim sagorevanjem (ICE) predstavlja put koji obećava ka postizanju visoko efikasnih pogonskih sklopova bez ugljenika za buduću mobilnost. Ovaj rad istražuje trenutno stanje, potencijal i izazove povezane sa motorima sa unutrašnjim sagorevanjem na vodonik. Sagorevanje vodonika nudi značajno smanjenje emisije CO_2, ali izazovi i dalje postoje, uključujući emisije NOx, stabilnost sagorevanja i razvoj sveobuhvatne infrastrukture vodonika. Analiza se bavi jedinstvenim svojstvima sagorevanja vodonika, koja se razlikuju od tradicionalnih goriva i zahtevaju napredne dizajne motora i inovativne strategije sagorevanja kako bi se optimizovala efikasnost. Pored toga, rad procenjuje ekološke implikacije, naglašavajući ulogu koju ICE na vodonik mogu igrati u postizanju ambicioznih ciljeva Pariskog sporazuma i Evropskog zelenog plana. Iako ICE na vodonik predstavljaju alternativu koja obećava, njihov uspeh zavisi od prevazilaženja značajnih tehnoloških i ekonomskih barijera, kao i od usklađivanja sa evoluirajućim regulatornim okvirima. Istraživanje zaključuje da, uprkos percepciji da ICE postaju zastareli u Evropi do 2035. godine, ICE na vodonik ostaju održivo rešenje za pogonski sklop, posebno za teška vozila (HDVs), gde mogu nadmašiti gorivne ćelije zbog nižih troškova proizvodnje i superiornih performansi. Ovo pozicionira ICE na vodonik kao ključnu komponentu u globalnim naporima za ugljeničnu neutralnost.

KLJUČNE REČI: *Motor sa unutrašnjim sagorevanjem na vodonik (H_2 ICE), ugljenično neutralni pogoni, efikasnost H_2 ICE, H_2 ICE tehnologija*

HYDROGEN AND INTERNAL COMBUSTION ENGINES – STATUS, PERSPECTIVES AND CHALLENGES IN PROVIDING HIGH EFFICIENCY AND CO_2 FREE POWERTRAIN FOR FUTURE

Nenad Miljić, Slobodan J. Popović

INTRODUCTION

Internal combustion engines have been driving the industry for more than a century. Powered mainly by fossil fuels and thus responsible for having a significant part in carbon dioxide emissions, within the global warming phenomena, the IC engine became a severely targeted technology as “obsolete”, “dirty”, and almost publicly sentenced to death.

So, how did we get here, and is there a stronghold for such claims? Is the hydrogen-fueled ICE only a hype or a viable solution that will provide ICE technology not only prolonged life but also a key role in decarbonising the future?

Global warming, characterised by the long-term rise in Earth’s average surface temperature, has become a defining challenge of our time. Since the late 19th century, the planet’s average surface temperature has risen by approximately 1.2°C, with most of this increase occurring in the past 40 years [1]. Processes driving the Earth’s climate are rather complex, and neither of the models can explain the current state without large margins of uncertainty for numerous reasons. The same applies even more when predicting the future state of the Earth’s climate.

In order to provide policymakers worldwide with the most relevant and regular scientific assessments on the current state of knowledge about climate change, United Nations Environment Programme (UNEPE) and World Meteorological Organization (WMO) established the IPCC (The Intergovernmental Panel on Climate Change) in 1988. In the First Assessment Report (FAR) of IPCC from 1990, greenhouse gases, particularly the rise of the carbon dioxide (CO_2) content in the Earth’s atmosphere, were identified as major contributors to climate change [2]. During the next thirty years, overall, six assessment reports contributed to a better understanding of climate change and gathered the vast majority of the global scientific community around the consensus that the rise of global surface temperature is highly correlated to the rise of carbon dioxide (CO_2) content in the atmosphere [3].

The analysis of the air bubbles trapped in the ice cores drilled from the Antarctic ice sheets older than a million years [4], provided substantial proof that the amount of CO_2 suddenly started to rise at the end of 19th century [5]. Moreover, the rise of the CO_2 level is stable and even accelerating, achieving current values that are more than 140% larger than the highest values in the past millennia [6]. It is a joint scientific standing that the rise of CO_2 is the most responsible for global warming due to the well-known greenhouse effect and that the rise correlates with intensive industrial activities and usage of fossil (carbon-based) fuels, i.e., that climate change is anthropogenic [3]. Greenhouse gases generally absorb and re-emit thermal (infrared) radiation and have a “blanketing” effect. Besides carbon dioxide, methane, nitrous oxide, ozone, and water vapour are also gases with significant greenhouse effect potential. In the current climate, for average all-sky conditions, water vapour is estimated to account for 50%, carbon dioxide 19%, ozone 4%, and other gases 3%, while clouds make up about 24% of the greenhouse effect [7].

The stated theory (on dominant anthropogenic causes of global warming by a massive release of CO_2 during the past 150 years) is still without sound challenge, although there are standings with claims that there are other significant phenomena that could be much more responsible for the Earth's temperature rise. One of them is that the increased presence of water vapour in the atmosphere, provoked by increased solar irradiation, is the leading cause of the intensive greenhouse effect [8]. Climate scientists soundly oppose these claims, explaining that water vapour has a minor effect on long-term global temperature change since its presence in the gaseous form in the atmosphere is relatively short. The abovementioned attitude of scepticism is also in opposition to a standard and well-established theory that increased atmospheric water vapour content, although highly involved in the overall greenhouse effect, is directly caused by the elevated level of greenhouse gases, i.e. that the increase of the water vapour content in the atmosphere is only a positive feedback of raised temperature mainly due to CO_2 increase. Some scientists focus on the long-term scale effects and changes of the Earth's Solar irradiation by the in-depth analysis of the Solar activity cycle [9] and Earth-to-Sun distance variations caused by so-called Sun Inertial motion, with a theory that the changes in the Earth's Solar irradiation contribute to a temperature increase even up to 80% (relative to the greenhouse effect itself) [10]. The predictions derived from this theory are much less alarming than those from IPCC Assessment Reports, claiming that the global temperature will drop and be well below what the IPCC predicted by the year 2053. This point of view is also under heavy criticism as a sceptic one [11].

All in all, knowledge on climate change gathered in IPCC Assessment reports, built upon a vast of various data sources and scientific expertise, became the core source of the guidelines for policymakers worldwide in defining strategies and decisions on how to fight climate change and prevent heavy consequences for the humanity which will follow by not acting. All these efforts provided essential material for governments to draw in the run-up adoption of the Kyoto Protocol in 1997, which further focused on measures and actions for limiting warming to 2°C toward the Paris Agreement in 2015. as a legally binding international treaty on climate change adopted by 196 Parties [12]. Although 2°C seems like a minor difference, the consequences of such a rise at a global level are immense. We are already seeing devastating consequences at the current level of temperature rise, including more frequent and severe heatwaves, droughts, and storms. All of this would escalate with higher temperatures rising even more, resulting in the loss of ecosystems and biodiversity on an unprecedented scale.

One of the critical measures defined as a measure for slowing down the increase of the CO_2 content in the atmosphere is related to a significant decrease in the usage of fossil fuels, i.e. limiting the overall emission of CO_2. This further implies a plan of action that will vastly increase the energy production capacities from renewable sources and emphasise the so-called carbon-neutral technologies that will provide CO_2 zero balance in their exploitation.

In December 2019, the European Union embarked on an ambitious journey to tackle climate change and environmental degradation by introducing the European Green Deal [13]. As the world grapples with the intensifying effects of global warming, the EU has taken a decisive stance with a comprehensive strategy to transform the continent into the first carbon-neutral economy by 2050. The EU Green Deal is more than just a climate policy; it's a roadmap for transforming Europe's economy to meet environmental challenges while fostering innovation and sustainable growth. At its core, the Green Deal seeks to reduce net greenhouse gas emissions by at least 55% by 2030 (compared to 1990) and reach net-zero emissions by 2050. This decarbonisation strategy spans multiple sectors, including energy, transport, agriculture, and industry.

1 PAVING THE WAY TO A CARBON-NEUTRAL FUTURE

According to the European Environment Agency (EEA), the EU's greenhouse gas emissions have already decreased by 31% between 1990 and 2021, driven mainly by a shift to renewables and improved energy efficiency [14]. However, reaching the 55% reduction target by 2030 requires even bolder actions and accelerated progress.

1.1 Cutting CO_2 Emissions: Key Measures and Strategies

One of the cornerstones of the Green Deal is the reduction of CO_2 emissions, which account for the majority of the greenhouse gas output. The European Union is implementing several measures to achieve this goal [15]:

1.1.1 Expansion of Renewable Energy Sources

Renewable energy is central to the Green Deal, with the EU aiming for renewables to account for 40% of total energy consumption by 2030. The shift from fossil fuels to wind, solar, and hydroelectric power is expected to drastically cut carbon emissions across member states. In 2022, renewables already accounted for more than 22% of the EU's energy mix, marking a significant step toward this target heading.

1.1.2 Carbon Pricing and the Emissions Trading System (ETS)

The EU's Emissions Trading System (ETS) remains one of its most effective tools for reducing carbon emissions. The ETS works on a "cap-and-trade" principle, setting a limit on total emissions while allowing companies to buy and sell emission allowances. Over time, the cap is reduced, pushing industries to invest in cleaner technologies. The recent reform of the ETS is designed to align it with the 2030 climate targets, with a more stringent cap and the inclusion of additional sectors such as maritime transport.

1.1.3 Energy Efficiency Improvements

Improving energy efficiency is crucial for reducing carbon emissions, and the Green Deal includes a "Renovation Wave" initiative aimed at doubling the renovation rate of buildings over the next decade. Buildings account for nearly 40% of the EU's energy consumption and 36% of CO_2 emissions. By enhancing insulation, upgrading heating systems, and installing smart energy management technologies, the EU hopes to significantly reduce emissions in this sector.

1.1.4 Decarbonizing Industry

The EU Green Deal emphasises the need to transition energy-intensive industries like steel, cement, and chemicals toward cleaner processes. The development of hydrogen as a key energy carrier and the deployment of carbon capture and storage (CCS) technologies are central to this effort. The EU's Hydrogen Strategy aims to establish hydrogen as a cornerstone of a decarbonised energy system, potentially reducing industrial CO2 emissions by up to 80%.

1.1.5 Sustainable Transport and Mobility

The transport sector is responsible for nearly a quarter of the EU's greenhouse gas emissions. The Green Deal targets a 90% reduction in transport-related emissions by 2050. This will be achieved by promoting electric vehicles, expanding high-speed rail networks, and introducing stricter CO_2 standards for passenger cars and Light and Heavy-duty vehicles. By 2030, the EU aims to have at least 30 million zero-emission vehicles on its roads.

1.2 Powertrains for the carbon-neutral society

Road transportation has one of the most significant impacts on total CO_2 emissions in the EU, amounting to approximately 24% (for 2020) [16]. More than 62% of that amount is emitted from Light-duty vehicles (LDVs -passenger cars and vans), while almost 25% is sourced by Heavy-duty vehicles (HDVs - trucks and buses).

With that in mind, the Green Deal agenda brought a set of regulations for restricting CO_2 emissions from vehicles:

- Regulation (EU) 2019/631 sets binding CO_2 emission targets for LDVs. It is updated in April 2023 to align the targets with the EU's 2030 and 2050 climate objectives. The ultimate goal of this regulation is the EU fleet-wide CO_2 emission target for LDVs of 0 g CO_2/km from the year 2035 onwards, corresponding to a 100% reduction [17].
- Regulation (EU) 2019/1242 sets binding CO_2 emission targets for HDVs. It is amended in 2024. by Regulation (EU) 2024/1610 [18] (as a part of the "Fit for 55" legislative package [19]) in order to broaden the scope and cover nearly all emissions from HDVs and applies to medium and heavy lorries, city buses, coaches and trailers. Revised targets are more ambitious, aiming to increase CO_2 emission reductions to 90% by 2040.

Since the vast majority of powertrains in both LD and HDVs are based on Internal Combustion Engines (ICE) fueled by fossil fuels, both regulations are aimed toward the heavy reduction of CO_2 emission from an ICE combustion process. This means the current EU "plan" is to establish the electrical powertrain as the only viable option in LDVs after 2035 and as a dominant option in HDVs beyond 2040. In order to achieve such an ambitious goal, two primary prerequisites must be achieved: Significant enlargement and optimisation of electric energy production capacities from renewable sources for the energy supply of such a massive fleet of electric vehicles (EVs) and advancements and innovations in the EVs design and production to make them affordable and available in needed numbers.

The increase in available renewable energy sources is planned to be achieved through the Renewable Energy Directive, which sets an overall renewable energy target of at least 42.5% binding (from 22% in 2022) at EU level by 2030 [20].

1.2.1 Electric Vehicles (EV)

Electric powertrain-based vehicle production and usage have been on the rise for years already, with all accompanying problems. The on-vehicle electricity could be stored primarily in batteries, supercapacitors, or a combination of two (hybrid batteries). Besides battery electric vehicles (BEVs), Plug-in hybrid vehicles (PHEVs) are also considered EVs. Although the technology of batteries is advancing, the battery modules are still bulky and heavy, giving the EVs a high mass and limited range compared to ICE-powered vehicles. The growing need to enlarge the electric charger network is still in demand and an obstacle to achieving comfortable and short charging times (comparable to ICE-powered vehicles). The EV prices are relatively high, mainly due to the high costs of a modest production scale. Despite all the problems, the number of newly registered Light-duty EVs has risen to a current share of 2.8%, with BEVs holding only 1.6% [21], where the rise strongly depends on the initial incentives and tax benefits.

In heavy-duty vehicles, the most intensive transformation is taking place in the city's public transportation fleet, where the EU yearly purchases of new BEV buses overtook diesel by numbers in 2023, with a share of 36%. The overall share of the BEV buses in the EU city public transportation fleet is at a level of 8.3% with a goal to reach zero-emission buses of 30% by 2030.

1.2.2 Alternative zero-emission powertrains

The goal of drastically cutting CO_2 emissions is built around the substantial buildup of electrical energy production capacities from renewable sources – primarily wind and solar energy. Being unpredictable and variable by nature, renewable sources-based energy production capacities require an accompanying energy buffer infrastructure, which can accumulate the energy in production peaks, thus enhancing longer-term stable availability. Multiple technologies are available for that, but each has advantages and drawbacks - from a very efficient pumped storage hydropower system via massive battery storage systems to systems that convert electricity to a gaseous or liquid fuel as energy storage.

The latter is an option with multiple potentials which will play a significant role in the overall decarbonisation process. One of the technologies that will be massively employed is the production of hydrogen from renewable energy sources based on electricity, i.e., hydrogen is considered to be the equally important energy carrier of electricity itself.

Moreover, renewable energy resources are unevenly distributed across the world. In a system reliant on renewable energy, hydrogen will serve as the energy carrier that can be efficiently transported and stored, enabling the delivery of renewable energy from resource-rich remote areas to where and when it is needed to meet energy demand [22].

From that point of view, powertrains using hydrogen as a fuel will find a significant place in building carbon-neutral industrial environments. One of the technologies already part of the decarbonisation process is fuel cell technology. It is very suitable for using gaseous hydrogen as a fuel for the direct and high-efficiency production of electrical energy. Several manufacturers are already offering passenger car models with fuel cell powertrains (Toyota Mirai and Hyundai Nexo). Although the number sold is modest, these vehicles entered the market as technology demonstrators and have been there for years, so much real-world experience is gathered.

Fuel cell powertrains are basically electrical and need relatively small battery capacities (only as a buffer) compared to BEVs. The main advantages of fuel cell technologies over BEVs are much less needed battery capacities and thus smaller system mass and much shorter "charging" times.

Fuel cell cars use onboard tanks with gaseous hydrogen stored at 700 bar with approximately 5 kg capacity (0.04 kg/l). Remarkable efficiency enables these vehicles to have an economy of 0.8-1 kg H2/ 100 km, giving them a range usually higher than in BEVs and closer to ICE-based vehicles. Besides, the hydrogen filling time is within the range of 5 minutes (in optimal conditions), making this technology more convenient and closer to the comfort of usage offered by ICE-based vehicles.

Fuel cell technology is also present in Heavy-duty vehicles – mostly in city public transportation buses. The fuel cell technology application in city buses offers more attractive performance than battery-based solutions (less weight, higher range and shorter fueling time). Although the presence of fuel cell-powered buses is still modest, the interest and number of orders are growing. For example, the biggest ever one-off contract in Europe for the delivery of fuel-cell-powered buses for an order of 130 buses was signed recently [23].

As a viable option for converting electricity to usable fuel (so-called e-fuel), technologies are available for synthesising carbon-based fuels from captured CO_2 (from some industrial processes) and hydrogen produced from renewable energy sources. A variety of synthetic fuels can be produced, like higher alcohols, ethers, and synthetic hydrocarbons (synthetic gasoline, paraffinic diesel, and paraffinic kerosene) [24], [25].

1.2.3 Internal combustion Engines-based powertrains?

The overall impression of introductory facts and trends could imply a conclusion that, within the Green Deal agenda, there is no more space for a powertrain technology, which has carried the industry on its shoulders for over a century – Internal Combustion Engines. Is it so?

Hydrogen

Legislative requirements and CO_2 *emission*

It is well known that ICE can use hydrogen as a fuel, thus providing water vapour as a dominant exhaust product. From that point of view, ICE is conforming to the future demands of zero CO_2 emission – at least according to currently defined and valid test and approval methodologies (Euro VI / post Euro VI legislative requirements). Hydrogen-powered ICE (H2ICE) technology appears very competitive to the Fuel cell technology, although with a few drawbacks on the ICE side:

- Due to the high-temperature combustion of hydrogen with atmospheric air, NOx emission is also present as an exhaust gas component. So, from that point of view, H2 ICE, inherently, is not an absolutely zero-emission powertrain unless an efficient Selective Catalytic Reduction system is implemented as a part of the engine’s exhaust after-treatment system. Also, if the current SCR technology (used in Diesel ICEs) is foreseen as a technology for the future hydrogen ICE, with urea as a reductant, the SCR system generates a very small amount of CO_2.
- Due to an unavoidable lubrication system, ICE operation is regularly followed by some oil consumption toward the combustion space, i.e., some oil combusts and generates non-zero CO_2 emission.

It is still unclear how exhaust emissions from H2 ICE will be treated. The future legislation basis for the H_2 ICE is currently under discussion, with an initial “lean” approach to encourage further developments and investments in H2 ICE technology [26], [27]. The current approach suggests that the H2 ICE emission will be treated similarly to conventional ICE, which means that the focus will be given to NOx emission and that the SCR system will be mandatory for H2 ICE.

Simulation of a long-haul heavy-duty application in the VECTO long-haul duty cycle shows that the CO_2 emission of the conventional diesel powertrain is 604 g/kWh. When the powertrain is replaced with H2 ICE, the CO_2 emission reduction is 100% if the emission from the urea-based SCR system is not considered. If this CO_2 emission is also taken into account (5 g/kWh), the overall reduction of CO_2 is still more than 99% [28].

Total Cost of Ownership (TCO)

Real-world experience shows that fundamental economic indicators drive market response and purchasing decisions. Fuel cell based powertrains CAPEX is higher due to a higher cost of the Fuel-cell specific power (approximately 3 x of H2 ICE). On the other hand, available data on maintenance costs are not consistent or completely coherent. Some analyses are based on maintenance costs of the fuel cell-based truck estimations, which are lower than those of ICE counterparts [29]. Others are relying on more realistic projections [30] or real-world experience, particularly from USA operators who have been in the maintenance business with fuel cell powered busses for years, delivering conclusions that hydrogen fleet maintenance is 20-125% more expensive than diesel fleet [31]. In both approaches, having in mind even the fact that the efficiency of the H2 ICE is lower (7 or more %), the conclusion is that the TCO of a Fuel cell truck is at least comparable but most likely considerably higher than those of the H2 ICE based truck. Not to mention that although the fuel cell technology has been present on the market for decades, the lifetime of the fuel cells is much shorter than those of potential H2 ICE. For example, claims for the latest generation of fuel cells lifetime for heavy-duty vehicle applications are 25000 hours [32], which implies that at least one (lifespan midterm) replacement is needed with a new power stack.

Therefore, H2 ICE has a lot of the potential to be TCO competitive, particularly if further progress is made in the area of H2 ICE combustion process research towards high efficiency.

“Zero-impact” for OEMs / truck makers

All truck manufacturers have established expertise with conventional ICE powertrains. They employ skilled professionals, and their systems are well-understood and optimised. Any modifications would be relatively minor compared to alternative approaches. Additionally, the impact on powertrain production would be minimal, as would the necessary changes to the supply chain. The hydrogen tank system would clearly introduce new requirements for vehicle integration and service operations. However, other components are already well understood, their behaviour is predictable, and the expert teams are already available to address any issues.

Alternative CO_2-neutral fuels

Besides hydrogen, as a most promising fuel option for zero-emission ICE, hydrogen-carrier fuels like ammonia are also attractive as zero CO_2 emission fuels [33]. The ammonia production and process equipment industry is mature and well-established, and that is why ammonia is foreseen as an attractive zero-emission fuel for ICEs in marine transport, mainly since the fueling capacities are already available (or can be built effectively) in large ports. Due to the high power demands required by ship propulsion, it is currently hard to imagine any other technology than ICE that can provide the required performance.

It is expected that the much larger scale production of synthetic fuels will be imminent in the future, taking a substantial part in overall decarbonisation in various applications – not only as CO_2 -neutral fuels for ICE powertrains and the aviation sector but also as a means of CO_2 storage. Due to high production costs, the prices of potential synthetic fuels are much higher than those of fossil fuels. However, with the production capacities upscaling and the expected fall of input prices, synthetic fuels can be expected not only to have a role in the decarbonisation process but also to be a competitive alternative to fossil-based fuels [34].

Viable and perspective options for ICE powertrains within the Green Deal agenda?

A comparable number and quality of uncertainties affect all drive technologies. Therefore, it is unjustified to point to any of the drive technologies as absolutely preferable [35]. Regulation (EU) 2019/631 is considered to ban ICE-based powertrains in LDVs starting in 2035. However, the potential consequences of such strict goals are still discussed, and public pressure is being put on to modify the regulation toward postponing and/or including synthetic fuels as a viable carbon-neutral option [36].

On the other side, ICE can still be used as a CO_2 zero-emission powertrain if powered by hydrogen. It is a question of how the ICE technology can be comparable to other alternatives – BEVs and fuel-cell powered vehicles in the LDVs area- in terms of costs, complexity, and range/efficiency [37]. ICE Efficiency is seen as the most significant disadvantage over other hydrogen powertrain technology – the fuel cells. Considering the feasible amount of hydrogen that can be stored in passenger cars (ca 5 kg), the range is heavily influenced by powertrain efficiency. The efficiency gap between fuel cells and ICE powertrains became smaller due to ICE technology advances, which is demonstrated on highly optimised large bore engines [38]. Still, the ultra-high efficiency hydrogen-powered ICE powertrain solution applicable to LDVs is yet something in which much R&D effort must be invested to be achieved.

Therefore, a hydrogen ICE-based powertrain is not yet seen as a viable option for the future. On the other hand, if the usage of synthetic fuels in LDVs is allowed (amended regulation scenario), the ICE will stay a very attractive option for powertrains.

In the HDV area, battery electric powertrains are already used, mainly in city public transportation buses. Due to a limited range and rather long charging time, the battery electric powertrain concept seems unpractical for HD applications covering longer distances. Therefore, fuel cells are in the spotlight of media and governing policies as preferred zero-emission future powertrains, emphasising high efficiency as a critical argument. Conversely, it is well known that fuel cells achieve the highest efficiency at partial loads, which suites a highly variable working cycle of HDVs like city buses but not trucks (medium and heavy lorries), which are much longer driven on higher loads. Having in mind other abovementioned disadvantages of fuel cell powertrains (maintenance costs, lifespan, total cost of ownership,…), it appears that high-efficiency Hydrogen ICE could be the most prominent candidate as a CO_2 zero-emission powertrain of the future in the HDVs area, particularly medium and heavy trucks/lorries.

In order to "secure" the future of hydrogen ICE powertrains, the utmost importance is for R&D capacities to offer a competitive and highly efficient ICE-based powertrain solution.

2 HYDROGEN AS A FUEL

As the world shifts toward cleaner energy, hydrogen is increasingly seen as a key player in the race to decarbonise transportation. The appeal is clear: hydrogen is the most abundant element in the universe. It emits no CO_2 when burned and can be used in both ICEs and fuel cells to power vehicles. Nevertheless, despite its promise, hydrogen remains a niche fuel in the global transport sector. What makes hydrogen a unique fuel, and what challenges lie ahead in making it a widespread solution for vehicles?

2.1 Properties and challenges in the widespread adoption of hydrogen as a fuel

2.1.1 Energy density

Hydrogen (H_2) is a colourless, odourless gas. As an element with the simplest atomic structure, it has the smallest density and is more than 14 times lighter than air at the common room temperature. As a fuel, hydrogen has a high energy density per unit of weight—approximately 120 MJ/kg, almost three times that of gasoline, but due to a small density, high pressures are required to store the comparable energy in tanks applicable for vehicle use.

To be stored onboard vehicles, hydrogen must be compressed to high pressures (typically 700 or 350 bar) or liquefied at extremely low temperatures (-253°C). Both methods are energy-intensive and require robust infrastructure. Although more than 900 hydrogen refuelling stations (HRS) were installed globally by the end of 2023, much work still needs to be done to define/update numerous standards for mass worldwide use [39], [40].

2.1.2 Onboard storage and refuelling

The HRS standards cover general requirements, dispenser, dispenser-vehicle communication, mechanical connection, hydrogen quality and fuelling protocol [41]. Standards addressing the mechanical connection and refuelling protocol are paramount for achieving safe, convenient, and fast hydrogen refuelling. Standards are also categorised in terms of vehicle class since the potential amount of hydrogen to store onboard differs significantly between LDVs and HDVs. One of the refuelling speed limitations is related to a maximum gas flow from the dispenser. Mechanical connections for LDVs and buses are designed to provide a maximum flow of 60 g/s of hydrogen. During refuelling, the temperature of the in-tank gas rises; therefore, an automation system must strictly control the process to limit the maximum in-tank temperature and pressure, and this is achieved by implementing the refuelling protocol. The refuelling automation system relies on information (in-tank pressure and temperature) supplied by the vehicle to the HRS via standardised communication. Overall refuelling time varies and depends on initial conditions met in the vehicle tank, and for LDVs, a refuelling speed is approximately 1kg of hydrogen per minute. HDVs (trucks), due to a much larger tank capacity, require higher, at least doubled refuelling capacities in terms of flow and speed. Thus, a newly proposed protocol within the PRHYDE project (if standardised) should provide a refuelling speed of 80kg of hydrogen in 10 minutes [41], [42]. Similar efforts are being made in the USA to improve adequate SAE norms [43].

2.1.3 Combustive properties of hydrogen

Hydrogen is a fuel, and such has stored chemical energy. It has associated hazards, but it is no more dangerous than the other fuels that store chemical energy. It is just different, and the science behind hydrogen flammability and combustion is well-known and well-understood [44].

Table 1 Flammability Properties of Hydrogen and Other Fuels

Property		Hydrogen	Methane	Propane	Gasoline Vapor
Flammability Concentration in Air (vol%) [45]	LFL	4.0 %	5.0 %	2.1 %	1.2 %
Flammability Concentration in Air (vol%) [45]	UFL	75.0 %	15.0 %	9.5 %	7.1 %
Most Easily Ignited Mixture in Air (vol%)		29% [46]	8.5% [47]	4% [48]	2% [49]
Adiabatic Flame Temperature [49]		2483 K	2236 K	2250 K	2289 K
Buoyancy (ratio to air)		0.07	0.54	1.52	4
MIE [50], [51]		0.011-0.017 mJ	0.28-0.30 mJ	0.25-0.26 mJ	0.8 mJ
Autoignition Temperature [49]		500 °C	580 °C	455 °C	246 – 280 °C

Hydrogen has properties which distinguish it from other widely used fuels in ICE. These impose hazards and risk concerns when used in vehicles and public transportation in general, which went through thorough analysis and checks in numerous studies on how to deal with them [52], [53]. Hydrogen is known as a gaseous fuel with the broadest range of flammability concentration limits in air - from 4.0 (LFL) to 75.0% (UFL) [45].

The hydrogen's minimum ignition energy (MIE) is an order of magnitude lower than the other fuel types, as seen in Figure 1[51]. As a result, an ignition source of an energy level far lesser than a typical automotive spark plug can be sufficient to ignite a hydrogen-air mixture in a wide concentration range – even a very lean one. Unfortunately, that also means that hot gases and hot spots on the ICE cylinder/head can serve as an ignition source, creating problems of premature ignition and flashback. Preventing this is one of the challenges of running an engine on hydrogen.

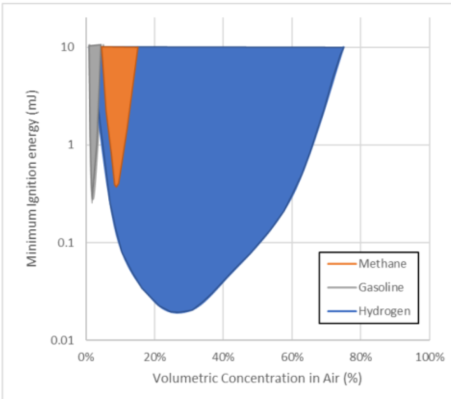

Figure 1 Minimum Ignition Energy for Different Fuels vs. Concentration [49]

Hydrogen has a shorter quenching distance compared to gasoline (0.6 mm vs. 2.0 mm), allowing hydrogen flames to approach the cylinder walls more closely before extinguishing [54]. As a result, quenching a hydrogen flame is more challenging than quenching a gasoline flame. Additionally, the shorter quenching distance increases the likelihood of backfire, as a hydrogen-air flame can more easily pass through a nearly closed intake valve compared to a hydrocarbon-air flame.

Hydrogen auto ignites at much higher temperatures than gasoline vapour, and therefore, it is considered suitable for use in ICE at higher compression ratios, which naturally have higher efficiency potential. Autoignition temperature is pressure-dependable, and it is way above 530°C (vs. 246-280°C for gasoline vapour) at pressures usually achieved in the compression stroke of an ICE [55]. The feature often promotes hydrogen as an ICE fuel that is much less prone to detonation/deflagration than gasoline, which is not quite so in real, state-of-the-art ICE applications. It is not simple to define the octane number (RON) of hydrogen since the standard ASTM procedures for determining the RON are designed for gasoline, and due to differences in combustion behaviour, these are not very usable in the case of hydrogen. Hydrogen-air mixture combustion speed and autoignition are heavily influenced by equivalence ratio, pressure and temperature, and thus, a comparison with the knocking behaviour of gasoline can be made only through modified RON-determination experiments by emphasising more comparable in-cylinder combustion conditions. When analysed from that point of view (modified RON), it appears that hydrogen has a higher octane number than gasoline (RON 93.7 @ λ=1, RON >120 @ λ=2), which is evident if hydrogen is used in typical gasoline engines with moderate compression ratios [56]. However, due to the complex relation of initial in-cylinder conditions (temperature, pressure, mixture non-homogeneities), low ignition energy and short ignition delay at higher compression ratios, hydrogen becomes a fuel considered highly prone to abnormal combustion, leading to preignition and engine knock, where the former is the most significant problem to cope with. Still, at the bottom line, despite not being knock insensitive, hydrogen can be employed as a fuel in ICE with higher compression ratios, i.e., in areas that are not reachable to gasoline, thus providing potential for reaching higher, diesel-like efficiencies.

Figure 2 presents an example of irregular hydrogen combustion in ICE. The process is captured in the ICE laboratory of the Faculty of Mechanical Engineering at the University of Belgrade during trials with specific engine configuration and λ=1.5 operation. As can be seen, combustion develops quite typically at a load of cca 8 bar IMEP without any visible “announcement” of potential combustion irregularities (Figure 2a), where the left (green) marker points to an end of injection angle and the next one (red) spark advance i.e. ignition angle. Suddenly, a late preignition occurs approximately 0.6 ms before regular spark (Figure 2b). Not being completely consumed by preignition flame, spark occurrence ignites another part of the mixture which is immediately followed by knock phenomena. This drastically rises the in-cylinder temperature providing even more favourable conditions for the preignition to appear in the following cycle. Another late preignition occurs in the upcoming cycle even closer to the TDC with an indication of a triggered volumetric combustion (Figure 2c). This further contributes to a deposited heat which in the next cycle triggers an early preignition which starts almost at the end of injection with a huge increase of the in-cylinder pressure and temperature and sharp drop of IMEP (Figure 2d). Intensive heat release sustains a sufficiently high temperature level during the compression stroke enabling successive cycles with hydrogen (early) autoignition (Figure 2e)with several overlapped successive irregular cycles with hydrogen autoignition).

Hydrogen combusts much faster than gasoline, which also contributes to the potential of enhancing ICE efficiency. Although the ignition delay rises and combustion speed drops with the enlargement of the air excess ratio, even a lean hydrogen mixture combusts at speeds comparable to gasoline. Fast combustion, even at higher air excess ratios, makes hydrogen an excellent fuel for the lean ICE operation.

Hydrogen has very high molecular diffusivity. It diffuses rapidly into the air, facilitating uniform mixture formation. In ICE with direct hydrogen injection, this property also influences the shape and range of the unignited (turbulent) jet. Combined with low density and high injection pressures, high diffusivity contributes to momentum-driven gas jets, which highly interact with all surfaces within the engine combustion chamber (cylinder head and lining, piston head) [57]. So, despite high diffusivity, this often results in a nonhomogenous mixture, which has consequences in combustion in general and, particularly, in enhancing abnormal combustion triggering mechanisms. That’s why tumble-driven mixture formation is favoured even in HD engines as a concept that contributes to better mixture formation and combustion flame kernel positioning away from the cylinderwalls.

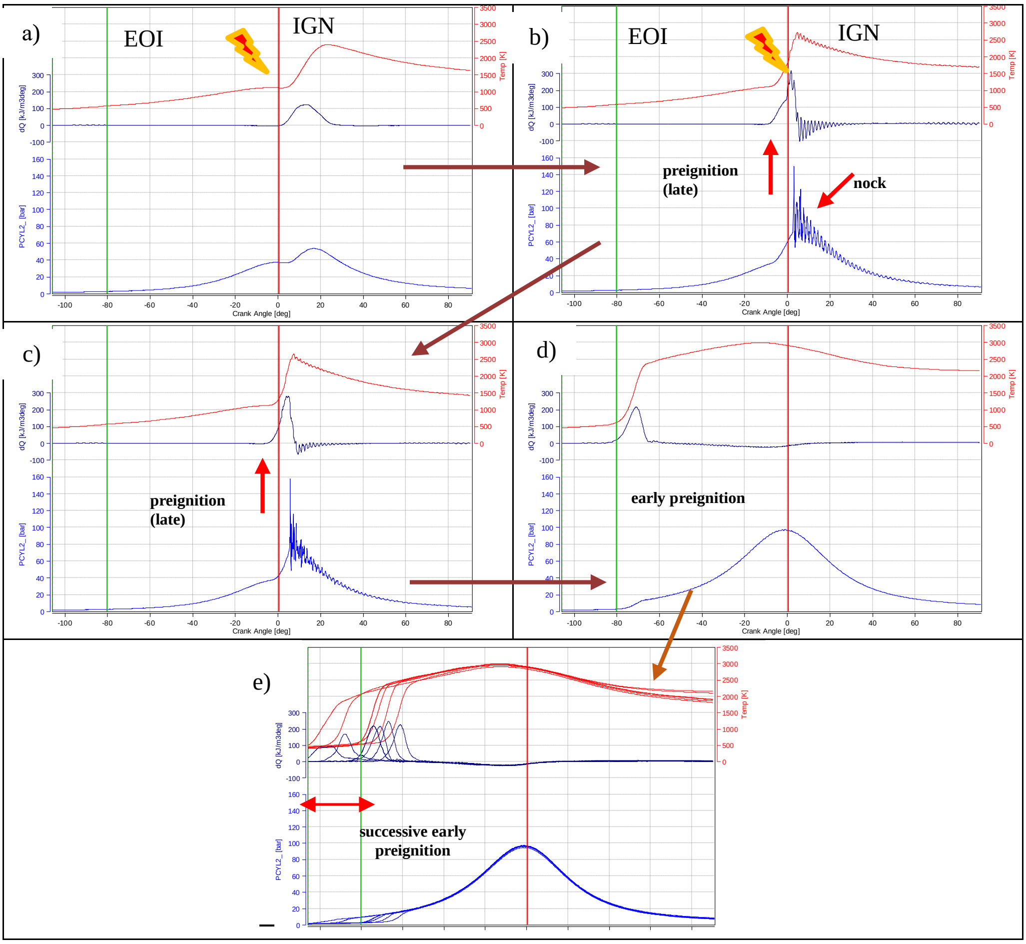

Figure 2 An example of developing irregular hydrogen combustion through four successive cycles (CR=13.7, λ=1.5, 2000 rpm, NA, IMEP≈8 bar)

2.2 Hydrogen in ICE

2.2.1 Technologies

The most significant advantage of hydrogen-fuelled IC engines is the existence of proven and well-established basis technology. Due to the specifics of the hydrogen, the well-known ICE needs some adaptation and additional R&D efforts, but all that the industry can provide in a short time with a minor modification of existing production and maintenance capacities. From that point of view, hydrogen-fuelled engines are considered a technology solution derived from existing spark-ignited (SI) or compression-ignited concepts.

Two general approaches can be used for hydrogen-air mixture formation: Low-pressure injection of the hydrogen into the intake port (PFI) and direct injection of the hydrogen into the cylinder (DI). The usage of PFI technology seems attractive and straightforward since it is implemented in many gas (CNG) engines. This approach seems adequate since the technology of high-flow, low-pressure gas injectors is mature (although not specifically for hydrogen). Using a low-pressure injection also maximises the utilisation of the pressurised hydrogen stored onboard in vehicle tanks. The most significant drawback of the MPI technology is the “easy-to-reach” condition of the flame backpropagation, as well as the occurrence of early preignition in the cylinder. Also, the MPI approach leads to a lower volumetric efficiency (considering the high hydrogen/air volumetric ratio needed even for a lean operation). Therefore, MPI technology is not seen as a pathway toward the high-efficiency hydrogen engine.

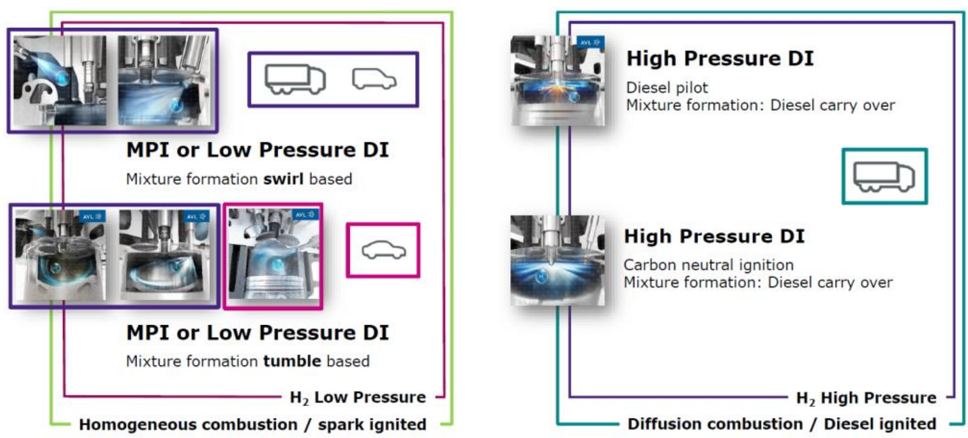

Figure 3 Hydrogen Combustion Concepts for Commercial Applications and Passenger Cars [58]

The DI approach diminishes the back flame issue and appears as a more versatile technology regarding combustion control potentials. Since the hydrogen is injected into the (already filled with air) cylinder, this approach can provide higher volumetric efficiency and, thus, higher specific power while keeping in mind that at lean operation, that can be achieved at the expense of high boosting pressures. A significant drawback of a DI approach is related to the needed capacity of the injection system since a large amount of hydrogen ought to be injected into the cylinder in a limited crankshaft angular (CA) window. Additionally, it is well-known that due to a high diffusivity, hydrogen can be absorbed by metals, which further can induce metal cracking. This hydrogen embrittlement is also an issue that must be carefully addressed when designing the hydrogen injection system, particularly injectors. Above that, hydrogen has a weak lubrication capability (even worse than CNG), which requires further mechanical development addressing friction issues toward reliable and durable injector solutions. Currently, much effort is invested in developing a new generation of both PFI and DI hydrogen injectors capable of delivering the required flow, mainly focusing on low-pressure solutions (20-30 bar) with high durability in mind [59], [60].

Low-pressure injection provides the best possible utilisation of the onboard stored hydrogen fuel. On the other side, since the injection occurs after inlet valve closure, the injection pressure has to be high enough to enable the free injection, opposing the in-cylinder pressure level reached during the compression stroke at the end of the injection. In summary, low-pressure DI has advantages but is generally limited by the necessity of delivering hydrogen through a long-duration single injection process.

Multiinjection strategies offer more versatility in controlling mixture formation, homogeneity, and combustion, which all influence and potentially enhance efficiency. Achieving this is possible by utilising higher injection pressures, i.e., with only high-pressure injection, the injection timing can be varied within a wide range, and thus, not only controlled fuel stratification can be realised but also an explicit control of the combustion process [61]. Thus, the high-pressure DI injection concept is considered one which could support combustion control concepts toward the highest possible efficiency. Although the low-pressure DI concept cannot offer as many degrees of freedom as the former, it can still provide many advantages of high-pressure while being closer to series-production readiness. That is why the low-pressure DI is the current focus of R&D.

The combustion system concept, foreseen for potential passenger cars hydrogen ICE, is based on a well-known technology used in gasoline engines – spark ignited with a pentroof combustion chamber and induced tumble air/fuel mixture motion. This concept is well-proven with hydrogen and provides, so far, the best results [62].

In the area of HDVs, currently, dominant CI diesel engines are swirl-based with a flat-top cylinder head. Current HD hydrogen-fuelled demonstrators rely on this concept to demonstrate that not-so-big changes are needed in the engine layout to “switch” them toward hydrogen use. Current R&D efforts are conducted on two tracks: One with a spark-ignited concept and another with a compression ignition to prove the highest possible efficiencies [58],[30]. Latter are actually dual-fuelled engines with a minor pilot amount of diesel fuel for stable auto-ignition of the hydrogen/air mixture [65]. Operating with a hydrogen energy ratio of 97.5% at full load, this setup meets potential CO_2 emission targets in HDVs and demonstrates an efficiency of 51.5% [66]. Also, controllable auto-ignition is demonstrated as possible with a spark plug assistance (ignition of lean pilot mixture followed by autoignition of late injected hydrogen [67]) or by means of a hot surface/glow plug [68].

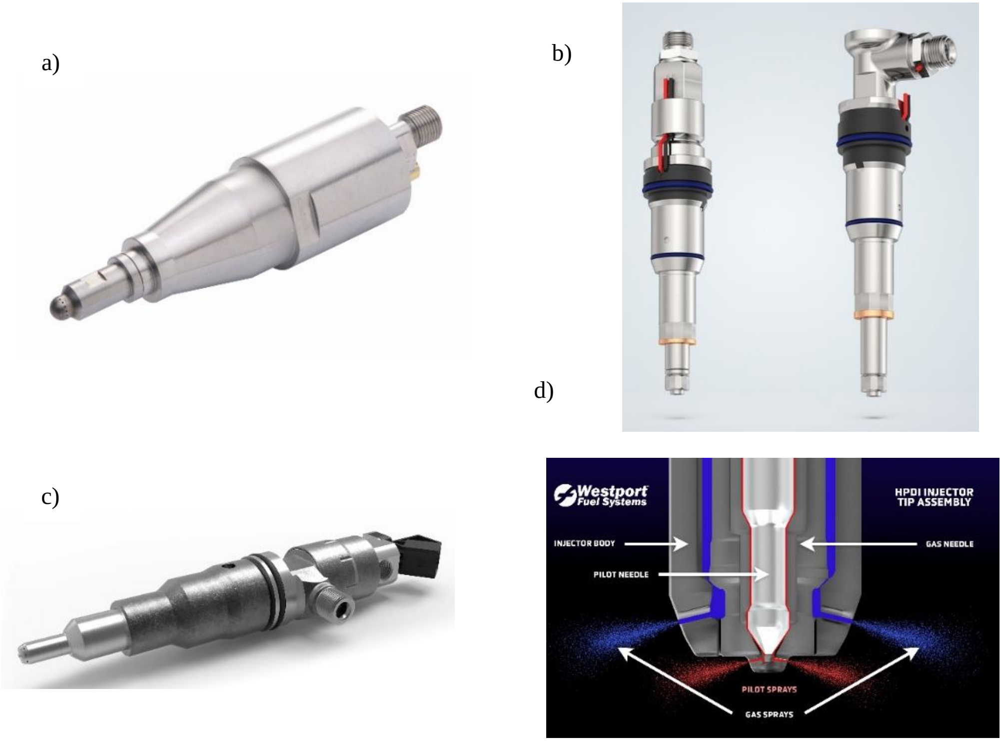

Figure 4 Hydrogen injector technologies: a) 300 bar DI injector from Hoerbiger for H2BVplus project [63];
b) low-pressure DI injector from Liebherr [64], [59]; c)-d) high-pressure HPDI hydrogen and diesel pilot injector as a single unit with injection pressures of up to 300 bar [30]

2.2.2 Combustion process control

Hydrogen is an extremely easy-to-ignite fuel with high-speed combustion. Therefore, there are two crucial aspects to deal with in order to achieve stable and controllable combustion. The first deals with a preignition, i.e., measures for its suppression. The second deals with a harsh pressure (and temperature) rise due to high-speed combustion, which further can easily lead to knock, thermal overload, extremely high in-cylinder pressures and high-pressure rise gradients challenging the mechanical integrity of the engine and causing harsh noise.

Using a stoichiometric ratio at high compression ratios gives a harsh, high-speed, and knock-provocative combustion process with the highest performance (specific power), the best transient behaviour and the highest NOx emissions. On the other side, lean combustion provides slower, much less knock-prone combustion, which is easier to handle even at high loads. Lean combustion also brings much less NOx emission and high efficiencies but with lower specific power and slower transient response as a drawback while needing much higher boost pressures for a higher load operation. So, depending on the application requirements, a mixture of approaches can be used to satisfy the stated objectives. However, in all cases, a kind of combustion moderator is needed to overcome harsh combustion behaviour on higher loads, which is not avoidable at high compression ratios and lower air excess ratios ($\lambda<2$).

One of the frequently used and discussed combustion moderators is water, which is injected through a dedicated PFI system and effectively influences the combustion speed, thus enabling stable combustion and control on higher loads even with stochiometric operation [62]. The drawback of this approach is the necessity to equip the vehicle with an additional water tank. Much research is involved in finding solutions that can avoid this, and one of the promising options is to use onboard-generated water by partially condensing engine exhaust gases. The second and largely exploited possibility is implementing the EGR concept, which significantly contributes to more stable and controllable combustion, simultaneously lowering cycle temperature and NOx emission.

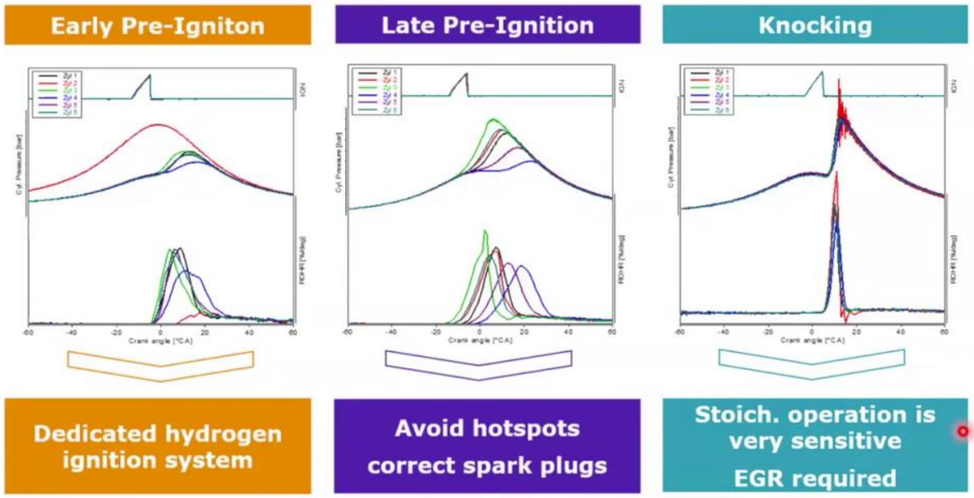

Figure 5 Hydrogen combustion anomalies - challenges in controlling hydrogen combustion process in ICE [69]

Due to the extremely low ignition energy required, special attention is given to suitable ignition systems. Spark plugs should be of highly heat conductive “cold” type and ignition coils, and their control should ensure needed spark plug electrodes potential explicitly when required, i.e. with high suppression of so-called “ghost spark phenomena” [70].

2.3 NOx emission control

The combustion of hydrogen/air mixtures inevitably leads to the formation of nitrous oxides through the well-known Zeldowich formation mechanism [71]. Highly temperature-dependable, the NOX formation rate in hydrogen engines is heavily influenced by the used air excess ratio and applied EGR.

For passenger car engines, two NOx after-treatment system options are considered as a potential solution for minimising tailpipe NOx emission. The so-called passive SCR (selective catalytic reduction) is a viable engine aftertreatment system (EAS) option for stoichiometric operation (Figure 6a). This concept features onboard ammonia (NH3) generation, formed in the three-way catalytic converter (TWC), closely coupled to the engine, which is then used as a reduction agent in a remotely placed (underfloor) SCR with or w/o additional external air [72], [73]. A conventional SCR system is needed for lean operation with an active SCR operation with a close coupled oxidation catalyst and SCR with active urea dosing (Figure 6b) [58].

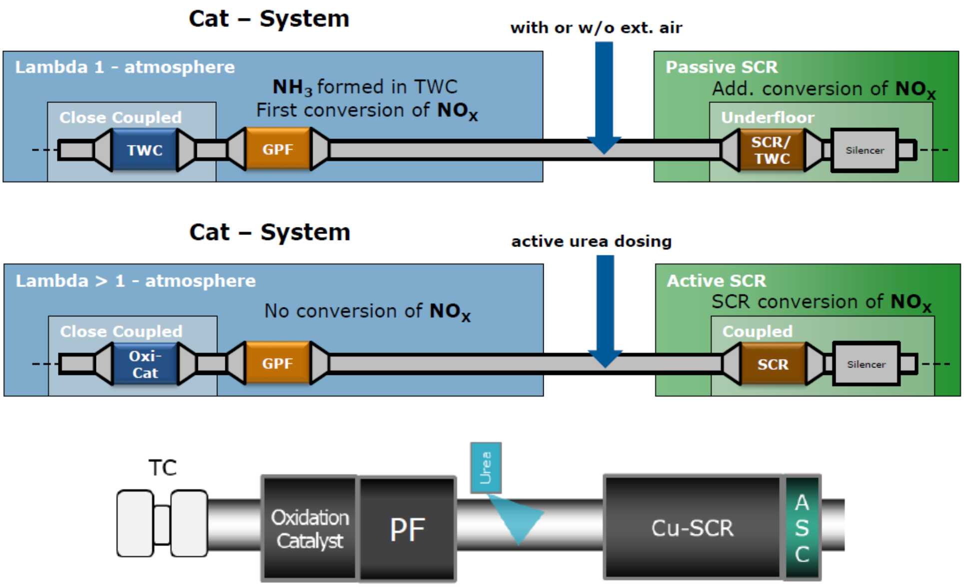

Figure 6 Exhaust aftertreatment systems layouts suitable for hydrogen ICE and fulfilment of Euro VI norms [58]

Foreseen EAS concepts for hydrogen HDVs are currently built with Euro VI norms in mind. The already tested and proven layout is a diesel-like concept and consists of an oxidation catalyst, an active SCR with a copper-based catalyst and an ammonia slip catalyst at the end (Figure 6c) [58]. Recently adopted EURO VII norms put further restrictions on NOx emissions, but it is considered that a two-stage SCR system is capable of providing the required performance in reducing NOx emissions below new limits [74].

3 H_2 ICE DEMONSTRATORS

R&D on hydrogen ICE has been conducted for decades, with its ups and downs, driven chiefly by the interests of its time. Much knowledge has been accumulated over time, and numerous examples of IC engines converted to hydrogen ICE are used as technology and various concept demonstrators [75], [76]. A significant milestone in hydrogen ICE development was the Hydrogen 7 project by BMW [77], [78]. It was the first hydrogen ICE vehicle produced in numbers sufficient to be used as a worldwide demonstrator. Hydrogen 7 car was powered by V12 6 litre bi-fuel engine with both hydrogen and gasoline tank onboard to achieve the highest possible range. The interesting aspect of the design is the choice and trial of liquid hydrogen storage as a measure for achieving an onboard mass of stored hydrogen fuel as large as possible. Having almost twice the volumetric density (0.071 kg/l for liquid H2 vs. 0.04 kg/l for gaseous H2 @ 700 bar), storing the hydrogen in liquid form seems a reasonable step for enhancing the capacity of onboard fuel storage and thus range. Unfortunately, hydrogen has to be cooled to at least -253°C to be kept in a liquid form since hydrogen boils off at a temperature above that limit -therefore, the storage tank has to be insulated (vacuum). Despite insulation, a heat transfer is unavoidable. This leads to permanent fuel boil-off, which must be vented to limit in-tank pressure buildup since the cryo tanks are low-pressure vessels. As an early hydrogen ICE demonstrator, the engine fueling system was built on many compromises. A PFI injection system was implemented, which mainly influenced the engine's volumetric efficiency and cut the gasoline "original" performance by more than 40%. The injection pressure was built by heating and evaporating the liquid fuel in a heat exchanger and thus kept at a level comparable to the gasoline PFI system (cca 3 bar). The original engine's compression ratio was lowered from 11.3 to 9.5. Furthermore, to avoid complex aftertreatment of the exhaust NOx, the control strategy was focused on using air excess ratios, which minimise the NOx generation. Thus, for "high power" operation, an air excess ratio of λ=0.97 was used since a slightly rich mixture provided a neglectable amount of NOx entirely handled by TWC with only a 0.1% hydrogen slip. An excess ratio of λ>1.8 was also used for part loads to minimise NOX emission [79]. Mixtures with $0.97<\lambda<1.8$ were avoided entirely as a range where NOx emission was substantial and could not be diminished by TWC. The concept was designed to demonstrate the capability to fulfil SULEV norms completely, and it proved successful despite its shortcomings – relatively low engine efficiency and fuel los due to boil-off.

At the same a larger-scale project HyICE was conducted in the EU [61]. An integrated project within the sixth framework of the European Commission gathered several key industry players around a quest to explore the possibilities and perspectives of hydrogen ICE and its optimisation. The project identified hydrogen direct injection as the most prospective concept. An efficiency of 42% was demonstrated on a specially built single-cylinder research engine with diesel-like geometry and injection pressures of 300 bars [80]. The concept was further explored within the H2BVplus project with experiments employing hydrogen self-ignition [63], [68]. The potentials of the low-pressure direct injection were also explored through a dedicated hydrogen ICE design and injector nozzles optimisation, which provided a 12.8-litre engine with a maximum power output of 200kW and an effective efficiency of 42%. This engine (MAN typ H2876 UH) is further tested in public transportation within the HyFLEET: CUTE project [81]. The HyICE also explored the concept of cryogenic port injection (CPI) - an injection of liquid hydrogen with a specially designed injector. CPI concept demonstrated a potential for the increase of specific power by 25% and providing performance comparable to a gasoline PFI engine but with substantially expanded range of good efficiency where 44% is demonstrated with increased compression ratio.

Both projects mentioned were conducted more than 15 years ago but brought to the engineering community a significant knowledgebase. In the meantime, ICE technology has advanced mainly in applying advanced mechatronic systems in the control of mixture formation and combustion process control. AVL presents one of the most recent examples of H2 ICE demonstrators, with two H2 ICE demonstration platforms, by following the in-the-meantime built general opinion and projections of the H2 ICE implementation in the future automotive technology.

According to all presented technology facts, current developments and EU policies, it is obvious that European automotive manufacturers do not see H2 ICE as a powertrain solution for passenger cars at the moment, mainly due to limited options for storing needed amounts of hydrogen onboard for a range comparable to a fuel cell or even battery electric vehicle. As a manufacturer that invested more than 40 years of R&D in H2 ICE, even BMW is abandoning the H2 ICE idea in cars and orienting itself toward fuel cell-based powertrains [82]. Supporting argument for this decision also lies in the fact that, as being electric, the majority of components of the fuel cell-based platform are compatible with the platform of battery electric vehicles, which are foreseen as a future of car production in Europe.

An exemption in the H2 ICE powertrain for cars is seen in racing sports. Therefore, AVL recently introduced a demonstrator of an H2 IC racing engine of remarkable performance: 300 kW @ 6500 rpm and 500 Nm @ 3000-4000 rpm from a two-litre four-cylinder inline engine. The concept proved the viability of a power density of 150 kW/litre and BMEP (break mean effective pressure) in a range of 32 bars.

Several concepts could be considered as potential H2 ICE operation concepts:

- Pure lean concept
- Lean + EGR
- Stochiomteric + combustion moderator

The pure lean concept relies on $\lambda \approx 2.5$ to achieve the lowest NOx emission. A drawback of a lean operation is the requirement for very high boost pressures to reach high power and the necessity of NOx aftertreatment with or without SCR. By introducing EGR, it is possible to slightly reduce boosting pressure with joint reduction of NOx, but NOx aftertreatment with or without SCR remains a requirement. Stoichiometric operations provide the highest power, but the combustion is very prone to irregularities, and thus, some combustion moderator is required to put the combustion process in stable control. Also, NOx emission at $\lambda=1$ can be handled with TWC. Therefore, AVL chose to use $\lambda=1$ operation with water as a combustion moderator (injected through a dedicated PFI system). AVL's H2 racing ICE has endured testing and is currently under analysis for further improvements in all possible aspects (***Figure 7***).

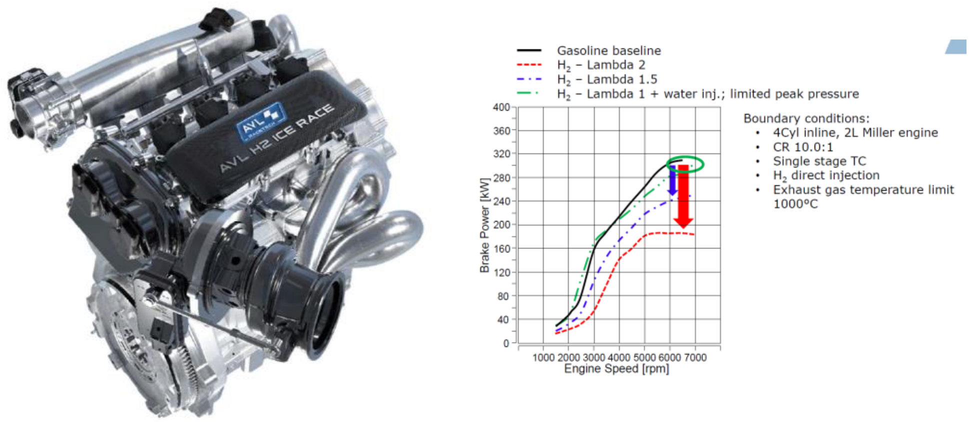

Figure 7 AVL H2 ICE racing engine demonstrator [62]

It is interesting to note that in Japan, Toyota is conducting similar testing of a racing H2 ICE but with a completely different idea and goal in mind. Toyota has been competing using a hydrogen-engine car (racing version of Corolla model) since 2021. As a first step, they used almost the exact version of the gasoline engine (3-cylinder turbocharged 1.6-litre engine) converted to a high-pressure DI hydrogen engine with hydrogen stored in a gaseous state in high-pressure tanks. Having in mind H2 ICE as the potential passenger car powertrain of the future, as a viable and more cost-effective option to a fuel cell, Toyota focused on solving the problem of onboard storage of sufficient amounts of hydrogen and therefore introduced liquid hydrogen storage in a racing car. However, their approach initially differs largely from the concept BMW introduced in the Hydrogen 7 project since it initially aimed to deliver the engine hydrogen at pressures needed for a high-pressure DI. So, Toyota's concept of liquid hydrogen storage is upgraded with a cryogenic high-pressure pump to raise the hydrogen pressure to 100 bar before evaporation and further transport to the engine injection system (***Figure 8***) [83]. Although Toyota deals with common problems like hydrogen boil-off, the size of the tank, and its design, the focus is on testing components and making progress in every aspect, mainly component durability and reliability. One of the crucial challenges is a cryogenic hydrogen pump with a plan to implement a pump with a superconducting drive. It is obvious that all efforts are being made toward exploring and finding solutions to overcome current limits in the implementation of hydrogen in both fuel cell and ICE-based passenger cars since hydrogen is seen as a critical enabler of the future carbon-neutral society in Japan [84]. The impression that engine efficiency is not in focus at the moment is only a misjudgment since Toyota's research in H2 ICE almost 14 years ago already demonstrated remarkable results in achieving high efficiencies with a goal to achieve H2 ICE efficiency at the level of state-of-the-art fuel cells. Research on a diesel-like engine geometry demonstrated the possibility of achieving an efficiency of 51% at part load with further potential of achieving similar eficinecies on higher loads by implementing a concept of spark assisted diffusive combustion with late injection strategy, injection concept which will minimise heat losses by limiting hydrogen jet penetration and wall interaction and application of largely humidified EGR [67].

A second worth-to-mention H2 ICE demonstrator is recently presented AVL heavy-duty hydrogen engine. Without any doubt, H2 ICE will be seen as a serious option for powering heavy-duty segments in the near future. The

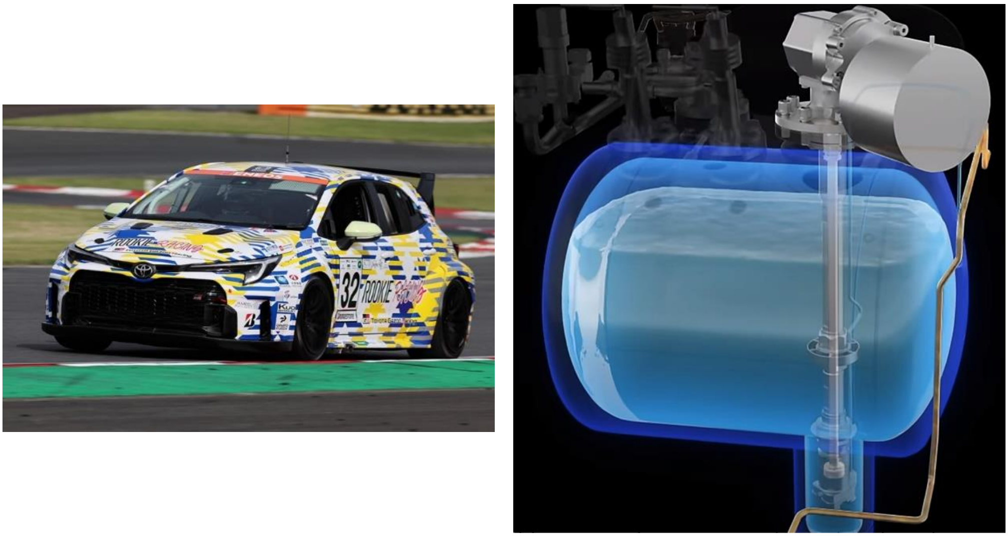

Figure 8 Toyota GR Corolla with lately introduced liquid hydrogen storage with cryogenic pump [83]

Demonstrator is a typical HD (truck 12.8 litres engine) derived from a natural gas-fueled engine. After conversion to hydrogen, the engine demonstrated performance comparable to a diesel engine of the same size with a power level of 350 kW, maximum load at 24 bar BMEP, and efficiency (BTE) of 43% (***Figure 9***). As a demonstrator, the engine is equipped with both a PFI and low-pressure DI injection system. In order to limit NOx emission, an air excess ratio of λ=1.8 is used at the highest loads while leaning the mixture toward lower loads (up to λ=2.4). A lean operation, even at λ=1.9, showed a significantly slower response on transient operation with a single-stage turbocharger and adding an e-booster or two-stage turbocharger is proposed for getting transient response behaviour comparable to a typical diesel engine (***Figure 10***).

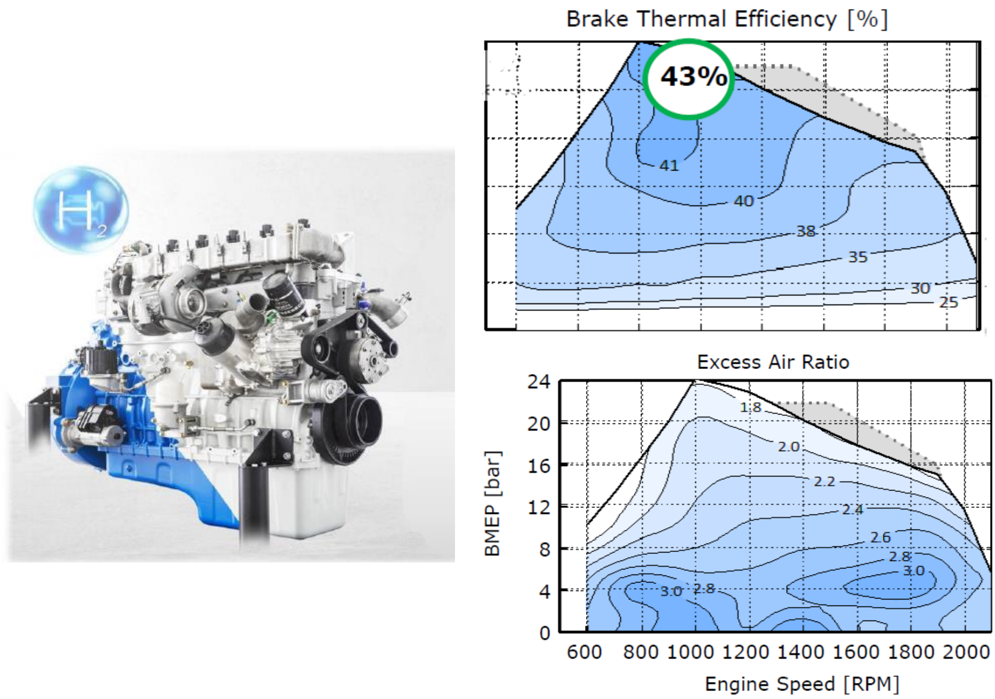

Figure 9 AVL HD H2 ICE demonstrator [69]

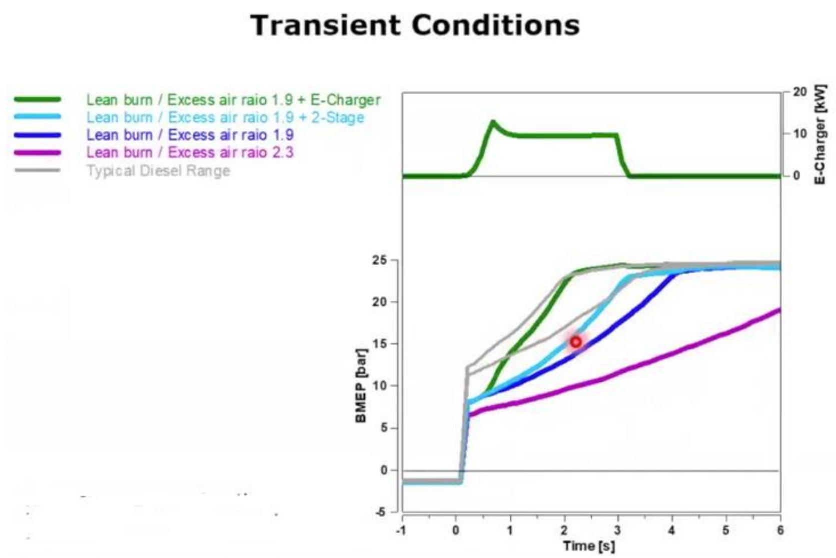

Figure 10 AVL HD H2 ICE demonstrator – air excess ratio dependable transient response and proposed solutions [69]

ICE Department of the Faculty of Mechanical Engineering of the University of Belgrade (UB FME ICED) recently (2023) upgraded its laboratory with a gaseous hydrogen supply facility and also started intensive research on controlling the modalities of the hydrogen combustion process on an adapted single-cylinder engine. The setup with a moderate high compression ratio gasoline-like engine in combination with high-pressure direct injection showed that efficiencies of 41% are achievable with the lean operation even without deep and thorough optimisation, signalling a lot of potential for extending efficiencies even higher.

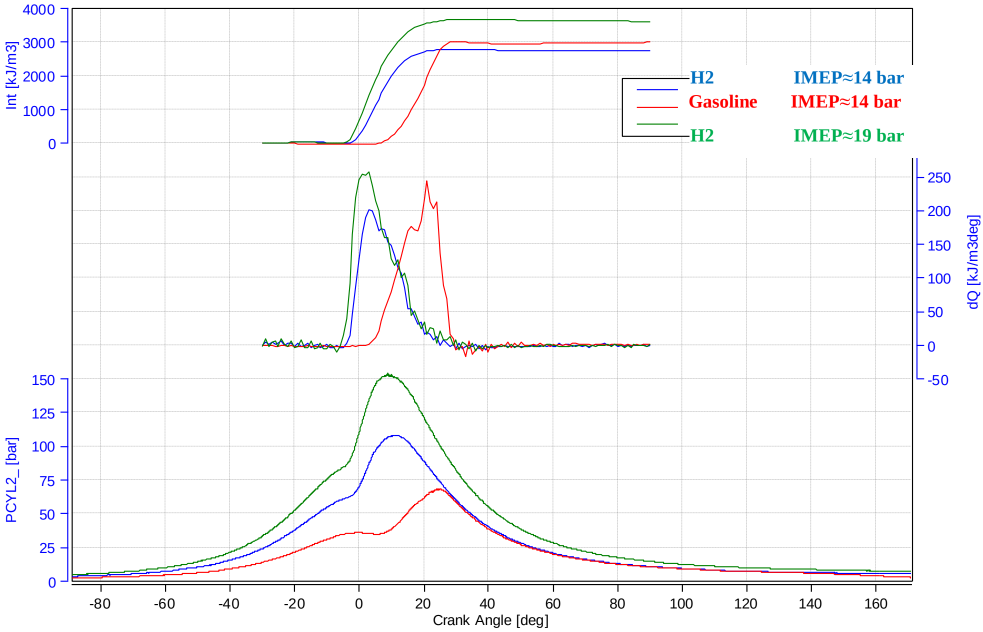

Figure 11 A comparison of H2 and gasoline ICE operation (CR=13.7, IMEP≈ 14 bar) @ UB FME ICED

Figure 11 presents a few ICE operation points measured at UB FME ICED Lab within a research area currently being conducted. Two operating points are selected for comparison – gasoline stoichiometric and lean H_2 operation with λ=2, both with high-pressure direct injection. Both operating points were conducted on a similar engine configuration (compression ratio 13.7) and at a similar load (≈14 bar IMEP). Clearly, the heat release rate and combustion speed of a lean hydrogen operation even outvies those of stoichiometric gasoline. While the spark advance of the gasoline operation has to be a result of a strong compromise toward the close knock limit (***Figure 12***), the spark advance of the lean hydrogen operation can be set at the optimal position for achieving high efficiencies i.e. MFB50 angular position for the gasoline operation is heavily retarded (MFB50=18 deg CA), while for H2 operation MFB50 can be positioned at 8 deg CA without any problem. Consequently, H2 operation easily achieves an efficiency of 40% - 7% higher than gasoline operation. Additionally, the third operational point shown is an operation on hydrogen on even higher loads (19 bar IMEP) with no evidence of irregular combustion and the same possibility for advancing the spark ignition for the best efficiency (achieved 41 %). Of course, lean operation on H2 required higher boosting pressures, i.e. 0.9 bar (relative) vs. 0.44 bar for stochiometric gasoline. At the same time, controllable and efficient, high loads with lean hydrogen operation can be achieved only at the expense of higher boosting pressure. A boosting pressure of 1.5 bar was needed for the highest load shown.

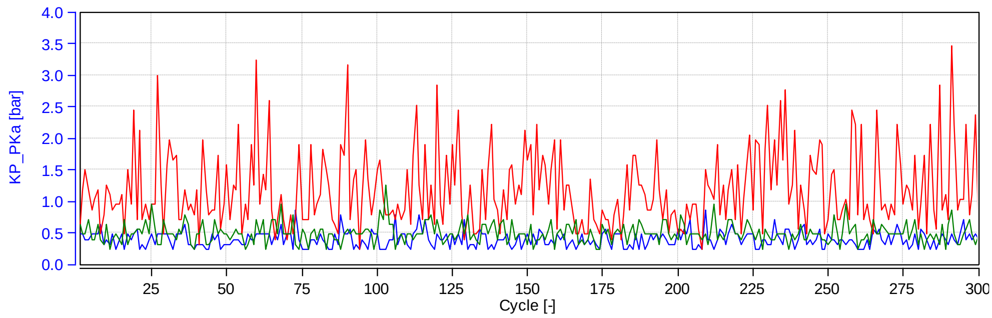

Figure 12 The maximum value of pressure deviation KP_PK (Knock Peak) for operating points from Figure 11

4 CONCLUSION

The ongoing EU Green Deal agenda implies that the IC engine has become obsolete. However, technological breakthroughs in achieving high efficiencies have positioned H2 ICE as a powertrain solution that has the potential to contribute significantly to the process of decarbonisation. Due to an onboard hydrogen storage limitation (still not efficiently solved), H2 ICE will likely not be seen as a part of the powertrain in LDVs in Europe beyond 2035. However, this is less likely to be the case in the rest of the world (particularly Japan).

In HDVs, H2 ICE is seen as a strong competitor to fuel cell-based powertrains, particularly in heavy trucks and non-road machinery powertrains.

It is also important to stress the fact that the production costs of a long-range battery vehicle are almost 2.5 times higher than those with a conventional ICE, which hugely influences the automotive industry's profit margin [85], [86]. This is also a significant motivating factor for the automotive industry to continue with the further development of ICE toward a viable, highly efficient powertrain solution that will be competitive enough in the upcoming decades.

ACKNOWLEDGMENTS

This research was supported by Ministry of Education, Science and Technological Development, Republic of Serbia, Grant no. 451-03-65/2024-03/200105

REFERENCES

[1] N. G. C. Change, “Global Surface Temperature | NASA Global Climate Change,” Climate Change: Vital Signs of the Planet. Accessed: Aug. 14, 2024. [Online]. Available: https://climate.nasa.gov/vital-signs/global-temperature?intent=121

[2] “First Assessment Report — IPCC.” Accessed: Aug. 14, 2024. [Online]. Available: https://www.ipcc.ch/assessment-report/ar1/

[3] V. Masson-Delmotte *et al.*, Eds., *Climate Change 2021: The Physical Science Basis. Contribution of Working Group I to the Sixth Assessment Report of the Intergovernmental Panel on Climate Change*. Cambridge, United Kingdom and New York, NY, USA: Cambridge University Press, 2021. doi: 10.1017/9781009157896.

[4] "Paleoclimatology: The Ice Core Record." Accessed: Aug. 14, 2024. [Online]. Available: https://earthobservatory.nasa.gov/features/Paleoclimatology_IceCores

[5] "CO2 Ice Core Data." Accessed: Aug. 14, 2024. [Online]. Available: https://www.co2.earth/co2-ice-core-data

[6] N. G. C. Change, "Carbon Dioxide Concentration | NASA Global Climate Change," Climate Change: Vital Signs of the Planet. Accessed: Aug. 14, 2024. [Online]. Available: https://climate.nasa.gov/vital-signs/carbon-dioxide?intent=121

[7] K. E. Trenberth, *The Changing Flow of Energy Through the Climate System*. Cambridge: Cambridge University Press, 2022. doi: 10.1017/9781108979030.

[8] H. D. Lightfoot and O. A. Mamer, "Back radiation versus CO2 as the cause of climate change," *Energy & Environment*, vol. 28, no. 7, pp. 661–672, Nov. 2017, doi: 10.1177/0958305X17722790.

[9] V. V. Zharkova, S. J. Shepherd, E. Popova, and S. I. Zharkov, "Heartbeat of the Sun from Principal Component Analysis and prediction of solar activity on a millenium timescale," *Sci Rep*, vol. 5, no. 1, p. 15689, Oct. 2015, doi: 10.1038/srep15689.

[10] V. Zharkova, "Millennial Oscillations of Solar Irradiance and Magnetic Field in 600–2600," in *Solar System Planets and Exoplanets*, J. Bevelacqua, Ed., Rijeka: IntechOpen, 2021. doi: 10.5772/intechopen.96450.

[11] V. V. Zharkova, S. J. Shepherd, S. I. Zharkov, and E. Popova, "Retraction Note: Oscillations of the baseline of solar magnetic field and solar irradiance on a millennial timescale," *Sci Rep*, vol. 10, no. 1, p. 4336, Mar. 2020, doi: 10.1038/s41598-020-61020-3.

[12] "History — IPCC." Accessed: Aug. 15, 2024. [Online]. Available: https://www.ipcc.ch/about/history/

[13] "The European Green Deal - European Commission." Accessed: Aug. 15, 2024. [Online]. Available: https://commission.europa.eu/strategy-and-policy/priorities-2019-2024/european-green-deal_en

[14] "EEA greenhouse gases — data viewer," European Environment Agency. Accessed: Aug. 15, 2024. [Online]. Available: https://www.eea.europa.eu/data-and-maps/data/data-viewers/greenhouse-gases-viewer

[15] "Delivering the European Green Deal - European Commission." Accessed: Aug. 15, 2024. [Online]. Available: https://commission.europa.eu/strategy-and-policy/priorities-2019-2024/european-green-deal/delivering-european-green-deal_en

[16] "Road transport: Reducing CO_2 emissions from vehicles - European Commission." Accessed: Aug. 16, 2024. [Online]. Available: https://climate.ec.europa.eu/eu-action/transport/road-transport-reducing-co2-emissions-vehicles_en

[17] *Regulation (EU) 2019/631 of the European Parliament and of the Council of 17 April 2019 setting CO2 emission performance standards for new passenger cars and for new light commercial vehicles, and repealing Regulations (EC) No 443/2009 and (EU) No 510/2011 (recast) (Text with EEA relevance)Text with EEA relevance*. 2023. Accessed: Aug. 16, 2024. [Online]. Available: http://data.europa.eu/eli/reg/2019/631/2023-09-05/eng

[18] *Regulation (EU) 2019/1242 of the European Parliament and of the Council of 20 June 2019 setting CO2 emission performance standards for new heavy-duty vehicles and amending Regulations (EC) No 595/2009 and (EU) 2018/956 of the European Parliament and of the Council and Council Directive 96/53/EC (Text with EEA relevance)*. 2024. Accessed: Aug. 16, 2024. [Online]. Available: http://data.europa.eu/eli/reg/2019/1242/2024-07-01/eng

[19] "Fit for 55: Delivering on the proposals - European Commission." Accessed: Aug. 16, 2024. [Online]. Available: https://commission.europa.eu/strategy-and-policy/priorities-2019-2024/european-green-deal/delivering-european-green-deal/fit-55-delivering-proposals_en

[20] "Renewable Energy Directive." Accessed: Aug. 17, 2024. [Online]. Available: https://energy.ec.europa.eu/topics/renewable-energy/renewable-energy-directive-targets-and-rules/renewable-energy-directive_en

[21] "European Union (EU27) | European Alternative Fuels Observatory." Accessed: Aug. 17, 2024. [Online]. Available: https://alternative-fuels-observatory.ec.europa.eu/transport-mode/road/european-union-eu27

[22] "Reports," Hydrogen Europe. Accessed: Aug. 11, 2024. [Online]. Available: https://hydrogeneurope.eu/in-a-nutshell/reports/

[23] "Press." Accessed: Aug. 18, 2024. [Online]. Available: https://www.solarisbus.com/en/press/solaris-in-the-booming-hydrogen-bus-market-2101

[24] S. Schemme *et al.*, "H2-based synthetic fuels: A techno-economic comparison of alcohol, ether and hydrocarbon production," *International Journal of Hydrogen Energy*, vol. 45, no. 8, pp. 5395–5414, Feb. 2020, doi: 10.1016/j.ijhydene.2019.05.028.

[25] S. Hänggi *et al.*, "A review of synthetic fuels for passenger vehicles," *Energy Reports*, vol. 5, pp. 555–569, Nov. 2019, doi: 10.1016/j.egyr.2019.04.007.

[26] K. Richter, F. Rost, and M. Schumacher, "Type Approval of H2 Engines," *87th GRPE Session*, Jan. 2023.

[27] "(WP.29/GRPE) Working Party on Pollution and Energy (87th session) | UNECE." Accessed: Aug. 18, 2024. [Online]. Available: https://unece.org/transport/events/wp29grpe-working-party-pollution-and-energy-87th-session

[28] "Vehicle Energy Consumption calculation TOol - VECTO - European Commission." Accessed: Aug. 18, 2024. [Online]. Available: https://climate.ec.europa.eu/eu-action/transport/road-transport-reducing-co2-emissions-vehicles/vehicle-energy-consumption-calculation-tool-vecto_en

[29] "H2-ICE Powertrain: can it be a serious long-term option for heavy-duty trucks? | AVL." Accessed: Aug. 18, 2024. [Online]. Available: https://www.avl.com/en/webinars/h2-ice-powertrain-can-it-be-a-serious-long-term-option-heavy-duty-trucks

[30] D. Mumford, S. Baker, and S. Munshi, "High Performance Hydrogen Engine Applications Using Westport Fuel Systems' Commercially Available HPDI Technology," presented at the 43rd International Vienna Motor Symposium, 2022.

[31] M. Barnard, "Hydrogen Fleets Are Much More Expensive To Maintain Than Battery & Even Diesel," CleanTechnica. Accessed: Aug. 15, 2024. [Online]. Available: https://cleantechnica.com/2024/01/26/hydrogen-fleets-are-much-more-expensive-to-maintain-than-battery-even-diesel/

[32] "FCMoveTM Spec Sheet." Accessed: Aug. 18, 2024. [Online]. Available: https://www.ballard.com/about-ballard/publication_library/product-specification-sheets/fcmovetm-spec-sheet

[33] P. Dimitriou and R. Javaid, "A review of ammonia as a compression ignition engine fuel," *International Journal of Hydrogen Energy*, vol. 45, no. 11, pp. 7098–7118, Feb. 2020, doi: 10.1016/j.ijhydene.2019.12.209.

[34] D. León, I. Amez, B. Castells, M. F. Ortega, and D. Bolonio, “Techno-economic analysis of the production of synthetic fuels using CO2 generated by the cement industry and green hydrogen,” *International Journal of Hydrogen Energy*, vol. 80, pp. 406–417, Aug. 2024, doi: 10.1016/j.ijhydene.2024.07.138.

[35] “Are battery electric vehicles the future? An uncertainty comparison with hydrogen and combustion engines,” *Environmental Innovation and Societal Transitions*, vol. 35, pp. 509–523, Jun. 2020, doi: 10.1016/j.eist.2019.03.003.

[36] K. Abnett and K. Abnett, “Biggest EU lawmaker group wants 2035 combustion car ban revised, draft shows,” *Reuters*, Jul. 02, 2024. Accessed: Aug. 21, 2024. [Online]. Available: https://www.reuters.com/business/autos-transportation/biggest-eu-lawmaker-group-wants-2035-combustion-car-ban-revised-draft-shows-2024-07-02/

[37] “Battery electric vehicles and fuel cell electric vehicles, an analysis of alternative powertrains as a mean to decarbonise the transport sector,” *Sustainable Energy Technologies and Assessments*, vol. 53, p. 102624, Oct. 2022, doi: 10.1016/j.seta.2022.102624.

[38] “Wärtsilä 31SG, the world’s most efficient 4-stroke engine,” Wartsila.com. Accessed: Aug. 21, 2024. [Online]. Available: https://www.wartsila.com/insights/article/wartsila-31sg-the-worlds-most-efficient-4-stroke-engine

[39] “Hydrogen Refuelling Infrastructure: Standardisation.” Hydrogen Energy Association, May 2024. [Online]. Available: https://energycentral.com/system/files/ece/nodes/674092/document_28.pdf

[40] J. Schneider, G. Dang-Nhu, and N. Hart, “ISO 19880-1, Hydrogen Fueling Station and Vehicle Interface Technical Specification,” *ECS Transactions*, vol. 71, pp. 155–172, Feb. 2016, doi: 10.1149/07101.0155ecst.

[41] V. Mattelaer, “H2 Fuelling Standards,” presented at the 8th HyTruck Breakfast Briefing, Apr. 03, 2024. [Online]. Available: https://interreg-baltic.eu/wp-content/uploads/2024/04/HyTruck-H2-Fuelling-Standards-Vincent-Mattelaer.pdf

[42] “PRHYDE,” Ludwig-Bölkow-Systemtechnik. Accessed: Aug. 25, 2024. [Online]. Available: https://lbst.de/prhyde/

[43] V. Mattelaer, “SAE J2601-5 HYDROGEN Heavy-Duty fuelling,” Dec. 01, 2023. [Online]. Available: https://cleanenergypartnership.de/wp-content/uploads/2023/12/CEP-SAE-J2601-5-Training-Session-Vincent-Mattelaer.pdf

[44] J. Keller and P. Benard, “Hydrogen Behavior – Myth Busting,” presented at the ICHS 2007, S. Sebastian Spain, Sep. 2007. Accessed: Aug. 24, 2024. [Online]. Available: https://conference.ing.unipi.it/ichs2007/indexb4cd.html?id=122

[45] C. L. Yaws and W. Braker, *Matheson gas data book*, 7th ed. Parsippany, NJ : New York: Matheson Tri-Gas ; McGraw-Hill, 2001.

[46] R. Ono, M. Nifuku, S. Fujiwara, S. Horiguchi, and T. Oda, “Minimum ignition energy of hydrogen–air mixture: Effects of humidity and spark duration,” *Journal of Electrostatics*, vol. 65, no. 2, pp. 87–93, Feb. 2007, doi: 10.1016/j.elstat.2006.07.004.

[47] C. J. R. Coronado *et al.*, “Flammability limits: A review with emphasis on ethanol for aeronautical applications and description of the experimental procedure,” *Journal of Hazardous Materials*, vol. 241–242, pp. 32–54, Nov. 2012, doi: 10.1016/j.jhazmat.2012.09.035.

[48] R. K. Eckhoff, M. Ngo, and W. Olsen, “On the minimum ignition energy (MIE) for propane/air,” *Journal of Hazardous Materials*, vol. 175, no. 1, pp. 293–297, Mar. 2010, doi: 10.1016/j.jhazmat.2009.09.162.

[49] C. LAFLEUR, “Large-Scale Hydrogen System Safety Issues.,” *Chemical Engineering Progress*, vol. 115, no. 8, pp. 42–46, Aug. 2019.

[50] H. Haase, *Electrostatic hazards: their evaluation and control*, Rev. ed., Adapted from the 2d German ed. Weinheim: Verlag Chemie, 1977.

[51] V. Babrauskas, *Ignition Handbook*. 2003.

[52] A. Glover, A. Baird, and C. LaFleur, “Hydrogen Fuel Cell Vehicles in Tunnels,” Sandia National Laboratories, SAND--2020-4507R, 1617268, 685771, Apr. 2020. doi: 10.2172/1617268.

[53] “National Hydrogen and Fuel Cell Emergency Response Training Resource | H2tools | Hydrogen Tools.” Accessed: Aug. 25, 2024. [Online]. Available: https://h2tools.org/national-hydrogen-and-fuel-cell-emergency-response-training-resource

[54] M. Fukuda, K. Korematsu, and M. Sakamoto, “On Quenching Distance of Mixtures of Methane and Hydrogen with Air,” *Bulletin of JSME*, vol. 24, no. 193, pp. 1192–1197, 1981, doi: 10.1299/jsme1958.24.1192.

[55] T. M. Cain, “Autoignition of hydrogen at high pressure,” *Combustion and Flame*, vol. 111, no. 1–2, pp. 124–132, Oct. 1997, doi: 10.1016/S0010-2180(97)00005-9.

[56] F. Poursadegh, M. Brear, B. Hayward, and Y. Yang, “Autoignition, knock, detonation and the octane rating of hydrogen,” *Fuel*, vol. 332, p. 126201, Jan. 2023, doi: 10.1016/j.fuel.2022.126201.

[57] P. G. Aleiferis and M. F. Rosati, “Controlled autoignition of hydrogen in a direct-injection optical engine,” *Combustion and Flame*, vol. 159, no. 7, pp. 2500–2515, Jul. 2012, doi: 10.1016/j.combustflame.2012.02.021.

[58] B. Raser and P. Kapus, “High Efficiency Hydrogen Internal Combustion Engine – Carbon-Free Powertrain for Passenger Car Hybrids and Commercial Vehicles,” presented at the 43rd International Vienna Motor Symposium, Vienna, Apr. 28, 2022.

[59] “LDI hydrogen injector | Liebherr.” Accessed: Sep. 03, 2024. [Online]. Available: https://www.liebherr.com/en/usa/products/components/injection-systems/injectors/product-highlights/ldi.html

[60] K. Wittek, V. Cogo, and G. Prante, “Development of a pneumatic actuated low-pressure direct injection gas injector for hydrogen-fueled internal combustion engines,” *International Journal of Hydrogen Energy*, vol. 48, no. 27, pp. 10215–10234, Mar. 2023, doi: 10.1016/j.ijhydene.2022.12.023.

[61] “Optimisation of hydrogen powered internal combustion engines (HYICE),” Feb. 2007. Accessed: Sep. 03, 2024. [Online]. Available: https://cordis.europa.eu/project/id/506604/reporting

[62] J. Caine, “The Development of a Hydrogen Race Engine,” UK, Feb. 28, 2024.

[63] “High-Pressure Direct-Injection Hydrogen Engine Achieves Efficiency of 42%; On Par with Turbodiesels,” Green Car Congress. Accessed: Sep. 08, 2024. [Online]. Available: https://www.greencarcongress.com/2009/03/high-pressure-d.html

[64] “Liebherr introduces H2 direct injection for heavy-duty combustion engines.” Accessed: Sep. 09, 2024. [Online]. Available: https://www.liebherr.com/en/ind/latest-news/news-press-releases/detail/liebherr-introduces-h2-direct-injection-for-heavy-duty-combustion-engines-conexpo.html

[65] D. Mumford, S. Ptucha, S. Baker, S. Munshi, A. Palmkvist, and E. Olofsson, “High Performance Hydrogen Engine Applications,” presented at the 44th International Vienna Motor Symposium, Vienna, 2023. [Online]. Available:

https://wfsinc.com/file_library/files/wfs-wfsinc/23-04-westport-h2-hpdi-vienna-motor-symposium.pdf

[66] "Commercial Hydrogen Engine with 50 % BTE | AVL." Accessed: Sep. 04, 2024. [Online]. Available: https://www.avl.com/en/expert-article/commercial-hydrogen-engine-50-bte

[67] S. Tanno, Y. Ito, R. Michikawauchi, M. Nakamura, and H. Tomita, "High-Efficiency and Low-NOx Hydrogen Combustion by High Pressure Direct Injection," *SAE International Journal of Engines*, vol. 3, no. 2, pp. 259–268, 2010.

[68] H. Eichlseder, C. Spuller, R. Heindl, F. Gerbig, and K. Heller, "Concepts for diesel-like hydrogen combustion," *MTZ Worldw*, vol. 71, no. 1, pp. 46–51, Jan. 2010, doi: 10.1007/BF03227001.

[69] B. Raser, M. Wieser, and F. Grabner, "CO2 reduction in commercial vehicles – the AVL hydrogen engine | AVL," AVL, Mar. 02, 2021. Accessed: Sep. 09, 2024. [Online]. Available: https://www.avl.com/en/webinars/co2-reduction-commercial-vehicles-avl-hydrogen-engine

[70] F. Ricci, J. Zembi, M. Avana, C. N. Grimaldi, M. Battistoni, and S. Papi, "Analysis of Hydrogen Combustion in a Spark Ignition Research Engine with a Barrier Discharge Igniter," *Energies*, vol. 17, no. 7, Art. no. 7, Jan. 2024, doi: 10.3390/en17071739.

[71] Y. B. Zeldovich, *Selected Works of Yakov Borisovich Zeldovich, Volume I: Chemical Physics and Hydrodynanics*. Princeton University Press, 1992. doi: 10.1515/9781400862979.

[72] V. Y. Prikhodko, J. E. Parks, J. A. Pihl, and T. J. Toops, "Passive SCR for lean gasoline NOX control: Engine-based strategies to minimize fuel penalty associated with catalytic NH3 generation," *Catalysis Today*, vol. 267, pp. 202–209, Jun. 2016, doi: 10.1016/j.cattod.2016.01.026.

[73] "Effects of including a NOx storage component on a TWC when using a lean spark ignition gasoline engine combined with a passive SCR system☆," *Applications in Energy and Combustion Science*, vol. 14, p. 100150, Jun. 2023, doi: 10.1016/j.jaecs.2023.100150.

[74] "Systemvergleich zwischen Wasserstoffverbrennungsmotor und Brennstoffzelle im schweren Nutzfahrzeug," e-mobil BW GmbH, Jul. 2021.

[75] A. Boretti, "Hydrogen internal combustion engines to 2030," *International Journal of Hydrogen Energy*, vol. 45, no. 43, pp. 23692–23703, Sep. 2020, doi: 10.1016/j.ijhydene.2020.06.022.

[76] S. Verhelst and T. Wallner, "Hydrogen-fueled internal combustion engines," *Progress in Energy and Combustion Science*, vol. 35, no. 6, pp. 490–527, Dec. 2009, doi: 10.1016/j.pecs.2009.08.001.

[77] "BMW INTRODUCES WORLD'S FIRST HYDROGEN-DRIVE LUXURY PERFORMANCE CAR FOR EVERYDAY USE - THE BMW HYDROGEN 7." Accessed: Sep. 05, 2024. [Online]. Available: https://www.press.bmwgroup.com/global/article/detail/T0012215EN/bmw-introduces-world-s-first-hydrogen-drive-luxury-performance-car-for-everyday-use-the-bmw-hydrogen-7?language=en

[78] T. Wallner *et al.*, "Fuel economy and emissions evaluation of BMW Hydrogen 7 Mono-Fuel demonstration vehicles," *International Journal of Hydrogen Energy*, vol. 33, no. 24, pp. 7607–7618, 2008, doi: https://doi.org/10.1016/j.ijhydene.2008.08.067.

[79] W. Enke, M. Gruber, L. Hecht, and B. Staar, "The Bi-fuel V12 engine of the new BMW Hydrogen 7," *MTZ Worldw*, vol. 68, no. 6, pp. 6–9, Jun. 2007, doi: 10.1007/BF03226832.

[80] "BMW HYDROGEN ENGINE REACHES TOP LEVEL EFFICIENCY." Accessed: Sep. 08, 2024. [Online]. Available: https://www.press.bmwgroup.com/usa/article/detail/T0020216EN_US/bmw-hydrogen-engine-reaches-top-level-efficiency?language=en_US

[81] "Hydrogen for clean urban transport in Europe | HYFLEET:CUTE Project | Results | FP6," CORDIS | European Commission. Accessed: Sep. 08, 2024. [Online]. Available: https://cordis.europa.eu/project/id/19991/results

[82] L. King, "Why BMW will not go back on the hydrogen engine," H2Today. Accessed: Sep. 08, 2024. [Online]. Available: https://hydrogentoday.info/en/bmw-hydrogen-engine/

[83] T. M. CORPORATION, "Evolved Liquid Hydrogen-Powered GR Corolla to Participate in Super Taikyu Fuji 24 Hours Race | Corporate | Global Newsroom," Toyota Motor Corporation Official Global Website. Accessed: Sep. 08, 2024. [Online]. Available: https://global.toyota/en/newsroom/corporate/40849748.html

[84] "Hydrogen is developing fast in Japan, closer to societal use," World Economic Forum. Accessed: Sep. 09, 2024. [Online]. Available: https://www.weforum.org/agenda/2024/04/hydrogen-japan/

[85] "The AlixPartners Global Automotive Outlook 2019." Accessed: Sep. 09, 2024. [Online]. Available: https://www.alixpartners.com/newsroom/alixpartners-global-automotive-industry-outlook-2019/

[86] "Automotive Engineering - July/August 2019." Accessed: Sep. 09, 2024. [Online]. Available: https://www.nxtbook.com/nxtbooks/sae/19AUTP08/index.php#/p/Intro

Intentionally blank

MOBILITY & VEHICLE MECHANICS

https://doi.org/10.24874/mvm.2026.52.01.02
UDC: 629.33.015.3:534.1:62-752

A CONTRIBUTION TO THE STUDY OF THERMAL LOADS CAUSED BY VERTICAL OSCILLATORY EXCITATIONS IN PASSENGER VEHICLES WITH CONVENTIONAL AND ELECTRIC POWERTRAINS IN THE CONCEPTUAL DESIGN PHASE

Miroslav Demić [1]*

Received in January 2026 *Accepted in March 2026*
ORIGINAL SCIENTIFIC ARTICLE

ABSTRACT: This paper analyses the thermal loading of damping elements in passenger vehicles caused by vertical oscillatory excitations for both conventional internal combustion engine (ICE) powertrains and electric powertrains (EM). A simplified oscillatory model with three lumped masses is applied, comprising the unsprung mass, the sprung mass, and the powertrain mass. The excitations originate from road micro-irregularities and from inertial forces of the power unit, for which representative analytical models are adopted for both powertrain types.

By numerically solving a system of nonlinear differential equations, relative velocities and forces in the damping elements are obtained, on the basis of which the dissipated mechanical energy, i.e. thermal power, is calculated. For comparative analysis, RMS values of thermal power are used, together with frequency-domain analysis employing partial coherence functions.

The results show that thermal loads are highest in the tyres and lowest in the powertrain mounts. In the case of electric powertrains, lower thermal loads are observed in the suspension damping elements and powertrain mounts, whereas in vehicles with conventional powertrains lower loads occur in the tyres. It is concluded that the energy aspect of oscillatory processes represents an important design criterion in the conceptual vehicle design phase.

KEY WORDS: *passenger vehicle, powertrain type, oscillatory model, thermal loads*

[1]*Miroslav Demić, Faculty of engineering University of Kragujevac, Sestre Janjić 6, Kragujevac, Serbia, Advisor at the Centre for Research and Development Activities in the Automotive Industry (CIRD), Belgrade, demic@kg.ac.rs , https://orcid.org/0000-0003-2168-1370, (*Corresponding author)*

PRILOG ISRAŽIVANJU TOPLOTNIH OPTEREĆENJA IZAZVANIH VERTIKALNIM OSCILATORNIM POBUDAMA KOD KLASIČNOG I ELEKTROPOGONA PUTNIČKIH MOTORNIH VOZILA U FAZI IDEJNOG PROJEKTOVANJA

REZIME: U radu je analizirano toplotno opterećenje prigušnih elemenata putničkog motornog vozila izazvano vertikalnim oscilatornim pobudama kod klasičnog pogona sa motorom sa unutrašnjim sagorevanjem i kod elektropogona. Primenjen je pojednostavljen oscilatorni model sa tri koncentrisane mase, koji obuhvata neoslonjenu masu, oslonjenu masu i masu pogonske grupe. Pobude potiču od mikroneravnina puta i od inercijalnih sila pogonskog agregata, pri čemu su za oba tipa pogona usvojeni reprezentativni analitički modeli.

Numeričkim rešavanjem nelinearnih diferencijalnih jednačina određene su relativne brzine i sile u prigušnim elementima, na osnovu kojih je izračunata disipirana mehanička energija, odnosno toplotna snaga. Radi uporedne analize korišćene su RMS vrednosti toplotne snage, kao i analiza u frekventnoj oblasti primenom parcijalnih funkcija koherenci.

Rezultati pokazuju da su toplotna opterećenja najveća u pneumaticima, a najmanja u osloncima pogonske grupe. Kod elektropogona uočena su manja toplotna opterećenja prigušnih elemenata sistema za oslanjanje i oslonaca pogonske grupe, dok su kod klasičnog pogona manja opterećenja u pneumaticima. Zaključeno je da energetski aspekt oscilatornih procesa predstavlja značajan kriterijum u fazi idejnog projektovanja vozila.

KLJUČNE REČI: *Putničko motorno vozilo, vrsta pogona, oscilatorni model, toplotna opterećenja*

A CONTRIBUTION TO THE STUDY OF THERMAL LOADS CAUSED BY VERTICAL OSCILLATORY EXCITATIONS IN PASSENGER VEHICLES WITH CONVENTIONAL AND ELECTRIC POWERTRAINS IN THE CONCEPTUAL DESIGN PHASE

Miroslav Demić

INTRODUCTION

Oscillatory motions are an inevitable phenomenon in the dynamic systems of passenger vehicles and occur as a consequence of various internal and external excitations [1–6]. They have a pronounced negative impact on ride comfort and occupant health, increase dynamic loads on structural components, and accelerate material fatigue, ultimately leading to reduced system reliability and service life [4]. Therefore, the analysis of oscillatory processes represents one of the key tasks in the design and optimisation of vehicle suspension systems and powertrain assemblies [7].

In the existing literature, this problem has been extensively investigated from the standpoint of dynamic stability, vibration comfort, mass distribution, and transmission of oscillations from the powertrain and the road to the vehicle body [1–7]. Special attention has been devoted to modelling vehicles as multi-mass oscillatory systems, where, depending on the level of detail, models with two or three lumped masses are frequently used. However, relatively few studies systematically address the energy aspect of oscillatory processes, i.e. the transformation of mechanical work into thermal energy due to damping.

It is well known that the presence of damping elements in a system leads to energy dissipation, whereby the mechanical work generated by oscillatory motion is converted into heat. This phenomenon results in local and global thermal loads of damping elements and adjacent structural components. Elevated temperature affects the mechanical and rheological properties of materials, degrades damping characteristics, and may cause accelerated ageing and potential component failure.

For oscillatory processes of stochastic and nonlinear nature, the RMS value of dissipated thermal power represents a physically meaningful indicator of the effective energetic intensity of damping, and is therefore suitable for comparative assessment of different powertrain concepts.

It is particularly interesting to analyse these effects in passenger vehicles with different powertrain types, such as vehicles with conventional internal combustion engines and those with electric powertrains. These concepts differ significantly in the nature and spectral content of oscillatory excitations, the level of unbalanced masses, and the manner in which dynamic forces are transmitted to the suspension system. In this respect, the application of a three-mass oscillatory model enables the interaction between the powertrain, suspension, and vehicle body to be examined, as well as the quantification of the associated thermal loads in the conceptual design phase.

The objective of this study is to quantitatively assess the thermal loads of damping elements caused by vertical oscillatory excitations during the conceptual design phase of a passenger vehicle and to perform a comparative analysis of vehicles with conventional and electric powertrains. Particular emphasis is placed on the energy aspect of oscillatory processes, namely the transformation of mechanical work resulting from relative motion into thermal energy dissipated in the damping elements.

Unlike most existing studies that primarily focus on vibration comfort, stability, and oscillation transmission [1–7], this paper employs dissipated thermal power as the principal criterion for comparing different powertrain concepts. By applying a nonlinear oscillatory model and analysing the system response in both the time and frequency domains, it is possible to separate the contributions of road micro-irregularities and powertrain excitations to the overall energy response of the system.

The contribution of this work lies in introducing the thermal load of damping elements as an additional design criterion when selecting a powertrain concept and dimensioning suspension systems and powertrain mounts, particularly in the early stages of vehicle development when many design parameters are still unknown.

Unlike conventional analyses based on accelerations, forces, or RMS displacement values, this study uses the thermal power dissipated in damping elements as the primary comparison criterion, as it directly reflects the energetic intensity of oscillatory processes.

1 METHOD

The aim of this study is to investigate, based on the analysis of oscillatory processes in the adopted dynamic model, the thermal loads arising from damping in both conventional and electric powertrains, and to highlight their influence on the operational characteristics and reliability of the system.

For the analysis of thermal loads caused by oscillatory processes, a simplified dynamic model of a passenger vehicle with three lumped masses is employed [3,4]. The use of such a model is considered justified and useful, given that the subject of investigation is primarily vertical vibrations and that all initial structural and material parameters of the system are known for the selected model. The three-mass model represents an acceptable compromise between realistic representation of vehicle dynamics and numerical complexity.

The method is applied to a passenger vehicle with a total mass of approximately 2 t, considered in two powertrain configurations: an internal combustion engine (ICE) and an electric powertrain (EM). The following masses are included in the model:

- unsprung mass, comprising the wheel, tyre, part of the axle, and associated suspension components,
- sprung mass, representing the vehicle body together with payload and passengers,
- powertrain mass, which for ICE vehicles includes the engine, gearbox, clutch, and associated structural components, while for electric vehicles it includes the electric motor, inverter, reduction gear, and related elements.

Vertical oscillations resulting from road micro-irregularities and inertial vertical excitations originating from the powertrain are considered. These excitations differ in character and intensity between ICE and electric powertrains, as discussed later.

Using dynamic simulation based on the system of differential equations of motion, time histories of vertical displacements, velocities, and accelerations of the unsprung mass, sprung mass, and powertrain mass are obtained. Particular attention is paid to relative motions between the masses, which are directly relevant to the operation of damping elements.

Based on the obtained relative forces and relative velocities in the damping elements, the mechanical work dissipated by damping, i.e. the corresponding thermal power, is calculated using the first law of thermodynamics [8,9]. This enables quantification of the thermal loads resulting from oscillatory processes in the system.

Given that the oscillatory excitations are of random or polyharmonic nature, comparison of different powertrain configurations is most appropriately carried out using RMS (root mean square) values of the calculated thermal power. The results are presented in tabular form and serve as a basis for comparative analysis of conventional and electric powertrains.

In addition to time-domain analysis, frequency-domain analysis is also performed. This includes calculation of ordinary coherence functions between excitations arising from road micro-irregularities and inertial vertical forces of the powertrain, with the aim of assessing the degree of linear dependence between excitation signals in different frequency ranges.

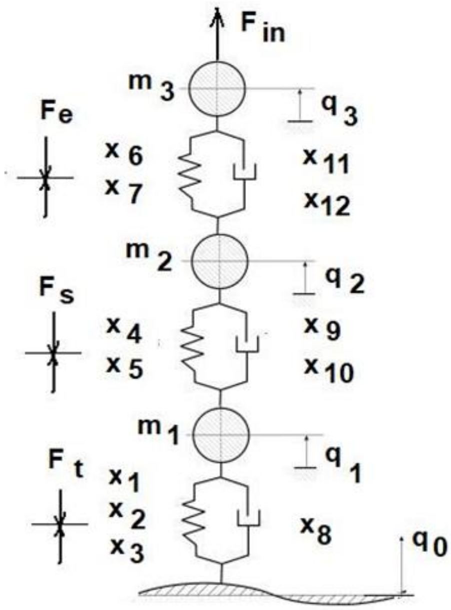

Figure 1. Oscillatory model of the passenger vehicle used

1.1 Mathematical model for the analysis of vertical vehicle oscillations

A large number of vehicle oscillatory models of different levels of complexity are available in the literature [1–7]. When selecting an appropriate model, it is necessary to use only the structure that can provide a reliable answer to the defined research problem. The application of models more complex than minimally required is not recommended, since such models require a large number of oscillatory parameters that are often not experimentally verified or are burdened with significant uncertainties [10].

Considering that in this study it is necessary to analyse the thermal power dissipated in damping elements for passenger vehicles equipped with an internal combustion engine (ICE) as well as with an electric motor, a three-degree-of-freedom model was assessed as an appropriate compromise between simplicity and physical representativeness. The adopted model is shown in Figure 1 and includes vertical oscillations of the sprung mass, the unsprung mass, and the powertrain mass.

Since models of this type have been described in detail in the available literature [4], only the basic relational expressions required for the formulation of the equations of motion are presented here. For clarity, the expressions are given in expanded rather than compact form.

With reference to Figure 1, the relative deformations and relative velocities of the elastic–damping elements are defined as:

$$\begin{aligned} D_1 &= q_1 - q_0 \quad & \dot{D}_1 &= \dot{q}_1 - \dot{q}_0 \\ D_2 &= q_2 - q_1 \quad & \dot{D}_2 &= \dot{q}_2 - \dot{q}_1 , \\ D_3 &= q_3 - q_2 \quad & \dot{D}_3 &= \dot{q}_3 - \dot{q}_2 \end{aligned} \tag{1}$$

where:

• q_i, $\dot{q}_i$ - denote the corresponding vertical displacements and velocities of the considered masses.

The forces in the elastic–damping elements are given by [4]:

$$\begin{aligned} F_1 &= x_1 D_1 + x_2 D_1^2 + x_3 D_1^2 + x_8 D_1 \\ F_2 &= x_4 D_2^3 + x_5 D_2^3 + x_9 \dot{D}_2 + x_{10} \dot{D}_2^2 Sign(\dot{D}_2) \ , \\ F_3 &= x_6 D_3 + x_7 D_3^3 + x_{11} \dot{D}_3 + x_{12} \dot{D}_3^2 Sign(\dot{D}_3) \end{aligned} \tag{2}$$

where:

•x_1........x_{12} are the corresponding oscillatory parameters, expressed in such units that multiplication by the relative deformation or relative velocity yields force in newtons (N).

Based on the adopted model (Figure 1) and applying Newton's laws, the differential equations of motion for each of the three masses can be written as:

$$\begin{aligned} m_1 \ddot{q}_1 &= F_2 - F_1 \\ m_2 \ddot{q}_2 &= F_3 - F_2 \ , \\ m_3 \ddot{q}_3 &= F_{in} - F_3 \end{aligned} \tag{3}$$

where F_{in} represents the vertical oscillatory excitation generated by the operation of the ICE or the electric motor, originating from unbalanced masses, electromagnetic forces, or periodic inertial effects of the powertrain.

Considering the stochastic nature of excitations caused by road micro-irregularities, the deterministic–periodic character of powertrain excitations, and the pronounced nonlinearity of forces in the elastic–damping elements, the equations of motion cannot be solved analytically. Therefore, the system of differential equations is solved numerically, using the fourth-order Runge–Kutta method.

For numerical integration, the system of second-order differential equations is transformed into an equivalent system of nonlinear first-order differential equations, which is a standard procedure and will not be discussed further here. Since the equations of motion include excitations from inertial forces and road micro-irregularities, these will be briefly described below.

1.2 Inertial forces of the internal combustion engine

In this study, a four-cylinder inline internal combustion engine is considered. In an ideal case, the primary inertial forces cancel each other, while the secondary components remain unbalanced and represent a significant source of vertical oscillatory excitations in the vehicle system, especially in the low- and mid-frequency ranges [11].

As is well known from the classical theory of slider–crank mechanism dynamics, such engines generate unbalanced inertial forces resulting from the reciprocating linear motion of the piston–connecting rod assembly [11]:

$$F_{in} = 4 m_k r \omega^2 \lambda \cos(2\omega t), \tag{4}$$

where:

- m_k - is the piston mass together with the associated portion of the connecting rod mass,
- r – is the crank radius,
- ω - is the angular speed of the crankshaft, and
- λ - is the ratio of the crank radius to the connecting rod length. ($\lambda = \frac{r}{l}$).

1.3 Excitations generated by the electric motor

Unlike internal combustion engines, electric motors do not include masses undergoing linear motion; however, oscillatory excitations occur due to [12]:

- unbalanced rotor masses (mechanical eccentricity),
- non-uniform air gap between rotor and stator,
- spatial and temporal harmonics of the electromagnetic field, and
- sideband components in the spectrum resulting from the interaction between eccentricity and the electromagnetic field.

The total excitation force of an electric motor is predominantly radial, and its vertical component acts directly on the vehicle structure through the motor mounts.

Based on available experimental and analytical results, the vertical excitation force of an electric motor can be approximated by [12]:

$$F_{in} = k_r \sum_{1}^{p\max} \varepsilon_p \frac{P_e}{\omega} \sin\left(p\omega t + \varphi_p\right), \tag{5}$$

- where:
- P_e – is the electric motor power (W),
- k_r – is the coefficient transforming tangential force into radial force (in this study, represents an effective energetic coefficient transforming electromagnetic torque into a radial excitation force),
- ω - is the rotor angular speed,
- p – is the harmonic order,
- p=1 – corresponds to the harmonic describing mechanical eccentricity,
- p=2,3, – correspond to harmonics originating from the electromagnetic field and sidebands,

- ε_p - are coefficients describing spatial and temporal harmonics of the electromagnetic field,
- φ_p – are phase angles of individual harmonics.

Expression (5) represents an energetic approximation, where the electromagnetic torque is transformed into an effective radial excitation force via the coefficient. It should be noted that k_r is not a universal constant but a combined coefficient that includes:

- electric motor geometry,
- pole–slot combination,
- air-gap non-uniformity, and
- motor mounting configuration.

Based on experimental data and [12], k_r≈0.02–0.08 can be adopted, while the most commonly used representative value in analytical models is k_r=0.05. It should be emphasized that the coefficient k_r is not intended to represent a direct physical constant, but rather an effective energetic transformation coefficient suitable for conceptual-level analysis.

The number of poles in electric motors used in passenger vehicles typically ranges from 6 to 8, which leads to dominant excitations in the mid- and high-frequency range (above 100 Hz). Compared to ICE engines, force amplitudes are usually smaller, but frequencies are significantly higher, which has important consequences for the vibro-acoustic behaviour of the vehicle.

Empirical data indicate that the maximum radial excitation of an electric motor is typically within:

$$F_{in\max} \approx (0,5 \div 2)\% G_{mot} ,$$

where G_{mot} is the weight of the electric motor.

In the following analysis, only the dominant harmonics p=1,2,3 are considered, with coefficients describing the intensity of mechanical and electromagnetic asymmetries.

Empirical data [12]: $n \leq 1200\text{min}^{-1}$, ε_1=0,01-0,03, ε_2=0,005-0,02. ε_3=0,002-0,01, are adopted data for analysis [12]: P_e=150000W, ε_1=0,02, ε_2=0,01, ε_3=0,005

1.4 Oscillatory excitations due to road micro-irregularities

Numerous data on road micro-irregularities are available in the literature, most of which are based on power spectral density definitions, which prevents the direct application of the inverse Fourier transform to determine the time-domain excitation function [4]. Therefore, this study adopts and briefly describes a procedure for defining the excitation time function according to [4].

The excitation function is assumed to be of the following form:

$$q_0(t) = \sum_{1}^{N} A(f) \sin\left[2\pi ft + \varepsilon(f)\right], \tag{6}$$

In this study, a polyharmonic excitation function with 83 harmonics distributed over the frequency range from 0.05 to 500, Hz is used.

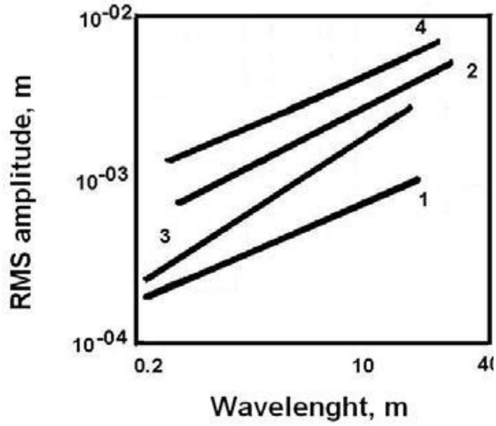

Figure 2. Limit values of road roughness (1 – modern road, 2 – road with poor concrete surface, 3 – repaired asphalt road, 4 – city street in good condition)

Based on Figure 2 [4], the following relation can be written:

$$A(f) = (A_o + B_o f)/v, \tag{7}$$

In the absence of more precise data, the phase angle is defined by:

$$\varepsilon(f) = 2\pi(rnd - 0.5), \tag{8}$$

where *rnd* denotes a set of random numbers uniformly distributed in the interval {0, 1}.

1.5 Thermal Loading of Damping Elements

The mechanical work generated in damping elements due to the action of relative velocities and damping forces is completely dissipated in the form of heat. The instantaneous dissipated power in a damping element is equal to the product of the damping force and the relative velocity between the connected masses. Since the damping force is a function of the relative velocity, the dissipated power exhibits a pronounced nonlinear character and directly depends on the oscillatory regime of the system.

The total thermal power generated in the damping elements represents the time integral of the instantaneous dissipated power and can be used as a quantitative measure of energy losses in the suspension system and powertrain mounts. This approach enables a direct connection between the dynamic behavior of the vehicle and the thermal loading of damping elements, which is of particular importance when comparing conventional and electric powertrains.

In the present case, the thermal power was calculated using the following expression:

$$P_t = F_{vrel} v_{rel}, \tag{9}$$

where:

- F_{vrel} - is the damping force in the corresponding damping element, and
- v_{rel} – is the corresponding relative velocity calculated using Eq. (1).

Considering the nature of the solutions of the differential equations (expressions 1-9), it is evident that the thermal power is also of a stochastic character, which will be discussed later.

Since the instantaneous thermal power exhibits a pronounced quasi-random character due to the stochastic nature of road excitations and nonlinear damping, RMS values were adopted as a representative measure of the effective thermal loading of individual damping elements.

2 DYNAMIC SIMULATION

The system of differential equations describing the oscillations of the observed passenger vehicle was solved numerically using the fourth-order Runge–Kutta method. For comparison purposes, both the internal combustion engine (ICE) and the electric motor (EM) were assumed to have a rated power of 150, kW and to operate at 1500, rpm under steady vehicle motion. It should be noted that this represents a simplified operating condition, particularly for electric vehicles, since power recuperation and similar effects were not considered.

During the conceptual design phase of a vehicle, many parameters are not precisely known-therefore, approximate relationships are commonly used. The mass of the powertrain can be related to the rated power of the propulsion unit. For ICE-driven vehicles, the ratio of maximum power to powertrain mass (engine, gearbox, clutch, and part of the driveline) typically ranges from 0.3 to 0.6, kW/kg, whereas for electric powertrains (electric motor, inverter, reducer) this ratio is significantly higher, ranging from 1.5 to 3, kW/kg. These relationships allow the estimation of the powertrain mass

In addition, empirical relations exist between the powertrain mass and the total vehicle mass. For ICE vehicles, the powertrain mass accounts for approximately 18 to 25,% of the total vehicle mass, while for electric vehicles this share is typically 8 to 12% (the battery is not included; in practice, the sprung mass of electric vehicles is usually 30 to 40% higher than in ICE vehicles).

In the present study, the inertial parameters listed in Table 1 were adopted.

Table 1. Inertial parameters of the analyzed vehicle

Powertrain type	m_1, kg	m_2, kg	m_3, kg
ICE	80	1600	375
EM	90	2150	75

For comparison purposes, it was considered appropriate to assume identical elasto-damping element properties for both powertrain types. These parameters are listed in Table 2.

Table 2. Characteristics of elasto-damping elements

Parameter	Value
x_1, N/m	$2*10^5$
x_2, N/m^2	$1*10^5$
x_3, N/m^3	$1*10^5$
x_4, N/m	$3*10^5$
x_5, N/m^3	$1*10^5$
x_6, N/m	$8*10^4$
x_7, N/m^3	$8*10^4$
x_8, Ns/m	$8*10^3$

x_9, Ns/m	$7*10^3$
x_{10}, Ns^2/m^2	$7*10^3$
x_{11}, Ns/m	$8*10^3$
x_{12}, Ns^2/m^2	$8*10^3$

In addition to these parameters, an equivalent piston mass of 1, kg was used for the ICE. An eight-pole electric motor was considered with the following parameters: ε_1=0,01; ε_2=0,01 ε_3=0,01, k_r=0,1.

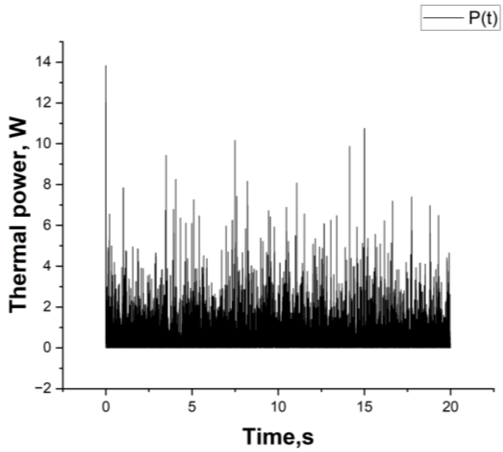

Figure 3. Time history of thermal power dissipated in the powertrain mounting damper of an electric vehicle

Numerical integration was performed using 20000 time steps with a time increment of 0.001, s, ensuring reliable analysis in the frequency range from 0.05 to 500, Hz [13]. This range covers the oscillations of the considered lumped masses, excitations due to road micro-roughness, and vertical excitations originating from both ICE and electric motors.

Based on the calculated relative velocities, the thermal power was determined using expression (1-9) for all damping elements of the vehicle and for both powertrain types. For illustration purposes, Figure 3 shows the time variation of the thermal power dissipated in the powertrain damper of the electric vehicle.

Analysis of all obtained time histories indicated that they are of a quasi-random nature. Therefore, for further analysis, RMS values were calculated and are presented in Table 3.

Table 3. RMS thermal power

	ICE - RMS, W	EM - RMS, W
Tire	3525741.6	3611390.5
Suspension system	42334.7	32103.5
Power train mounting	3.429	1.070

For more detailed analysis, it was considered appropriate to apply an approach commonly used in automatic control theory [14,15]. The oscillatory model was treated as a system with two inputs (road micro-roughness excitation and inertial force of the powertrain) and three outputs (thermal power in the tires, suspension system, and powertrain mounts), as illustrated in Figure 4a.

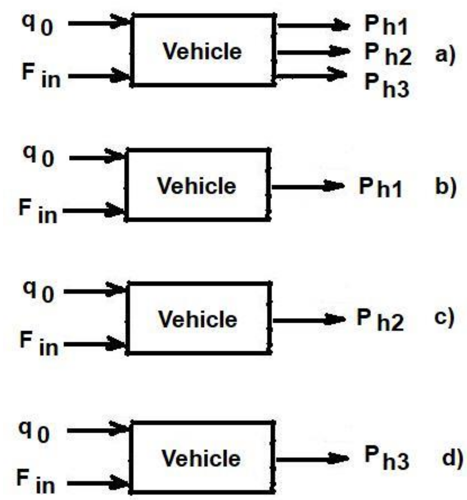

Figure 4. MIMO system (a) and its transformation into MISO systems (b, c, and d)

Such systems are known as multi-input multi-output (MIMO) systems [14,15]. They are analyzed by transforming them into multi-input single-output (MISO) systems (Figures 4b–4d), under the condition that the input signals are mutually independent. To verify this condition, the ordinary coherence function between the two analyzed inputs (F_{in} , q_0), was calculated. The obtained results are shown in Figure 5.

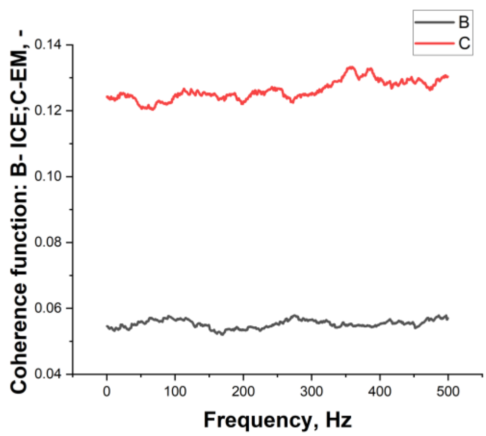

Figure 5. Ordinary coherence functions of the input signals: road micro-roughness excitation and vertical component of the powertrain inertial force; B – ICE, C – EM

Analysis of Figure 5, shows that the ordinary coherence function is approximately 0.06 for the ICE and about 0.13 for the electric motor. Both values are well below 0.3, which is commonly considered the lower threshold for significant frequency-dependent energetic coupling between input signals [13]. This indicates that signal decoupling is not required.

Based on the adopted MIMO approach, partial coherence functions were calculated, enabling a more reliable assessment of the influence of individual excitations on the system responses in the presence of multiple simultaneous inputs. This approach allows clearer separation of the contributions of road micro-roughness and powertrain inertial excitations to the overall dynamic and energetic response of the system.

Accordingly, partial coherence functions were calculated using a custom program developed in Dev Pascal. The results are shown in Figures 6–11.

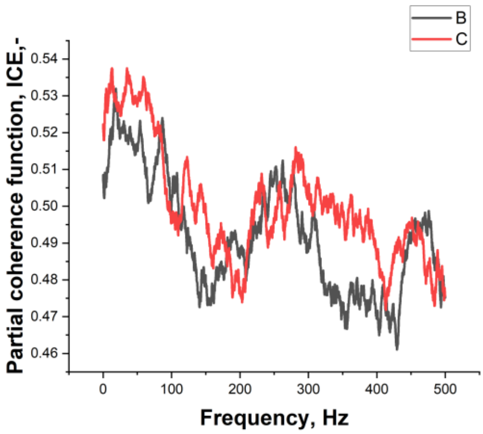

Figure 6. Partial coherence functions for the tire in ICE-driven vehicles: B – powertrain inertial forces, C – road micro-roughness

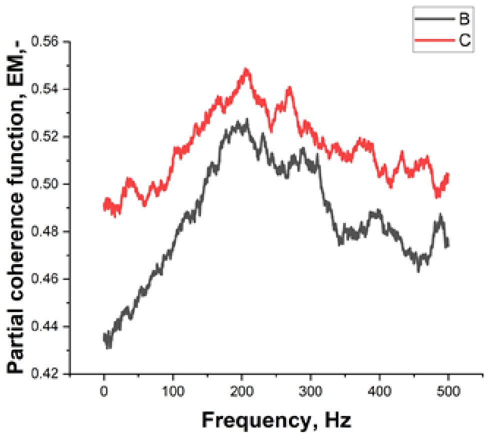

Figure 7. Partial coherence functions for the tire in EM-driven vehicles: B – powertrain inertial forces, C – road micro-roughness

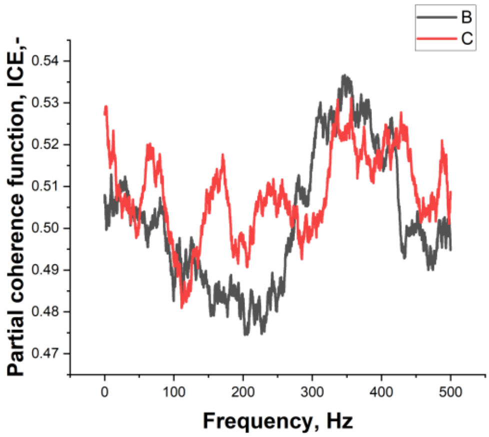

Figure 8. Partial coherence functions for the suspension system in ICE-driven vehicles: B – powertrain inertial forces, C – road micro-roughness

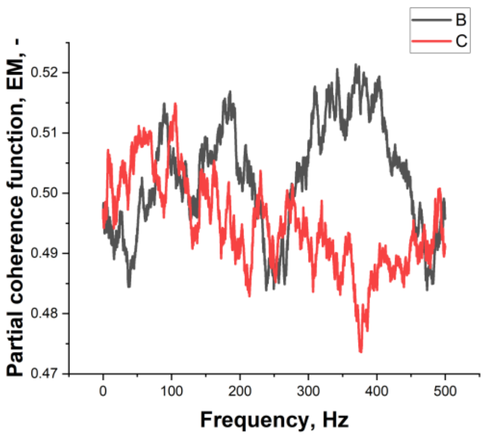

Figure 9. Partial coherence functions for the suspension system in EM-driven vehicles: B – powertrain inertial forces, C – road micro-roughness

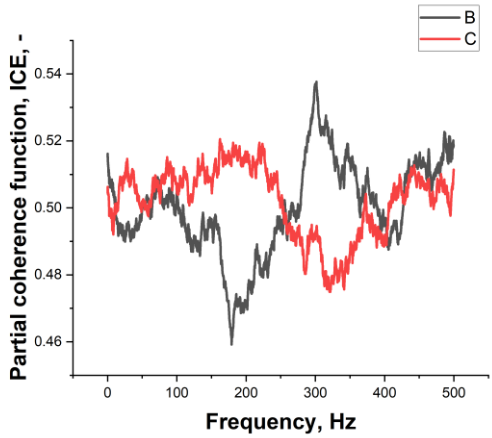

Figure 10. Partial coherence functions for powertrain mounts in ICE-driven vehicles: B – powertrain inertial forces, C – road micro-roughness

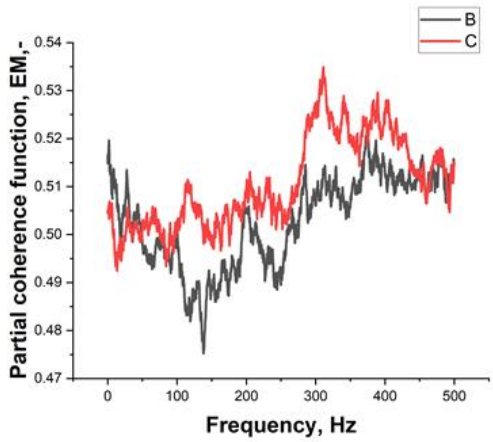

Figure 11. Partial coherence functions for powertrain mounts in EM-driven vehicles: B – powertrain inertial forces, C – road micro-roughness

3 DATA ANALYSIS

The analysis begins with Table 3. It is evident that, for both types of powertrain, the thermal power is highest in the tires and lowest in the powertrain mounts. When comparing the considered powertrain systems, the thermal power in the electric powertrain is higher in the tires than in the ICE-powered vehicle, whereas it is lower in the remaining damping elements. This can be explained by the fact that the sprung mass is significantly larger in the electric vehicle considered.

In practice, this issue is addressed by an appropriate selection of elasto-damping elements; however, in the present study, identical characteristics were assumed for both powertrain types in order to ensure comparability.

The obtained results reveal markedly different orders of magnitude of the thermal power dissipated in individual damping elements of the system. At first glance, it may appear unexpected that the RMS values of thermal power in the tires are of the order of megawatts, while those in the powertrain mounts are of the order of watts. However, this relationship is fully consistent with the physical nature of the processes involved and with the overall energy balance of the system.

The tire represents the primary element in the transmission chain of excitations originating from road micro-roughness and is subjected to the largest relative deformations and velocities, particularly over a wide frequency range. At the same time, damping forces in the tire are substantial, and energy dissipation occurs continuously along the tire–road contact patch, resulting in very high instantaneous and RMS thermal power values.

It should be emphasized that this energy is not accumulated within a single structural component but is distributed over a large tire volume and dissipated into the surrounding environment during vehicle motion. It is also noted that the influence of tire dimensions on the oscillatory excitation of the tire center was not included in the present model; therefore, the predicted excitations are more severe than in reality, leading to an overestimation of the thermal power dissipated in the tire.

In contrast, powertrain mounts are designed to operate with significantly smaller relative displacements and velocities, and their primary function is vibration isolation rather than the dissipation of large amounts of energy. Consequently, the thermal power dissipated in these elements is several orders of magnitude lower and remains within the watt range. The suspension system occupies an intermediate position, with thermal loads on the order of tens of kilowatts, which corresponds to its role in absorbing oscillatory energy between the unsprung and sprung masses.

The pronounced differences in the orders of magnitude of thermal power indicate that the energy balance of oscillatory processes cannot be properly assessed without clearly distinguishing the roles of individual damping elements. Furthermore, direct comparison of absolute values is meaningful only within the same component and for the same type of powertrain.

Analysis of Figure 6 shows that road micro-roughness has a greater influence on the thermal power dissipated in the tire, while the frequency-dependent energetic coupling decreases with increasing frequency. The highest values occur in the regions around 50, Hz and 300 Hz. The fact that the partial coherence function is less than unity indicates the presence of significant nonlinearities in the system. A similar behavior is observed for the electric powertrain (Figure 7), with the difference that the maximum coupling occurs at approximately 180 Hz.

Figure 8 shows that, over a wide frequency range, road micro-roughness dominates the thermal power in the suspension system for the ICE-powered vehicle, except around 300, Hz. The highest frequency-dependent energetic coupling occurs near 350 Hz. In the case of the electric powertrain, road micro-roughness also has a dominant influence over a broad frequency range, except around 50, Hz (Figure 9), with the strongest contribution observed near 350, Hz. These phenomena can be explained by the nonlinear dynamic nature of the vehicle suspension system.

From Figure 10, it can be observed that road micro-roughness has a greater influence up to approximately 250, Hz, while around 300, Hz the influence of engine inertial forces becomes dominant. Up to about 500, Hz, the frequency-dependent energetic coupling is relatively uniform. In the case of electric propulsion, road micro-roughness exhibits a stronger influence on the thermal power over a broader frequency range, as shown in Figure 11.

Based on the preceding analysis, it can be concluded that a frequency-dependent energetic coupling exists between the considered excitation sources in the vehicle and the thermal power dissipated in all damping elements. The influence of these excitations is not identical for the two powertrain types, which can be attributed to the nonlinear behavior of the system. Therefore, in subsequent stages of the project, further research should be conducted using more accurate input data and appropriately optimized elasto-damping elements for both propulsion concepts.

The applied oscillatory model is intended for use in the conceptual design phase and, accordingly, has certain limitations. The influence of road slope was not considered, which implies that additional static and dynamic load components arising from changes in normal reactions and mass redistribution during uphill or downhill driving were neglected.

Furthermore, the model does not account for the longitudinal dynamics of the vehicle, such as acceleration, deceleration, and variations in driving torque; therefore, only approximately steady-state operating conditions were analyzed. In addition, temperature feedback effects-i.e., the dependence of elasto-damping element properties on temperature-were not included, although it is well known that temperature rise can significantly affect stiffness and damping characteristics. Incorporation of these effects represents a logical direction for further model development and would enable a more realistic assessment of thermal loads under real operating conditions.

4 CONCLUSION

This paper investigated the influence of the powertrain type on the thermal loading of damping elements in a passenger motor vehicle subjected to vertical oscillatory excitations. By applying a multi-mass oscillatory model with three lumped masses and a nonlinear description of elasto-damping elements, a quantitative assessment of mechanical energy dissipation and its transformation into heat was achieved.

The results of numerical simulations show that, for both propulsion types, the highest thermal loads occur in the tires, while the lowest are observed in the powertrain mounts. Compared with conventional ICE propulsion, electric vehicles exhibit lower thermal loads in the damping elements of the suspension system and powertrain mounts, which can be attributed to lower excitation force amplitudes and a different mass distribution. On the other hand, the higher sprung mass associated with electric powertrains leads to increased thermal loads in the tires.

Frequency-domain analysis based on partial coherence functions demonstrated that the contributions of road micro-roughness and powertrain excitations depend on the frequency range and the type of propulsion, and that neither excitation source can be neglected. A pronounced nonlinear behavior of the system was observed, confirming that the energetic response cannot be reliably predicted using linear models.

The investigations conducted in this study confirm that the analysis of thermal loading in damping elements can serve as an important additional criterion during the conceptual vehicle design phase, particularly in the selection of the propulsion concept and the sizing of elasto-damping elements. Further research should focus on the application of more advanced vehicle models, inclusion of temperature-dependent damping characteristics, and consideration of realistic operating conditions, including acceleration, deceleration, and energy recuperation in electric vehicles.

RMS thermal power was shown to be a robust and physically meaningful criterion for comparing the energetic impact of different powertrain concepts under stochastic and nonlinear oscillatory conditions.

The obtained results indicate that the choice of propulsion concept affects not only the dynamic and vibro-acoustic response of the vehicle but also the energetic and thermal loading of key damping elements, which should be taken into account already in the early stages of vehicle design.

REFERENCES

[1] Genta, A.: Motor Vehicle Dynamics. Politecniko di Torino, 2003.

[2] Miliken, WF., Miliken, DL.: Race Car Vehicle Dynamics, SAE, Warrendale, 1995.

[3] Mitschke, M.: Kraftfahrzeugkonstruktion, Teil D., TU Braunschweig, Forlesung, 1997.

[4] Demić, M.: The optimization of vibration systems of motor vehicles (in Serbian). University of Kragujevac, Mechanical Engineering Faculty, 1997.

[5] Gillespie, T.: Fundamentals of Vehicle Dynamics, SAE, Warrendale, 1992.

[6] Rajamani, R., Vehicle Dynamics and Control, University of Minesota, 2005.

[7] Demić, M., Diligenski, Đ.: A contribution to the study of thermal loads of hydraulic and active mounts of powertrain of a freight motor vehicle, Journal of Applied Engineering Science, doi:10.5937/jaes16-15905,

[8] 16, 521, pp. 217 – 224, 2018.

[9] Atkins, P.: The Laws of Thermodynamics (A Very Short Introduction) Oxford, 2010.

[10] Bojić, M.: Thermodynamics (in Serbian). University of Kragujevac, Mechanical Engineering Faculty, 2011.

[11] Demić, M.: Design of passenger cars (in Serbian). University of Kragujevac, Mechanical Engineering Faculty, 2004.

[12] Khachiyan, A. S., et al.: Internal Combustion Engines, Vysshaya Shkola, Moscow, 1978 (in Russian).

[13] Soresini, F. at all: Noise and Vibration Modeling of Permanent Magnet Synchronous Motors: A Review, IEEE Transactions on Transportation Electrification, Institute of Electrical and Electronics Engineers (IEEE), Vol. 10, Issue 4, pp. 8728–8745, 2024.

[14] Bendat, J., Piersol, A.: Random data analysis and measurement, John Wiley and Sons, London, 2000.

[15] Doule, J., et al.: Feedback Control Theory, Mc Millan Publishing Co, 1990.

[16] Tomović, R. et al.: Introduction to nonlinear systems of automatic control (in Serbian), Naučna knjiga, Belgrade, 1974.

MOBILITY & VEHICLE MECHANICS

https://doi.org/10.24874/mvm.2026.52.01.03
UDC: 656.11.021:519.857

TRAFFIC SIGNAL OPTIMIZATION AT A QUADRATIC ROAD INTERSECTION USING A SWARM INTELLIGENCE ALGORITHM

*Aleksandar Jovanović [1]**

Received in March 2026 *Accepted in May 2026*

ORIGINAL SCIENTIFIC ARTICLE

ABSTRACT: Quadratic Road Intersection (QRI) belongs to the group of traffic intersections with alternative designs, which have become popular due to their ability to alleviate traffic congestion and reduce travel time. A common feature of all alternative intersection designs is their implementation in suburbs, since they require more space compared to traditional intersections. The second common characteristic of the family of alternative intersections is treating left-turning vehicles in an unconventional way. QRI eliminates all left-turn movements at the main intersection, using quadratic bypasses to accommodate the missing turns. This creates two secondary intersections downstream from the main one, typically controlled by traffic lights. There are two phasing schemes that are used to control QRI: with one controller (Reid phases) and with three controllers, one for each intersection. The latter assumes optimization of traffic progression between the separated intersections that the QRI consists of. In this study, the QRI layout from the field is used to investigate control delay discrepancies in the implementation of the two phasing schemes. Moreover, this study develops a unique offset optimization approach, especially suited for QRI. In that endeavour, a swarm optimization technique, Bee Colony Optimization (BCO), is leveraged to optimize traffic control parameters: cycle, splits, and offsets. BCO is a well-known metaheuristic approach, based on the natural process of collecting nectar by honeybees. BCO has already shown high performance in traffic control optimization tasks. Although more complex to implement, the results show that the three-controller phase scheme, with offset optimization, outperforms the Reid phase scheme in terms of control delay as the primary performance measure in traffic signal control optimization problems.

KEY WORDS: *Quadratic road intersection, Reid phase scheme, offset optimization, bee colony Optimization, control delays*

[1]*Aleksandar Jovanovic, Faculty of Engineering, University of Kragujevac, Sestre Janjic 6, 34000 Kragujevac, Serbia, a.jovanovic@kg.ac.rs, https://orcid.org/0000-0003-4208-5703*
*(*Corresponding author)*

OPTIMIZACIJA SVETLOSNIH SIGNALA NA KVADRATNOJ RASKRSNICI PRIMENOM INTIGENCIJE ROJA

REZIME: Kvadratna raskrsnica (QRI) pripada grupi saobraćajnih raskrsnica sa alternativnim dizajnom, koje su postale popularne zbog svoje sposobnosti da ublaže saobraćajna zagušenja i smanje vreme putovanja. Zajednička karakteristika svih alternativnih raskrsnica je njihova primena u prigradskim područjima, zbog činjenice da zahtevaju više prostora u poređenju sa tradicionalnim raskrsnicama. Druga zajednička karakteristika ovih nekonvencinalnihi saobraćajnih rešenja je tretiranje vozila koja skreću levo na alternativan način. QRI eliminiše sva leva skretanja na glavnoj raskrsnici, koristeći kvadratne obilazne saobraćajne trake kako bi se opslužila vozila u levom skretanju. Na taj način nastaju dve sekundarne raskrsnice nizvodno od glavne, koje su obično kontrolisane svetlosnim signalima. Postoje dva plana faza koje se koriste za upravljanje QRI: sa jednim kontrolerom (Reid faze) i sa tri kontrolera, po jednim za svaku raskrsnicu. Ova druga podrazumeva optimizaciju progresije saobraćaja između odvojenih raskrsnica od kojih se QRI sastoji. U ovom istraživanju koristi se QRI geometrija sa terena kako bi se ispitale razlike u vremenskim gubicima vozila pri primeni predmetnih planova faza. Pored toga, u radu je razvijen jedinstveni pristup optimizacije pomaka zelenog vremena, posebno prilagođen QRI raskrsnicama. Za optimizaciju parametara upravljanja svetlosnih signala: ciklusa, raspodele zelenog vremena i pomaka zelenog vremena, koristi se algoritma iz klase optimizacije roja: optimizacija kolonijom pčela (BCO), dobro poznata metaheuristička metoda zasnovana na prirodnom procesu prikupljanja nektara kod pčela. BCO je pokazao visoke performanse u zadacima optimizacije upravljanja saobraćajem. Iako je složenija za implementaciju, rezultati pokazuju da plan faza sa tri kontrolera, uz optimizaciju pomaka zelenog vremena, daje bolje rezultate od Reid faza u pogledu vremenskih gubitaka vozila, kao primarne mere performansi u problemima optimizacije upravljanja svetlosnim signalima.

KLJUČNE REČI: *Kvadratna raskrsnica, Reid faze, optimizacija pomaka zelenog vremena, optimizacija kolonijom pčela, vremenski gubici vozila*

TRAFFIC SIGNAL OPTIMIZATION AT A QUADRATIC ROAD INTERSECTION USING A SWARM INTELLIGENCE ALGORITHM

Aleksandar Jovanović

INTRODUCTION

Traffic engineers, researchers, and practitioners seek solutions that will mitigate the global problem of traffic congestion, which causes emissions and urban contamination. Among all approaches to this problem, intersections with Alternative Geometrical Design (AGD) arose as a practical solution that improves traffic performance measures such as vehicle delay and travel time [5]. AGDs are typical suburban facilities, where urban streets meet rural highways. The reason for this lies in the space requirements and the specific demand patterns that suit these intersections. For instance, some types of AGD fit well with high through traffic demands on the main road and relatively low demands on the side streets. On the other hand, Quadratic Road Intersection (QRI) might accommodate relatively high traffic demands from both the main and side roads, which makes it suitable for implementation in inner parts of cities.

QRI eliminates left-turn movements from the main intersection and redirects them toward two downstream intersections, which are connected by a quadratic bypass road. At first glance, it might look that vehicles travel more compared to the traditional layout. However, by significantly improving the capacity of the main intersection, studies [13] show improvement in overall travel time and vehicle delays.

Due to relatively simplified phase plans, fixed-time traffic control is the preferred way to control traffic demands at QRI. However, it remains an open problem whether it is preferable to use a single controller for all three intersections that the QRI consists of, or to implement a separate controller for each intersection. In the first case, the so-called Reid phase plan was developed [12], and it is recommended in the case of shorter distances between the three intersections and unbalanced traffic demands on the main intersection. On the other hand, when intersections are farther apart and traffic demands on the main intersection are relatively balanced between the two directions, the solution with three controllers is preferable [13].

The aim of this study is to investigate these recommendations under different traffic demand patterns using the geometrical layout of a field QRI. The first objective is to optimize traffic signal parameters at QRI to minimize vehicle delay using both Reid phases and the three-controller phase scheme. The second objective is to develop offset optimization especially suitable for implementation in QRI.

As the optimization tool, the Bee Colony Optimization (BCO) technique is leveraged for obtaining control parameters: cycle, splits, and offsets. BCO is inspired by bee behaviour in nature during the process of nectar collection. The first mathematical formulation and application of BCO were proposed by [10]. Since then, BCO has been shown to be a reliable tool for traffic control optimization at signalized intersections [7,9]. Also, BCO has already been applied to the optimization of AGD [8].

In recent decades, QRI has attracted moderate research interest. In his study, Reid (2000) found that QRI lowers overall travel time by 22% compared to the traditional intersection layout. At the same time, travel time for left-turning vehicles is not significantly changed. The Federal Highway Administration (FHWA) provides a detailed guide on QRI, including recommendations for geometry, markings, and pedestrian accommodation [5]. During the construction of QRI in Fairfield, Ohio, the project team found that the implemented QRI had a positive influence on the environment and the economy of the community [1].

The literature review opens a vast space for research on QRI, especially in the area of traffic signal control optimization. The contribution of this study is to examine two recommended phase plans on a QRI from the field under different traffic demand patterns. In addition, a unique set of equations is developed for offset optimization in the case of the three-controller phase scheme.

After the introduction, the second section presents the problem statement. The third section is dedicated to the mathematical description of the problem and the proposed solution. The fourth section shows a numerical example with results. Finally, the fifth section concludes the study and outlines possible directions for future research.

1 PROBLEM STATEMET

In this study the QRI layout from Fairfield, Ohio (39°19'26.16" N 84°30'16.50" W), which opened in January 2012, is used. Figure 1 presents the geometry of subject QRI, with marked traffic movements (A, B… R). Right-turn movements, except for traffic movement H, are not controlled by traffic lights. Pedestrian demands are neglected.

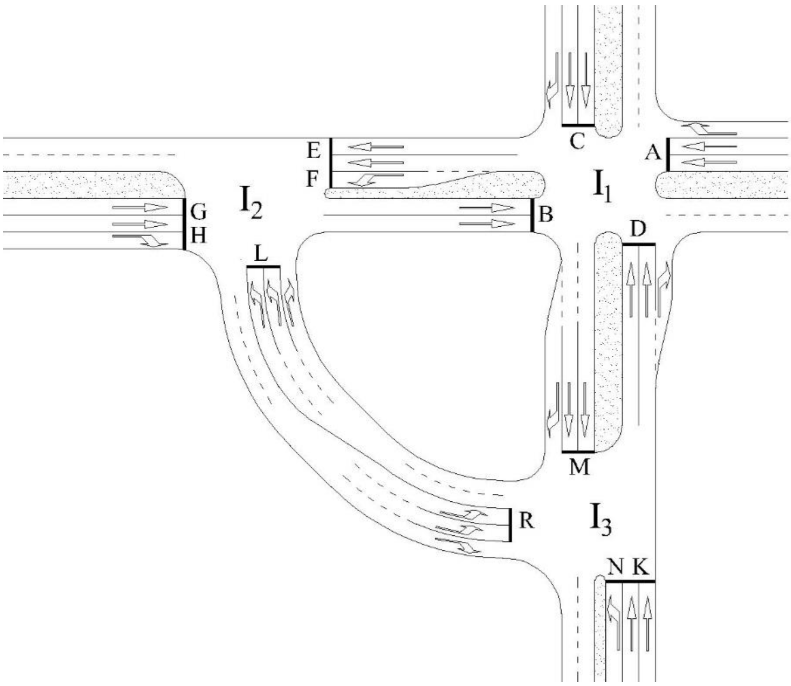

Figure 1. The graphical representation of QRI layout

Two possible signal phase schemes used to control QRI are presented in Figure 2. In the upper part of Figure 2, the Reid scheme is shown, while the lower part presents the signal phase scheme with three controllers. In the latter case, the main intersection is controlled by two phases, while the two downstream intersections are each controlled by three phases.

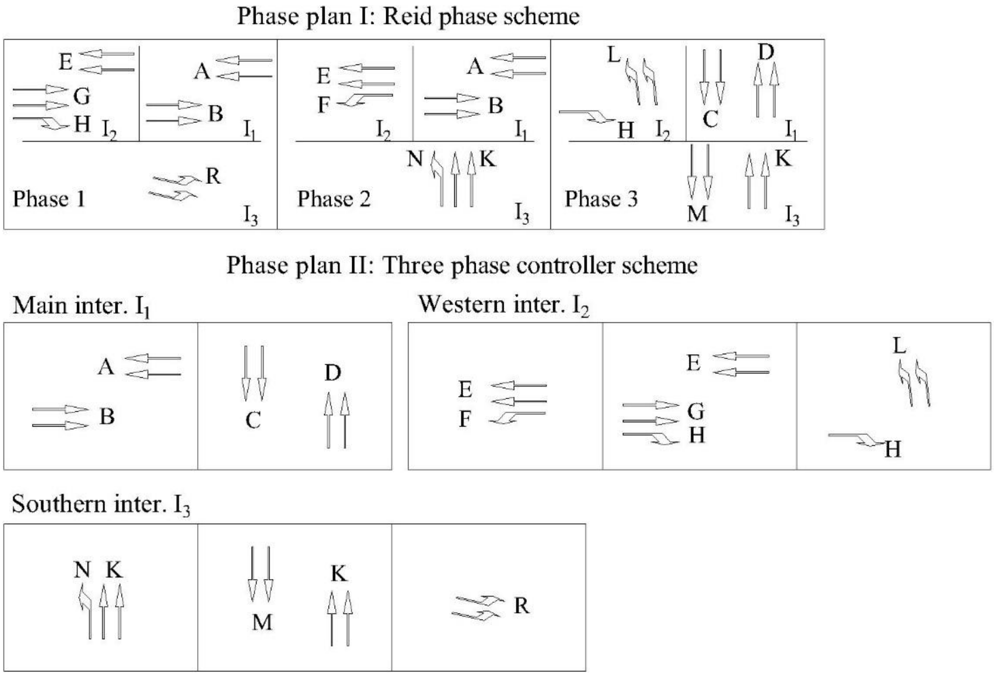

Figure 2. Two phases' planes for QRI

Because right-turning vehicles are served without traffic light control, the extra travel time for left-turning vehicles will be negligible. However, this is not the case for left-turning vehicles in movements R and B. Approximately, the extra travel time is equal to the double travel time between intersections (t_{tr}). Because delay is the main performance measure in this paper, these additional travel times will not affect the optimization results and will not be considered in the mathematical model.

Engineering questions that arise from the problem statement are: (1) which signal plan should be applied considering different traffic demand patterns and the distances between the three intersections that the QRI consists of; (2) for the applied signal plan, what should be the values of the control parameters: cycle, splits, and, in the case of signal plan 2, offsets; (3) how to set up the offset optimization for this unique node of three intersections.

To compare these differences, vehicle delay is used as the traditional performance measure in the case of unsaturated traffic conditions. Because QRI is designed for high traffic demands, oversaturated traffic conditions are not expected. Therefore, this study does not consider traffic congestion at QRI.

2 MATHEMATICAL FORMULATION AND PROPOSED SOLUTION

According to the QRI layout showed in Figure 1, let us define by M the set of traffic movements, where m is the traffic movement index, m = A, B, ... R. Let us define the vehicle delay (d_m) of m-th movement in the following way [4]:

$$d_m = d_{1m} \cdot (PF_m) + d_{2m} \quad \forall m \in M \tag{1}$$

where d_{1m} – uniform delay in the m-th movement (s/veh), which can be calculated as:

$$d_{1m} = \frac{0.5 \cdot C \cdot \left(1 - \frac{g_m}{C}\right)^2}{1 - \left[min(1, X_m) \cdot \frac{g_m}{C}\right]} \tag{2}$$

where:

C – cycle length (s),
g_m – green time in the m-th movement (s),
X_m – volume-to-capacity ratio of the m-th group, which can be calculated as:

$$X_m = \frac{q_m/s_m}{g_m/C} \tag{3}$$

where:

q_m – traffic demand in the m-th movement (veh/h),
s_m – saturation flow rate in th m-th movement (veh/h),
d_2 – incremental delay in the m-th movement (s/veh), which can be calculated as:

$$d_{2m} = 900T \cdot \left[(X_m - 1) + \sqrt{(X_m - 1)^2 + \frac{4 \cdot X_m}{c_m \cdot T}}\right] \tag{4}$$

where:

T – analysis time (1 h),
c_m – capacity in the m-th movement, can be calculated as:

$$c_m = s_m \cdot \frac{g_m}{C} \tag{5}$$

Progression factor (PF) can take values between 0 and 1, where 0 means that the whole platoon of vehicles faces red at the downstream intersection, while 1 means that the whole platoon passes through green at the downstream intersection. PF is calculated based on the formulas presented in the study by [2].

PF_m – progression factor in the m-th movement, which can be calculated as:

$$PF_m = 1 - \left\{\frac{1}{B_m}\left[max(0, min(\tilde{r}_m + B_m, g_{down\,m}) - \tilde{r}_m) + max\big(0, min(\tilde{r}_m + B_m - C_m, g_{down\,m})\big)\right]\right\} \tag{6}$$

where:

B_m - the platoon bandwidth. It is assumed to be equal to the green time of the upstream intersection for movement m,
$g_{down\,m}$ - the green time of the downstream intersection for movement m,
$\tilde{r}_m$ - the relative arrival time of the beginning of the platoon at the downstream intersection for movement m, measured within the signal cycle, which can be calculated as:

$$\tilde{r}_m = (t_{tr} - \theta_m) mod C \tag{7}$$

where θ_m is the offset for the m-th movement. The offset is the time difference between phase initiation at the upstream and downstream intersections. It affects the movement at the downstream intersections.

Let us define I as the set of all intersections that QRI consist of, where i is the intersection index, i = 1,2,3. In a similar way, let us define P as the set of phases that control i-th intersection, where p is the phase index, p = 1,2,3. For instance, considering phase plan II from Figure 2, offset $\theta_{31\text{-}23}$ represents the time difference between the initiation of phase 1 at intersection 3 and phase 3 at intersection 2. Because it affects movement L, it will be denoted as θ_L.

In the case of phase plan I from Figure 2, the mathematical formulation of the problem is defined as:

$$min \ \frac{\sum_{m=1}^{|M|} d_m \cdot q_m}{\sum_{m=1}^{|M|} q_m} \tag{8}$$

subject to:

$$C_{min} \leq C \leq C_{max} \tag{9}$$

$$g_{p\,min} \leq g_p \leq g_{p\,max}, \quad \forall p \in P \tag{10}$$

$$\sum_{p=1}^{|P|} g_p + L = C \tag{11}$$

$$C, g_p \ and \ L \ \in Z_{>0} \tag{12}$$

where:

g_p – the green time of the p-th phase (s),
L – the cycle lost time at the QRI (s).

Equation (8) presents the total average vehicle delay at the QRI, which needs to be minimized. In this case, PF is equal to 1 for all traffic movements. Equation (9) sets the cycle length between minimum and maximum values, while Equation (10) does the same for each control phase. Equation (11) defines the relation between green time, cycle lost time, and cycle length.

In the case of phase plan II from Figure 2, the mathematical formulation of the problem is defined as:

$$min \ \frac{\sum_{m=1}^{|M|} d_m \cdot q_m}{\sum_{m=1}^{|M|} q_m} \tag{13}$$

subject to:

$$C_{min} \leq C \leq C_{max} \tag{14}$$

$$g_{ip\,min} \leq g_{ip} \leq g_{ip\,max}, \quad \forall p \in P, \forall i \in I \tag{15}$$

$$\sum_{p=1}^{|P|} g_{ip} + L_i = C, \quad \forall i \in I \tag{16}$$

$$\theta_D + \theta_M = n \cdot C + g_{31} + (\Delta t + y) \tag{17}$$

$$\theta_B + \theta_E = n \cdot C - g_{21} - (\Delta t + y) \tag{18}$$

$$\theta_R + \theta_L = n \cdot C - g_{33} + g_{22} \tag{19}$$

$$0 \leq \theta_m \leq C, \quad \forall m \in M \tag{20}$$

$$C, g_{ip} \; and \; L_i \; \in Z_{>0} \tag{21}$$

$$\theta_m \; and \; n \; \in Z_{\geq 0} \tag{22}$$

where:

g_{ip} – the green time of the p-th phase at the i-the intersection (s),
L_i – the cycle lost time at the i-th intersection (s),
$\Delta t + y$ – all-red time plus yellow time. In this study, this value is equal to 5 s in all cases.

Equations (17–22) are developed in accordance with area traffic control principles. More details can be found in the papers by [5,6].

The mathematical optimization is conducted using the BCO metaheuristic. The pseudocode of the BCO algorithm is presented below [11]:

Pseudocode for BCO

Set number of bees: *B*
Set the number of iterations: *IT*
Set the number of forward and backward passes in a single iteration: *NP*
Set number of changes: *NC*
REPEAT
    For *i* = 1 to *B*
        Determine an initial solution for the *i*th bee
        Evaluate the solution of the *i*th bee
    Set *S*: calculate the best solution of the bees
    For *j* = 1 to *IT*:
        For *i* = 1 to *B*:
            Set the initial solution for bee *i*
        For *k* = 1 to *NP*:
            For *i* = 1 to *B*:
                For *r* = 1 to *NC*:
                    Evaluate modified solutions generated by possible changes of the *i*th bee solution
                    By roulette wheel selection choose one of the modified solutions
        For *i* = 1 to *B*:
            Evaluate solution of the *i*th bee
        For *i* = 1 to *B*:
            Decide whether the *i*th bee is loyal
        For *i* = 1 to *B*:
            if the bee *i* is not loyal
                Choose one of the loyal bees to be followed by the *i*th bee
            if the best solution of the bees is better than the solution *S*
                Set *S*: the best solution of the bees
UNTIL criterion is met
RETURN *S*

More details about the BCO application and the optimization parameter settings in traffic signal timing control problems can be found in [6].

3 A NUMERICAL EXAMPLE AND RESULTS

Fixed-time optimization, using BCO, is conducted on the geometrical layout presented in Figure 1, with the following parameters:

- Travel time between all intersections is 14 seconds (t_{tr} = 14 s). The travel time (t_{tr}) between all intersections is assumed to be the same.
- Minimum and maximum cycle values are 30 and 120 seconds, respectively (C_{min} = 30 s; C_{max} = 120 s),
- Minimum and maximum green time values are 5 and 70 seconds, respectively ($g_{p\ min}$ = 5 s; $g_{p\ max}$ = 70 s),
- Cycle lost time is 15 seconds (L = 15 s), except in the case of phase plan II for the main intersection, where L = 10 s.

Based on prior experience, the following BCO parameters were adopted:

- Number of bees involved in the search: 20,
- Number of forward/backward passes in a single BCO iteration: 20,
- Number of changes in one forward pass: 1, and
- CPU time allocated to artificial bees to search for the solutions (in all tests): 6 min.

The base traffic demand pattern (TD #1 in veh/h) is adopted from the FHWA report on QRI (Hughes et al., 2010), while saturation flow rates (s in veh/h) are calculated according to HCM (2010) and presented in Table 1. Additionally, four more traffic demand patterns (TD #2-5) were developed to address the questions stated in the problem statement. Finally, to investigate the influence of different geometries on QRI performance, the travel time between intersections is changed to 7 s and 21 s under all traffic demand scenarios.

Table 1. Traffic demands and saturation flow rates

q (veh/h)	A	B	C	D	E	F	G	H	L	K	N	M	R
TD #1	750	770	750	850	800	150	620	500	160	650	160	600	200
TD #2	750	700	450	450	800	150	620	450	160	300	160	370	150
TD #3	1050	1070	750	850	1000	250	920	500	160	650	160	600	200
TD #4	750	1070	750	850	800	150	920	700	160	650	160	600	250
TD #5	450	400	450	450	550	100	320	450	160	300	160	370	150
s (veh/h)	3800	3800	3800	3800	3800	1500	3800	1500	2800	3800	1500	3800	2800

All traffic scenarios (from TD #2 to TD #5) deviate from TD #1 to capture fluctuations in traffic demand within the QRI. TD #2 represents a decrease in demand in one direction at the main intersection, while TD #3 represents an increase in demand in one direction of the main intersection. TD #4 reflects an increase in traffic demand at the west intersection, whereas TD #5 represents a decrease in demand in both directions at the main intersection.

Table 2 shows the optimization results in terms of control delay as the primary performance measure. Furthermore, for the base traffic demand pattern, the lower part of Table 2 presents the corresponding control parameters.

Table 2. The results of average vehicle delays (in seconds/veh)

<table>
<tr><td colspan="30">t_{tr} = 14 s</td></tr>
<tr><td colspan="12">TD #</td><td colspan="4">1</td><td colspan="4">2</td><td colspan="4">3</td><td colspan="3">4</td><td colspan="3">5</td></tr>
<tr><td colspan="12">Reid phase</td><td colspan="4">12.71</td><td colspan="4">10.51</td><td colspan="4">16.66</td><td colspan="3">15.1</td><td colspan="3">9.67</td></tr>
<tr><td colspan="12">The three phase controller</td><td colspan="4">7.74</td><td colspan="4">7.52</td><td colspan="4">9.39</td><td colspan="3">8.85</td><td colspan="3">6.89</td></tr>
<tr><td colspan="30">The three-phase controller (the average delay values in seconds/veh)</td></tr>
<tr><td colspan="6">TD #1</td><td colspan="6">TD #2</td><td colspan="6">TD #3</td><td colspan="6">TD #4</td><td colspan="6">TD #5</td></tr>
<tr><td colspan="3">t_{tr} = 7 s</td><td colspan="3">t_{tr} = 21 s</td><td colspan="3">t_{tr} = 7 s</td><td colspan="3">t_{tr} = 21 s</td><td colspan="3">t_{tr} = 7 s</td><td colspan="3">t_{tr} = 21 s</td><td colspan="3">t_{tr} = 7 s</td><td colspan="3">t_{tr} = 21 s</td><td colspan="3">t_{tr} = 7 s</td><td colspan="3">t_{tr} = 21 s</td></tr>
<tr><td colspan="3">10.14</td><td colspan="3">7.67</td><td colspan="3">7.76</td><td colspan="3">7.35</td><td colspan="3">9.92</td><td colspan="3">9.65</td><td colspan="3">10.36</td><td colspan="3">8.52</td><td colspan="3">8.59</td><td colspan="3">6.22</td></tr>
<tr><td colspan="30">Intersection control parameters (in seconds). For Reid phase: C=46 s, g_1=10 s, g_2=7 s, g_3=14 s</td></tr>
<tr><td colspan="2">C</td><td colspan="2">g_{11}</td><td colspan="2">g_{12}</td><td colspan="2">g_{21}</td><td colspan="2">g_{22}</td><td colspan="2">g_{23}</td><td colspan="2">g_{31}</td><td colspan="2">g_{32}</td><td colspan="2">g_{33}</td><td colspan="2">θ_D</td><td colspan="2">θ_M</td><td colspan="2">θ_B</td><td colspan="2">θ_E</td><td colspan="2">θ_R</td><td colspan="2">θ_L</td></tr>
<tr><td colspan="2">40 s</td><td colspan="2">19 s</td><td colspan="2">11 s</td><td colspan="2">6 s</td><td colspan="2">14 s</td><td colspan="2">5 s</td><td colspan="2">8 s</td><td colspan="2">11 s</td><td colspan="2">6 s</td><td colspan="2">13 s</td><td colspan="2">40 s</td><td colspan="2">10 s</td><td colspan="2">19 s</td><td colspan="2">19 s</td><td colspan="2">29 s</td></tr>
</table>

Considering the results, one might consider the three-phase controller to be more suitable for the QRI from the perspective of average vehicle delays. For the base traffic demand pattern and travel time from the field of 14 s, the three-phase controller outperformed the Reid phase by 39.1%. For TD #2, TD #3, TD #4, and TD #5, the three-phase controller performed better than the Reid phase by 28.45%, 43.64%, 41.39%, and 28.75%, respectively. Figure 3 presents a graphical representation of the results.

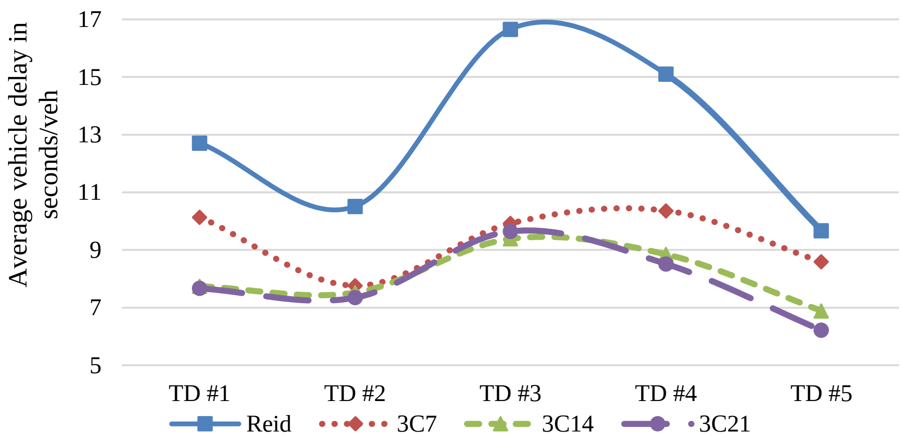

Legend: 3C – The three-phase controller; 7, 14, 21 – seconds of travel time

Figure 3. The results

By changing the travel time, it is shown that Reid phases perform better for shorter distances between the intersections that form the QRI compared to longer distances. However, with properly optimized offsets, the three-phase controller is still the preferable choice.

CONCLUSIONS

This paper addresses the problem of fixed traffic signal control optimization at QRI, an alternative intersection design that has gained popularity in the USA and has potential for implementation in other parts of the world. BCO, a well-known swarm-based metaheuristic, is used as the optimization technique. Two recommended phase plans are examined: one that assumes a single controller, the so-called Reid phase scheme, and another with three controllers and offset optimization.

It has been shown that, with proper optimization of offsets, the three-controller phase plan outperforms the Reid phase in all traffic scenarios and for all tested changes in travel time. It has also been noted that the Reid signal plan provides acceptable results when the distances between intersections are shorter, although the three-controller solution remains the preferable option. In addition, the contribution of this paper lies in the formulation of offset optimization equations that are unique for the QRI.

In future research, travel time, number of stops, and ecological parameters could be considered during fixed-time optimization. In addition, it should be examined whether real-time traffic control algorithms can further improve performance measures at QRI.

REFERENCES

[1] Bypass Project Team: Lessons learned from Fairfield's Quadratic Road Intersection. APWA Reporter, July 2013. American Public Works Association.

[2] Fambro, D. B., Chang, E. C. P., and Messer C. J.: Effects of the Quality of Traffic Signal Progression on Delay. Vol. 339. Transportation Research Board, 1991.

[3] Gartner, N.: Area traffic control and network equilibrium. In Traffic Equilibrium Methods: Proceedings of the International Symposium Held at the Université de Montréal, November 21–23, 1974 (pp. 274-297). Berlin, Heidelberg: Springer Berlin Heidelberg.

[4] Highway Capacity Manual (HCM): Transportation Research Board, Washington, DC, National Academies, 2010.

[5] Hughes, W., Jagannathan, R., Sengupta, D. and Hummer, J.: Alternative intersections/interchanges: informational report (AIIR), 2010.

[6] Jovanović, A., Nikolić, M. and Teodorović, D.: Area-wide urban traffic control: A Bee Colony Optimization approach. Transportation Research Part C: Emerging Technologies, 77, pp.329-350, 2017.

[7] Jovanović, A. and Teodorović, D.: Multi-objective optimization of a single intersection. Transportation planning and technology, 44(2), pp.139-159, 2021.

[8] Jovanović, A. and Teodorović, D.: Fixed-time traffic control at superstreet intersections by bee colony optimization. Transportation research record, 2676(4), pp.228-241, 2022.

[9] Jovanović, A., Uzelac, A., Kukić, K. and Teodorović, D.: The shortest-path and bee colony optimization algorithms for traffic control at single intersection with NetworkX application. Demonstratio Mathematica, 57(1), p.20230160, 2024.

[10] Lucic, P. and Teodorovic D.: Bee System: Modeling Combinatorial Optimization Transportation Engineering Problems by Swarm Intelligence. Proc., TRISTAN IV Triennial Symposium on Transportation Analysis, Sao Miguel, Azores Islands, 2001.

[11] Nikolić, M. and Teodorović, D.: Empirical study of the Bee Colony Optimization (BCO) algorithm. Expert Systems with Applications, 40(11), pp.4609-4620, 2013.

[12] Reid, J.D.: Using Quadrant Roadways to Improve Arterial Intersection Operations. ITE Journal, 70(6), pp. 34–45, 2000.

[13] Reid, J. and Hummer, J.E.: Quadrant Roadway Intersection Informational Guide, 2020.

Intentionally blank

MOBILITY & VEHICLE MECHANICS

https://doi.org/10.24874/mvm.2026.52.01.04
UDC: 623.4.014:624.042.8:519.673

ANALYSIS OF PLACING ADDITIONAL SUPPORTS OF THE INTEGRATED ARTILLERY SYSTEM CALIBER 130 MM

Andjela Mitrović[1], Vladimir Milovanović[2], Nebojša Hristov[3], Damir Jerković[4], Mladen Josijević[5], Djordje Ivković[6]*

Received in August 2024 *Accepted in October 2024*

ORIGINAL SCIENTIFIC ARTICLE

ABSTRACT: As part of this work, the vehicle platform on which the 130 mm caliber artillery tool was integrated was analyzed. The analysis of the platform was performed in the numerical program FEMAP. As it is a fast variable impulsive process, a dynamic analysis was performed. The type of analysis, Direct Transient, allows the determination of various parameters of a structure that is loaded with a force that is variable over time. The platform was analyzed with 2D and 3D finite elements, which show different values of the final results. Analyzing the results leads to the most suitable final element for further analysis. The further course of analysis involves analyzing additional supports on the vehicle platform. Extra supports are placed at different angles about the vertical plane. The analyzed angles are 15°, 45°, and 60°, while the tool is placed at various angles of elevation and direction. Through this analysis, certain laws were observed in the behavior of the construction, and the best variant that could be realized in the future was observed. This is the variant that would be the most suitable in terms of the load on the supports during the action of the weapon. Since the process takes place in a short period, the optimal variant should handle rapid load changes.

KEY WORDS: *artillery system, integration of artillery system, numerical analysis, FEMAP, Direct Transient*

[1] *Andjela Mitrović, Faculty of Engineering University of Kragujevac, Kragujevac, andjamit99@gmail.com, - (*Corresponding author)*
[2] *Vladimir Milovanović, Faculty of Engineering University of Kragujevac, Kragujevac, vladicka@kg.ac.rs, https://orcid.org/0000-0003-3071-4728*
[3] *Nebojša Hristov, University of Defence, Military Academy, Belgrade, nebojsahristov@gmail.com, https://orcid.org/0000-0002-8163-2223*
[4] *Damir Jerković, University of Defence, Military Academy, Belgrade, damir.d.jerkovic@gmail.com, https://orcid.org/0000-0001-5182-7057*
[5] *Mladen Josijević, Faculty of Engineering University of Kragujevac, Kragujevac, mladenjosijevic@gmail.com, https://orcid.org/0000-0001-9619-0897*
[6] *Djordje Ivković, Faculty of Engineering University of Kragujevac, Kragujevac, djordje.ivkovic@fink.rs, https://orcid.org/0000-0002-5747-7876*

ANALIZA UTICAJA POLOŽAJA DODATNIH OSLONACA INTEGRISANOG ARTILJERIJSKOG SISTEMA KALIBRA 130 MM

REZIME: U okviru ovog rada analizirana je vozna platforma na koju je integrisano artiljerijsko oruđe kalibra 130 mm. Analiza platforme sprovedena je u numeričkom softveru FEMAP. S obzirom na to da se radi o brzo promenljivom impulsnom procesu, izvršena je dinamička analiza. Primenjeni tip analize, Direct Transient, omogućava određivanje različitih parametara konstrukcije opterećene silom koja se menja tokom vremena.

Platforma je analizirana primenom dvodimenzionalnih (2D) i trodimenzionalnih (3D) konačnih elemenata, pri čemu su dobijene različite vrednosti rezultata. Uporednom analizom utvrđen je najpogodniji tip konačnih elemenata za dalja istraživanja. U nastavku rada izvršena je analiza dodatnih oslonaca na voznoj platformi. Dodatni oslonci postavljeni su pod različitim uglovima u odnosu na vertikalnu ravan, pri čemu su razmatrani uglovi od 15°, 45° i 60°. Artiljerijsko oruđe je istovremeno postavljano pod različitim uglovima elevacije i pravcima dejstva.

Rezultati sprovedenih analiza ukazali su na određene zakonitosti u ponašanju konstrukcije, kao i na najpovoljniju konstrukcionu varijantu za buduću realizaciju. Kao optimalno rešenje izdvojena je varijanta koja obezbeđuje najpovoljnije opterećenje oslonaca tokom dejstva oruđa. Budući da se proces odvija u veoma kratkom vremenskom intervalu, optimalna konfiguracija treba da omogući efikasno preuzimanje i podnošenje naglih promena opterećenja, čime se povećava pouzdanost i stabilnost celokupne konstrukcije.

KLJUČNE REČI: *artiljerijski sistem, integracija artiljerijskog sistema, numerička analiza, FEMAP, direktna tranzijentna analiza*

ANALYSIS OF PLACING ADDITIONAL SUPPORTS OF THE INTEGRATED ARTILLERY SYSTEM CALIBER 130 MM

Andjela Mitrović, Vladimir Milovanović, Nebojša Hristov, Damir Jerković, Mladen Josijević, Djordje Ivković

INTRODUCTION

The 130 mm caliber artillery system chosen for analysis in this paper is the 130 mm M46 gun, a towed artillery piece. It was developed in the 1940s by the Soviet Union after World War II [1]. While it was first used in the 50s of the last century. It has been developed in more than 40 countries and is still an important tool in most countries [1].

Figure 1. View of the 130 mm M46 gun [2]

The selected artillery system of caliber 130 mm, gun 130 mm M46, as a towed artillery tool, consists of the following assemblies:

- barrel assembly,
- upper carriage assembly,
- assembly of the anti-roll device and
- lower carriage assembly [3, 4, 5].

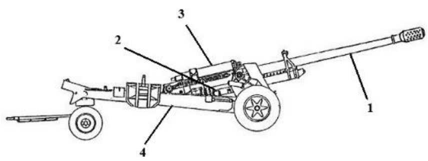

Figure 2. View of the 130 mm M46 gun with assembly positions: 1 – barrel assembly; 2 - upper carriage assembly; 3 - assembly of the anti-roll device; 4 - lower carriage assembly [6]

There are different variants of the 130 mm M46 gun, which are made identically to the original version, i.e. under license, made with the same caliber or another, whereby certain tactical-technical (TT) characteristics were reduced or increased. Also, there are variants when this tool is integrated into different vehicles.

1 VEHICLE INTEGRATION

To carry out the integration of the gun, first of all, a wheeled vehicle that is in use by the Serbian Armed Forces, the FAP 3240 vehicle, was chosen.

FAP 3240 (figure 3) is an off-road truck developed for the needs of the Serbian Army. According to the information so far, 4 such vehicles have been produced, while the 5th is a prototype [7]. Table 1 shows the characteristics of the FAP 3240.

Figure 3. FAP 3240 [7]

Table 1. *Characteristics FAP 3240 [7]*

FAP 3240	
Permissible total mass [kg]	24300
Payload [kg]	10000
Engine	OM 457 LA EU 3
Power [KW (KS)/min-1]	295 (401)
Maximum speed [km/h]	95
Maximum climbing ability [%]	60
Cargo Box [mm]	5500x2430x1700

1.1 Display of the forces acting on the tool

When the bullet is fired, the weapon recoils, that is, the recoil force P_{kn} occurs, which is caused by the accelerated movement of the projectile in the channel of the barrel and powder gases [3, 4, 5]. The recoil force depends on the resistance of the weapon and its firing stability. Total recoil force:

$$R = F_k + F_p + F_T - Q_t \sin\varphi \tag{1}$$

In which:

- F_k – hydraulic brake force,
- F_p – return force,
- F_T – total frictional force and
- $Q_t \sin\varphi$ – force component of the weight of the recoiling mass [3, 4, 5].

Due to the lack of data needed to calculate the force of the total recoil resistance based on the previous equation, the force R was calculated based on the recoil force P_{kn} and the recoil impulse I_t. The force R was caused by the total declaration by breaking the movement of the pipe. While the force It represents the internal recoil force. Figure 4 shows the forces acting on the tool. The mentioned forces can be calculated based on the conditions of the balance of forces, i.e. of the condition that the force of inertia of the twitching parts is by definition:

$$I_t = P_{kn} - R \tag{2}$$

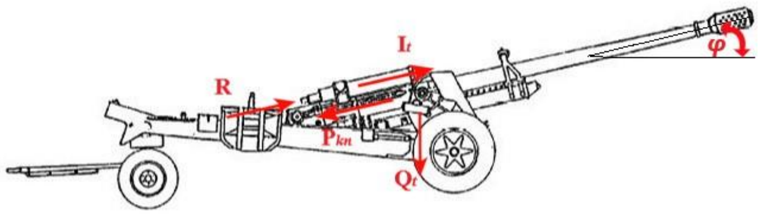

Figure 4. Force acting on the tool

The internal ballistic characteristics are shown in Table 2. To determine the internal ballistic characteristics, an internal ballistic calculation was performed using the Drozdov method [8].

***Table 2.** Internal ballistic characteristics*

Internal ballistic characteristics	
v_o [m/s]	924.22
p_m [Pa]	331425536
t[s]	0.01308

1.2 Defining constraints and assumptions

Figure 5 shows the forces acting on the tool and the vehicle.

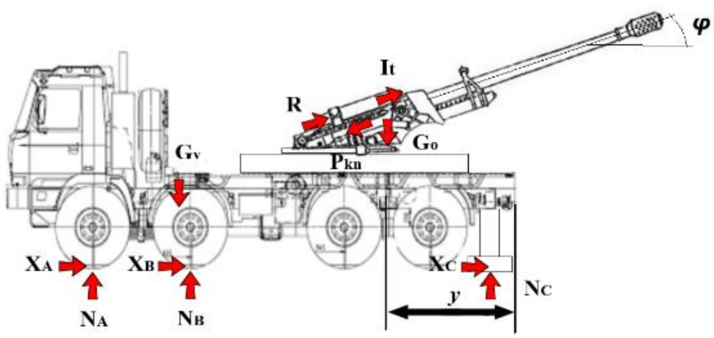

Figure 5. The forces acting on the tool and the vehicle

First, during the analysis of the reactions of the supports, certain assumptions were adopted to solve the problem more easily.

The adopted assumptions are:

- parts of the tool, the connection between the tool and the truck are rigid,
- the truck wheels are on a horizontal and solid surface,
- relying on the last four wheels is excluded,
- the effect of the weight of the tool (G_o) and the truck (G_v) is ignored and

- all forces act in the plane of symmetry.

The integration of the cannon on the vehicle was carried out on half the width of the vehicle, with the center of mass of the weapon located in the middle of the cargo box, marked with the symbol y (figure 5).

When integrating the cannon FAP 3240 needs to have additional supports at the end of its cargo area (figure 5). When the cannon is fired, the two end supports are lowered, disabling the other two pairs of truck wheels.

1.3 Defining the effect of force

To simplify the calculation, it is defined that the force acts at one point. The chosen point of action is localized at half the width and half of the cargo box. The magnitude of the force depends on the elevation angle ϕ and the direction angle ψ.

However, as the force P_{kn}-R (symbol F) acts in space and the plane of symmetry of the tool, it is necessary to determine its components in space. Figure 6 shows the force in space.

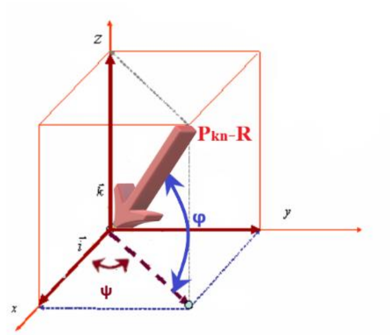

Figure 6. Force components in space

The equations for calculating the force components in space are as follows:

$$X = -F * cos\psi * sin\varphi; \tag{3}$$

$$Y = -F * sin\psi * cos\varphi; \tag{4}$$

$$Z = -F * sin\varphi. \tag{5}$$

How it is necessary to perform a dynamic analysis of the problem, i.e. to analyze a structure loaded over time, it is necessary to define a function in time. That is why a function is created to be analyzed. In this case, P_{kn}-R is analyzed over time (figure 7).

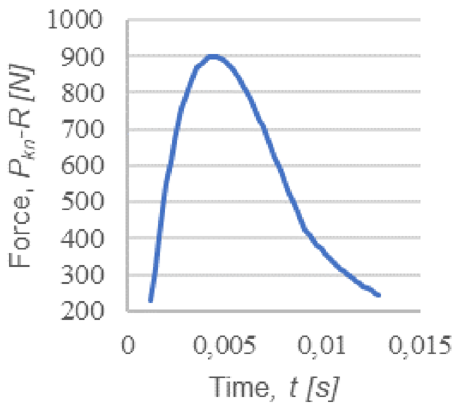

Figure 7. Force value over time

2 ANALYSIS WITH DIFFERENT FINITE ELEMENTS

To get the best results, an analysis of the problem with different finite elements was done first. Since the given force acts in space, the linear finite element is not considered. With a 1D finite element, it is necessary that the load acts along one axis ([9, 10]), which is impossible to establish here. So, the analysis comes down to comparing the results obtained with 2D and 3D finite elements.

Necessary data for the further course of analysis are geometric data of the structure and data on the material. Baseline data are given in Table 3.

Table 3. *Initial data*

Initial data	
Vehicle length [mm]	8500
Vehicle width [mm]	2800
Wheel height [mm]	1000
Wheelbase [mm]	2000
Width of supports [mm]	500
Modulus of elasticity, E [N/mm^2]	$2.1*10^{11}$
Poisson's coefficient, ν [/]	0.3
Material density, ρ [kg/mm^3]	$7.850*10^{-6}$

When creating a model using 2D finite elements, it is necessary to add the thickness of the shell in addition to the initial data. Wherein in the case of 2D finite element thickness is added symmetrically in half about the created surface [9, 10]. In this case, the default thickness of the 2D finite element is 100 mm. 3D finite elements are volume elements, by creating a shell in the required shape of a simplified construction, volume is added.

Figure 8 shows a comparative view of the reaction results of the supports of the analyzed structure with 2D and 3D finite elements. As the action was performed at a direction angle of 0°, the pairs of supports have identical values of the reactions of the supports. Therefore, diagrams are presented for pairs of supports.

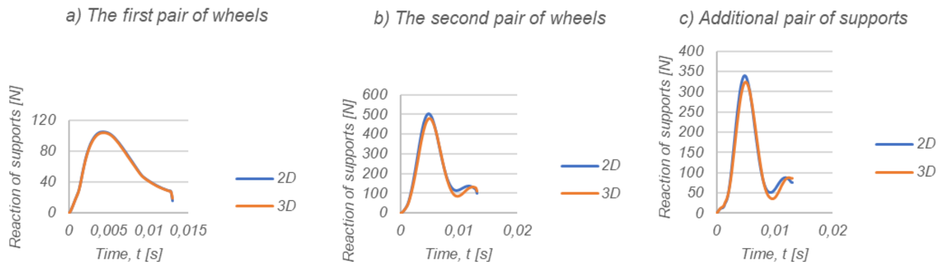

Figure 8. Comparative view of the results

The presented diagrams show that higher values of support reactions are obtained during the analysis of the structure made of 2D finite elements. Whereby the second pair of wheels bear the greatest load. Also, it is observed that the reactions of the supports when analyzing the structure with 2D finite elements have a faster response to the load. At the end of the firing process, they have a smaller increase in the reactions of supports, compared to analyzing the reactions of the supports with 3D finite elements.

Figures 9 and 10 show the displacement field for both types of finite elements shown at the moment of the highest load.

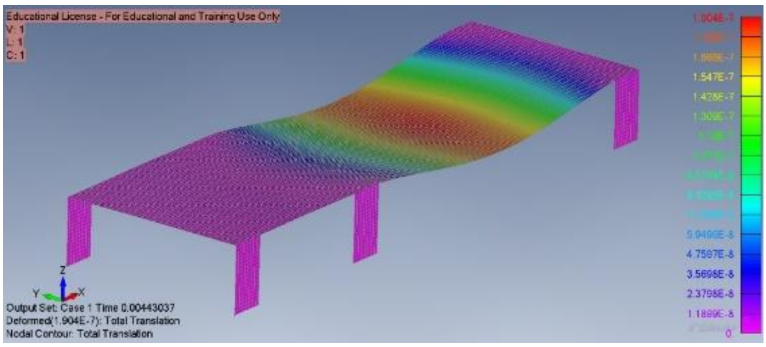

Figure 9. The displacement field of the analyzed structure made of 2D finite elements

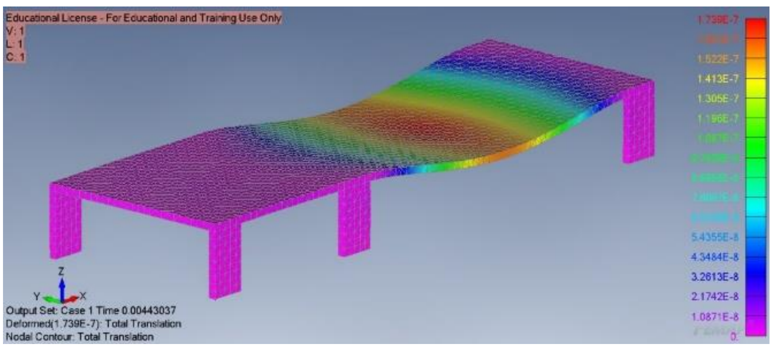

Figure 10. The displacement field of the analyzed structure made of 3D finite elements

With these images, it can be seen that the structure analyzed with 2D finite elements has a slight but larger field of displacement, compared to the structure analyzed with 3D finite elements. Based on the presented pictures of the comparative diagrams of the support reactions for pairs of supports, as well as based on the analyzed displacement field of the structure with different finite elements, certain conclusions can be made. First, the structure analyzed with 2D finite elements gave higher values of support reactions, which can be suitable for further calculations. For the reason that in real conditions it can be observed with a certain degree of certainty, because the real values can be smaller, and the analysis gives higher values, which represents a certain degree of certainty for constructors. Also, 2D finite element analysis shows a larger displacement field, which also represents a certain degree of certainty. The differences between the analyzed construction with different finite elements are not significantly greater, but there is still a certain difference. For this reason, the method where the structure is analyzed with 2D finite elements is used as a method for further calculations.

3 ANALYSIS OF DIFFERENT ANGLES OF ADDITIONAL SUPPORTS

Varying the angles at which the additional supports are placed about the vertical plane is the next step. The analyzed angles are 15°, 45° и 60°, shown with the symbol α. Figures 11 and 12 show the longitudinal and transverse views of the structure, respectively.

Figure 11. Longitudinal view of the structure

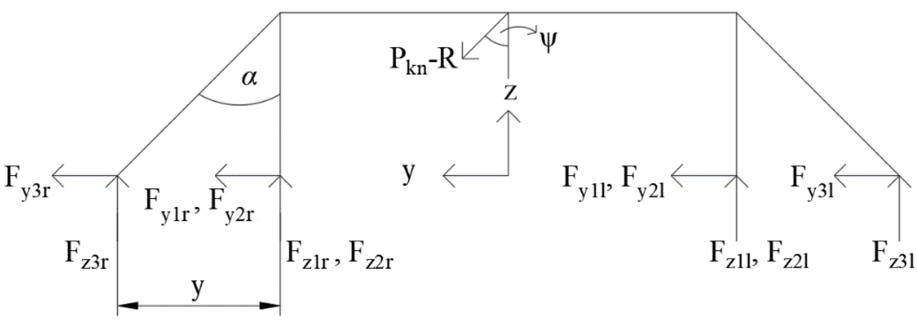

Figure 12. Cross-sectional view of the construction

Analyzing certain laws that have been established has been observed. Like that when acting with a positive angle of direction, the largest loads are borne by the left side of the structure. Conversely, by acting with a negative direction angle, the greatest load is borne by the right side of the structure. As well as that, when acting at any angle of elevation and direction, the biggest load is borne by the second pair of wheels. The exception that occurs is the effect of a negative elevation angle. In this case, the opposite situation occurs when acting at a positive or negative direction angle. For example, due to the negative elevation angle and the positive direction angle, the right side of the structure bears the greatest load, and vice versa.

Also, it was observed that the greatest load is borne by the supports when the action is performed at an elevation angle of 45°, at different angles of placement of additional supports.

Furthermore, a comparison of the angles of additional supports will be given when acting at an elevation angle of 45° and a direction angle of 0°. figure 13 shows a comparison of pairs of supports.

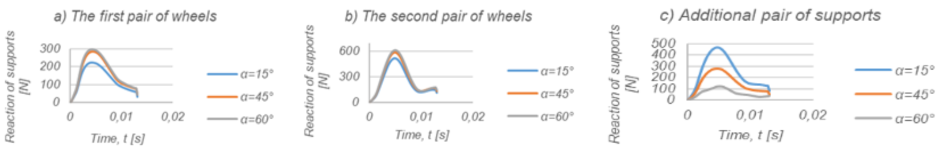

Figure 13. Comparative view of support reactions for pairs of supports

A comparative view shows that by placing additional supports at an angle of 15° about the vertical plane, the first and second pair of wheels bear the least load compared to placing additional supports at other angles. The exception is a pair of additional supports, which bear the higher load at an angle of 15°.

Also, it should be noted that when placing additional supports at a certain angle about the vertical plane, the reaction curves of the supports do not increase drastically at the end of the firing process, which was the case when the analysis of the structure with additional supports placed vertically was performed.

Analyzing the effect at an elevation angle of 45° and a positive or negative direction angle of ±25°, the following values are obtained for pairs of supports, shown in Figure 14.

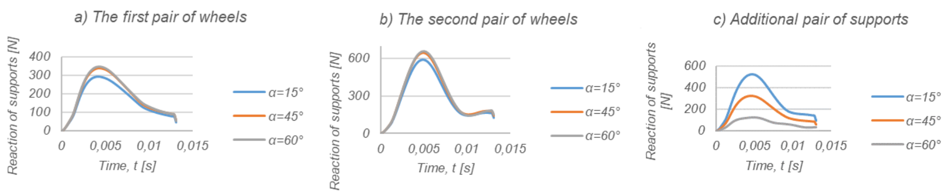

Figure 14. Comparative view of support reactions for pairs of supports

Based on the presented comparative analysis, the same pattern can be observed. Where a pair of additional supports bears the greatest load when placed at an angle of 15°, contrary to the first and second pair of supports which then bear the least load.

4 CONCLUSIONS

The selected 130 mm artillery system is integrated into the wheeled vehicle. In which a dynamic analysis was performed for the vehicle set up in this way, during the analysis, supports were added at the end of the cargo area so that the last two pairs of wheels were eliminated from the analysis. Additional supports, in that case, are vertical

The dynamic analysis was performed in the numerical program FEMAP. The type of analysis used is dynamic analysis, which enables problem-solving over time. Also, at the same time, it allows more realistic problem-solving. Making it possible to understand the magnitude of the problem, which happens in a fraction of a second, during which there is a huge effect of the load caused by the combustion of gunpowder gases at very high temperatures.

By comparing the results obtained from the analysis of these two elements, the analysis with a 2D finite element was taken as the optimal variant of the finite element. It is precisely with the help of this final element that higher values of support reactions and displacement of elements are obtained. Such values in real conditions may represent a certain degree of certainty.

The analysed additional supports are 15°, 45° and 60°. wherein the action was carried out at different angles of elevation and direction prescribed for the aforementioned artillery system.

By analysing the obtained values, certain regularities are observed. First, when operating with a positive angle of elevation and at a zero angle of direction the pairs of supports are identically loaded, with the second pair of wheels carrying the largest load. When the action is performed, also with a positive angle of elevation, and with a positive angle of direction, the left side of the structure bears the greatest load. Where the largest load is borne by the left second wheel. On the contrary, due to the negative direction angle, the greatest load is borne by the right side of the structure, i.e. right section wheel. The exception is the action with a negative angle of elevation, where when acting with a positive angle of direction, the greatest load is borne by the right side of the structure. Which is the opposite behaviour of the action with a positive elevation angle. Also, when the action is performed with a negative angle direction, the left side of the structure bears the greatest load.

By comparing the results obtained from the analysis of different angles of additional supports, it was observed that in the case of an action with an elevation angle of 45° and a direction angle of 0°, the highest load is borne by the first and second pair of supports when the structure is with additional supports that are at an angle of 60°, then with 45°, while at 15° they bear the least loads.

The exception is the behaviour of additional support. When the construction is with additional supports that are at an angle of 15°, then they are the most loaded. While at an angle of 45° they bear a slightly smaller load, and at an angle of 60° they bear the least load.

Such behaviour also occurs when the action is performed at the same elevation angle, i.e. 45°, and at a positive or negative direction angle.

For this reason, the variant where the additional supports are at an angle of 15° about the vertical plane was chosen as the optimal variant of constructions with additional supports. The reason for such a choice is that case the first and second pair of wheels bear the smallest loads. It was the second pair of wheels that was always the most loaded, in all analyses.

Based on the results shown, as well as the observation that the second pair of wheels bears the greatest load, it would be best to study the situation of installing additional supports just behind the second pair of wheels to secure the structure in that place, as well as to reduce the loads on the additional pair of supports.

REFERENCES

[1] Web page: https://armyrecognition.com/military-products/army/artillery-vehicles-and-weapons/towed-howitzer-guns/m-46-m1954-130-mm-gun-russia-uk, accessed: 30.10.2023.

[2] Web page: https://bit.ly/44DwFRo, accessed: 30.10.2023.

[3] Ristić Z.: Mechanics of artillery weapons, textbook, Military Academy, Belgrade, 2013. (in Serbian)

[4] Kari A., Ilić S.: Basis of weapon construction, textbook, Military Academy, Belgrade, 2020. (in Serbian)

[5] Kalezić M.: Designing artillery systems - Book 1, Belgrade, 2010. (in Serbian)

[6] Web page: https://bit.ly/3pavM2w, accessed: 30.10.2023.

[7] Web page: http://www.fap.co.rs/fap/3240nam.htm, accessed: 30.10.2023.

[8] Tančić Lj.: Classic internal ballistics, Belgrade, 2005. (in Serbian)

[9] Kojić M, Slavković R., Živković M., Grujović N.: Finite element method I - Linear analysis; University of Kragujevac, Faculty of Mechanical Engineering, Kragujevac, 2010. (in Serbian)

[10] Dunica Š., Kolundžija B.: Nonlinear analysis of structures; University of Belgrade, Faculty of Civil Engineering, Belgrade, 1985. (in Serbian)

MOBILITY & VEHICLE MECHANICS

https://doi.org/10.24874/mvm.2026.52.01.05
UDC: 629.113.012.55:504.5

TIRE WEAR: VEHICLE SAFETY AND ENVIRONMENTAL PROBLEM

Saša Vasiljević[1], Jasna Glišović[2], Marko Maslać[3], Milan Đorđević[4], Sonja Kostić[5], Dobrivoje Ćatić[6]*

Received in August 2024 *Accepted in October 2024*

ORIGINAL SCIENTIFIC ARTICLE

ABSTRACT: The vehicle consists of a large number of elements that make it safe and prevent traffic accidents. One of the important elements on the vehicle are tires. Tires are one of the key elements on a vehicle that prevent the occurrence of a traffic accident, bearing in mind that they are the only contact between the vehicle and the ground. The wear of tires or their tread basically has two key problems that occur. The first problem is the problem of vehicle safety, with the reduction of the depth of the pattern or tread of the tire, the characteristics of the tire decrease. These characteristics are primarily related to the fact that in some cases the braking distance of the vehicle is extended, the adhesion between the tire and the surface is reduced in the case of wet pavement, ... Another problem is an environmental problem that occurs due to tire wear. Tire wear leads to the formation of particles. Tires consist of different materials, and their wear and tear and the formation of particles contain materials that can be harmful to humans and the environment. In this paper, tire wear is analyzed from the aspect of vehicle safety and ecology, where the pollution caused by the wear of vehicle tires is analyzed.

KEY WORDS: *Vehicle, tires, safety, ecology*

[1] *Saša Vasiljević, Academy of Professional Studies Šumadija, Department in Kragujevac, Kosovska 8, Kragujevac, Serbia, vasiljevic.sasa036@gmail.com, svasiljevic@asss.edu.rs. https://orcid.org/0000-0002-2235-1309 (*Corresponding author)*

2 Jasna Glišović, University of Kragujevac, Faculty of Engineering, Kragujevac, Serbia, Sestre Janjic 6, jaca@kg.ac.rs, https://orcid.org/0000-0002-8251-1722

[3] *Marko Maslać, Academy of Professional Studies Šumadija, Department in Kragujevac, Kosovska 8, Kragujevac, Serbia, mmaslac@asss.edu.rs. , -*

[4] *Milan Đorđević, Academy of Professional Studies Šumadija, Department in Kragujevac, Kosovska 8, Kragujevac, Serbia, mdjordjevic@asss.edu.rs, -*

[5] *Sonja Kostić, Academy of Professional Studies Šumadija, Department in Kragujevac, Kosovska 8, Kragujevac, Serbia, skostic@asss.edu.rs, https://orcid.org/0000-0002-2522-9501*

[6] *Dobrivoje Ćatić, University of Kragujevac, Faculty of Engineering, Kragujevac, Serbia, Sestre Janjic 6, caticd@kg.ac.rs, .https://orcid.org/0000-0003-3636-8301*

HABANJE PNEUMATIKA KAO PROBLEM BEZBEDNOSTI VOZILA I ZAŠTITE ŽIVOTNE SREDINE

REZIME: Vozilo se sastoji od velikog broja elemenata koji doprinose njegovoj bezbednosti i sprečavanju nastanka saobraćajnih nezgoda. Jedan od važnih elemenata na vozilu jesu pneumatici. Pneumatici predstavljaju jedan od ključnih elemenata koji utiču na bezbednost saobraćaja, imajući u vidu da predstavljaju jedinu vezu između vozila i podloge.

Habanje pneumatika, odnosno njihovog gazećeg sloja, dovodi do dva osnovna problema. Prvi problem odnosi se na bezbednost vozila. Smanjenjem dubine šare, odnosno gazećeg sloja pneumatika, dolazi do pogoršanja njegovih eksploatacionih karakteristika. To se pre svega ogleda u produženju zaustavnog puta vozila u određenim uslovima vožnje, smanjenju prianjanja između pneumatika i kolovoza na mokrim površinama i drugim negativnim efektima koji mogu povećati rizik od nastanka saobraćajne nezgode.

Drugi problem predstavlja uticaj na životnu sredinu koji nastaje usled habanja pneumatika. Habanje pneumatika dovodi do stvaranja čestica koje se oslobađaju u životnu sredinu. Budući da se pneumatici sastoje od različitih materijala, čestice nastale njihovim habanjem mogu sadržati supstance koje su potencijalno štetne za ljude i životnu sredinu.

U ovom radu analizirano je habanje pneumatika sa aspekta bezbednosti vozila i zaštite životne sredine, pri čemu je posebna pažnja posvećena zagađenju koje nastaje kao posledica habanja pneumatika motornih vozila.

KLJUČNE REČI: *vozilo, pneumatici, bezbednost, zaštita životne sredine*

TIRE WEAR: VEHICLE SAFETY AND ENVIRONMENTAL PROBLEM

Saša Vasiljević, Jasna Glišović, Marko Maslać, Milan Đorđević, Sonja Kostić, Dobrivoje Ćatić

INTRODUCTION

Pneumatics (tires) on motor vehicles is one of the most important elements on the vehicle when it comes to vehicle safety. Tires represent elements that have the only contact with the surface [1]. Thus, tires represent an important element from the aspect of vehicle safety. The braking distance of the vehicle depends on the tires, but also the stability of the vehicle during its movement. Today, there are a number of different types of tires that differ according to their names, construction or composition, depending on the purpose. Also, tires have their own characteristics related to driving conditions, their behavior on the road in different driving conditions, the level of noise created and the impact of fuel consumption [2]. One of the basic divisions of tires is according to the weather conditions in which they are used. According to this classification, the first type are winter tires, which are used in the winter months and in bad road conditions. Summer tires are used in the summer months and in better weather conditions and can be used in the rain and at temperatures above 7oC. The third group of tires is all-season tires, which are a compromise between summer and winter tires and can be used in almost all conditions. These tires are designed differently according to the tread and the tire itself consists of a mixture of different materials. Applications in conditions for which the tires are not designed can lead to a negative effect on the braking distance and behavior of the tires [3].

The problem that occurs with tires is their wear. Tire wear leads to two basic problems. The first problem that occurs during wear is the pollution of the environment by particles that are created during tire wear. In jargon, pneumatics are often called tires, however, the tread consists of a mixture of different materials. During the movement of the vehicle, wear of the tread occurs in the form of particles of different sizes. Another negative phenomenon that occurs with tire wear is the reduction of the tread, i.e. the pattern on the tread. By reducing the tread, the characteristics of the tires are reduced and lead to a negative effect on the braking distance [4].

In this paper, an analysis and review of other results related to the impact of different characteristics of tires from the aspect of safety, as well as an analysis of the formation of particles resulting from tire wear, was performed. The impact of tires on vehicle safety and above all on braking distance was analyzed with several characteristics such as tire tread depth, tire type from the aspect of weather conditions for which the tire was designed, tire pressure, etc. The impact of tires on the environment is also analyzed in this paper, as well as the overall impact of tires on the environment in relation to other pollutants.

1 INFLUENCE OF TIRES ON VEHICLE SAFETY

1.1 The influence of the type of tire according to its purpose on the braking distance of the vehicle

It was noted that tires can differ according to their purpose in different climatic conditions, that is, when the vehicle moves in different road conditions. Thus there are so-called winter tires, summer tires and all-season tires. According to the legislation of the Republic of Serbia, it is mandatory to use winter tires in the period from November 1st to April 1st if there is ice, snow or ice on the road. However, if the road is dry, it is allowed to use summer tires. The problem that can arise then is the ambient temperature. Summer tires have uniform characteristics up to a temperature of 7ºC, if the temperature is lower they become rigid, which has a negative effect when braking. So you have to take that into account, so if the temperature during the day is higher, you can use summer tires, but in this period, if the temperature is lower, you still need to use winter tires, whose characteristics do not change below the specified temperature. Figure 1 shows the level of tire compatibility depending on the external temperature and climatic conditions.

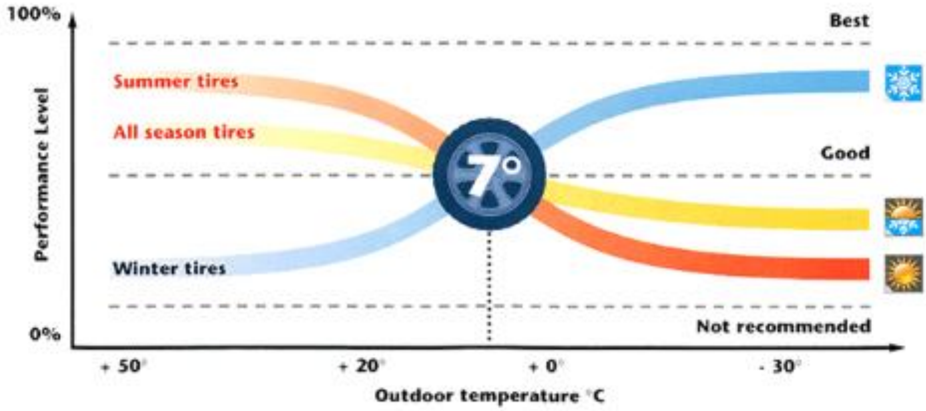

Figure 1 Tire compatibility level depending on ambient temperature [5]

The influence of the ambient temperature on the tires and finally the stopping distance is shown in Figures 2 and 3. Figure 2 primarily shows the influence of the ambient temperature depending on the tires and on dry and wet pavement. It can be seen that the stopping distance differs significantly from the temperature and road conditions. In the case of dry pavement and when the temperature is higher than 20ºC, in that case it is unfavorable to use winter tires because the braking distance increases significantly. Summer tires, on the other hand, showed favorable characteristics at all temperatures and when the pavement is dry. In the case of wet pavement, the use of summer tires at a temperature of 5ºC is very unfavorable because the braking distance is significantly extended compared to a temperature of 20ºC. The displayed data is related to braking at an initial speed of 100 km/h. Figure 3 shows the values of the braking distance depending on the conditions and the tire used, where it can be seen that at a temperature of 15ºC and on dry and wet pavement, summer tires have the shortest braking distance, all season and winter tires. In snow conditions, winter, all-season and summer tires have the shortest braking distance.

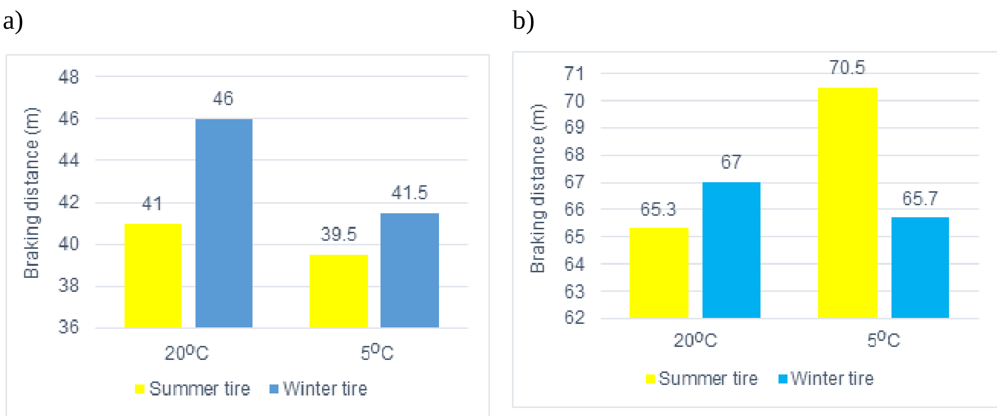

Figure 2 Braking distance from 100 km/h to 0 km/h depending on tires and ambient temperature, a) braking on dry pavement, b) braking on wet pavement [6,7]

Figure 3 Dependence of braking distance on tires and braking conditions [8]

From May 2021, all tires have their own markings or EU tire label related to tire application, fuel consumption, i.e. economy, noise level, but also wet grip rating, such a marking is shown in Figure 4a. The wet grip rating is further linked to the stopping distance. The difference of the braking distance depending on the grip distance rating depending on the category is shown in Figure 4b. Tires with category F tires have 18 m longer stopping distance compared to tires with category A.

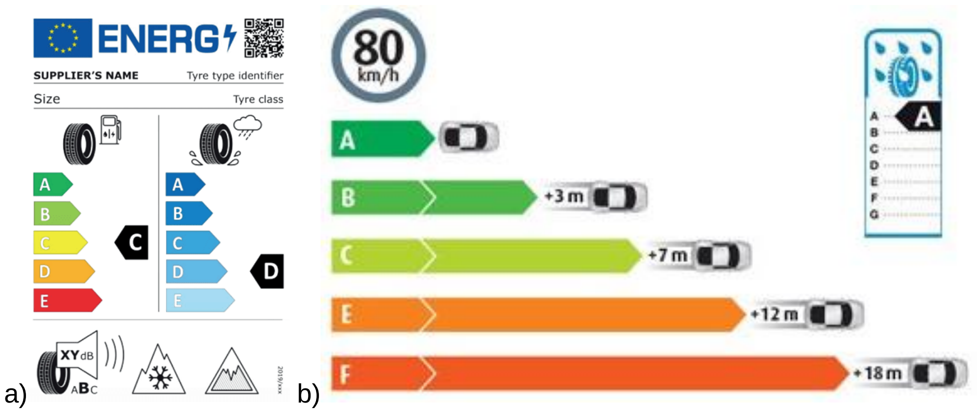

Figure 4 EU tire label and the influence of the category on the braking distance on wet roads: a) the appearance of the tire label, b) the difference in the length of the braking distance of different categories [9, 10]

Tires also have an impact on the vehicle's ability to turn. Figure 5 shows the possibility of turning the vehicle when moving the vehicle on snow. It is noticeable that winter tires have the best and more favorable turning, followed by all-season tires, and summer tires have the worst turning angle, at least when turning on snow.

Figure 5 The influence of the type of tire on the cornering of the vehicle [11]

1.2 Effect of tire tread depth on braking distance

The depth of the tire tread is one of the important elements when it comes to the influence of the tire on the stopping distance of the vehicle. Minimum tire tread depth values are legally prescribed. There is a significant influence of the depth of the pattern on the stopping distance, so as shown in Figure 6, as the depth of the pattern decreases, the stopping distance increases. Thus, it is necessary to always take care of tire wear because new tires have a significantly shorter braking distance compared to worn tires.

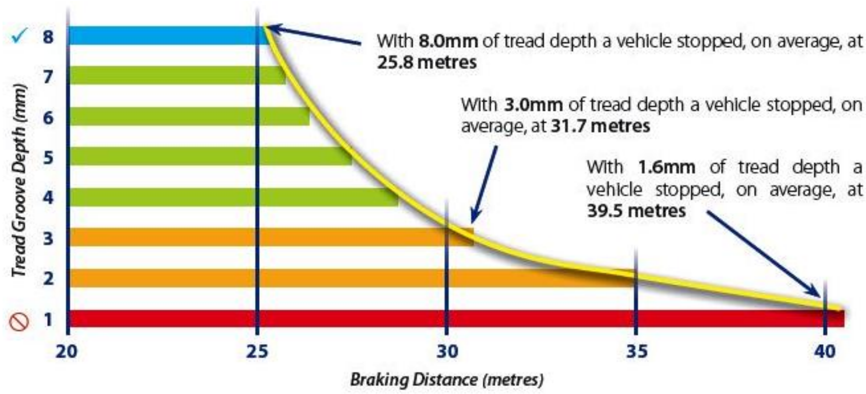

Figure 6 The length of the braking distance depending on the depth of the tire tread [12]

As mentioned, the depth of the pattern has a significant influence on the stopping distance, but it must be noted that the impact of the stopping distance also depends on the manufacturer. Figure 7 shows the background paths of two tires from different manufacturers in the case of new and worn tires. It is noticeable that there is a difference in the stopping distance even with new tires, but they also differ when the tires are worn. If the tires are analyzed according to the manufacturers, it is noticeable that in the case of some tires, when the tires wear out, the stopping distance increases significantly. There is always an increase in braking distance, but with some tires that distance increases significantly.

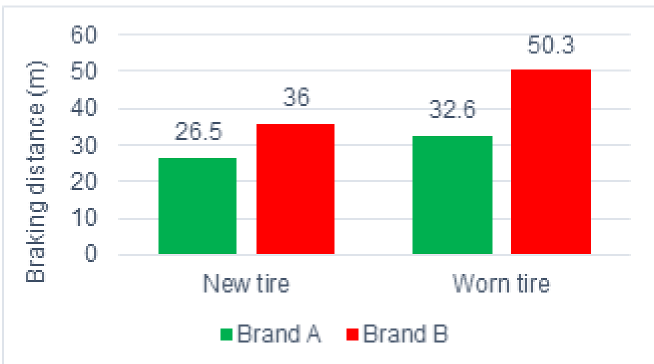

Figure 7 The length of the braking distance in the manufacturer and the condition of the tires [13]

1.3 Influence of tire pressure on braking distance

When it comes to braking, tire pressure is an important factor. In the study [14], different tires and pressure were shown, where it was shown that they have a different effect on the stopping distance, but that they differ according to the type of tire. Figure 8a shows the influence of tire pressure on the friction coefficient depending on the surface. When it comes to stopping distance, it is noticeable that the stopping distance is longer when the pressure in the tire is higher. Which can be related to the surface of the tire tread.

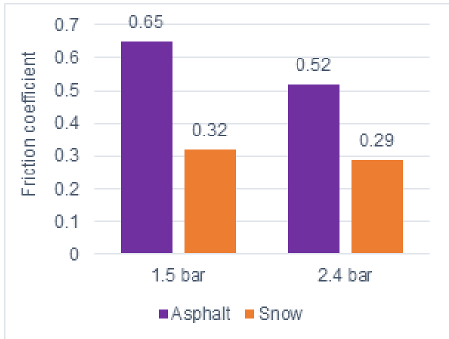

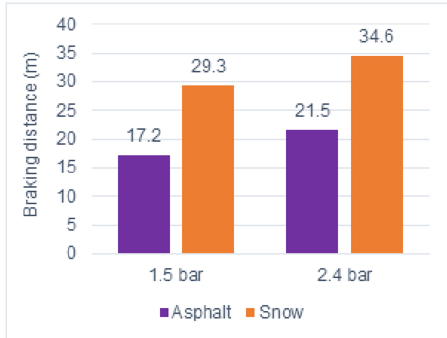

Figure 8 Braking distance depending on tire pressure and road conditions: a) coefficient of friction, b) stopping distance [15]

Figure 9 shows the values of the stopping distance at different pressures and road conditions. Thus, the shortest braking distance is at medium pressure, while at the lowest and highest pressure. Thus, it can be concluded that neither the highest, nor the lowest pressures are the most favourable. It is recommended that the pressure be the one prescribed by the manufacturer.

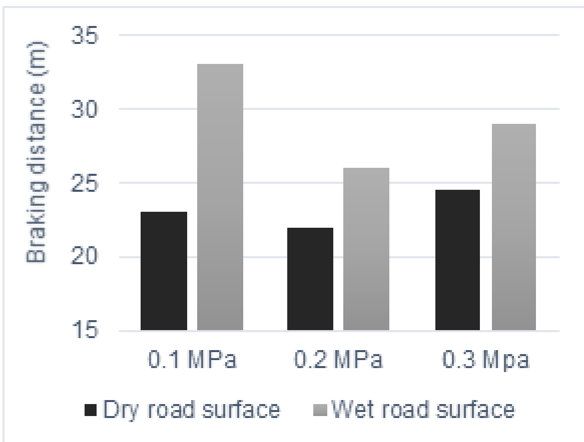

Figure 9 Braking distance depending on tire pressure and road conditions [16]

1.4 Effect of tire age on braking distance

It is known that each tire has its own year of production. As the tire ages, the characteristics of the tire deteriorate due to oxidation or other effects on the materials from which the tire is made. Figure 10a shows the recommendation that as tires age, the risk of tire failure increases. It is recommended not to use tires older than six years. Figure 10b shows that as the tire ages, the adhesion coefficient decreases. This was determined by applying a correlation where it was observed that there is a negative correlation between the coefficient of friction and the age of the tire. Due to the age of the tires, their oxidation occurs or the tire becomes stiff. In this case, cracks may form on the tire. It is certainly necessary to check the age of the tires through the so-called DOT number that is written on each tire. In addition to all the information, the DOT also contains information about the year of manufacture and the week of the year in which the tire was manufactured. Thus, there are recommendations to change tires every six years from the date of manufacture, but it is also recommended to never operate and use tires that are older than ten years.

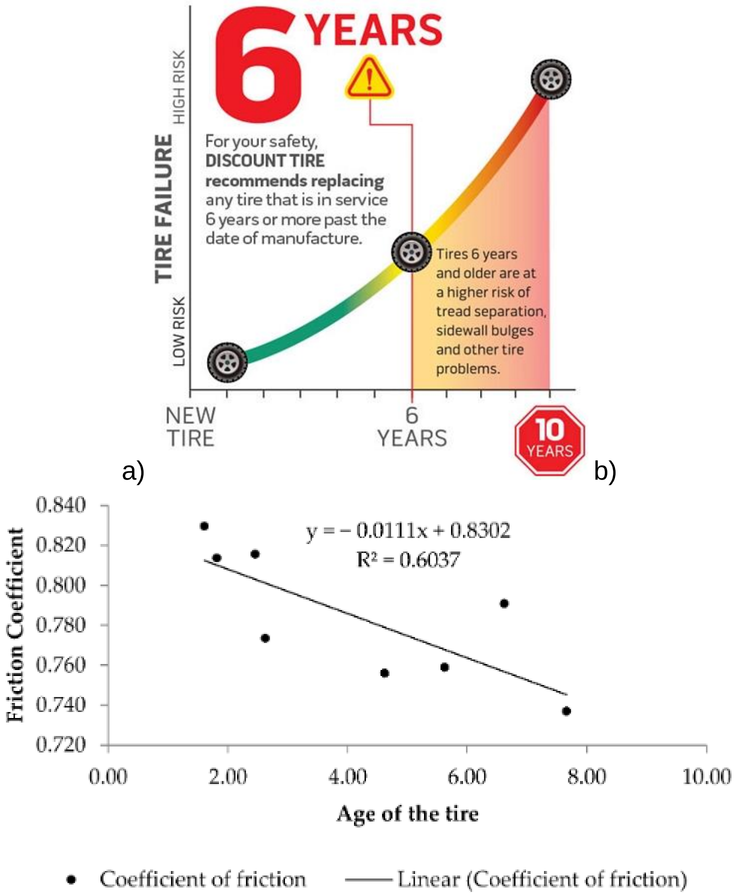

Figure 10 Tire age and influence on the friction coefficient: a) Dependence of tire age and tire failure, b) Correlation between tire age and friction coefficient [16, 17]

2 IMPACT OF TIRES ON THE ENVIRONMENT

The life of a tire is determined by its age or tread depth. After a certain number of years, when the tire exceeds the limit mentioned in the previous section, when the depth of the tread pattern falls below the permitted limit or due to damage, it is no longer usable; it can be treated as waste. When looking at the number of tires that are discarded in just one year, they become a global problem of environmental pollution [19]. According to data [20], over 280 million tires are discarded every year, of which around 30 million are remanufactured so that they can be reused, while 250 million tires remain as waste. Thus, one of the ways to reduce harm to the environment is the recycling of tires for reusing materials or generating energy [21]. The problem that occurs with tires is that tires are not biodegradable, so they do not break down in nature like some natural materials, so they can only pile up when dumped in nature. They are also very durable and can pile up and take up a lot of space in landfills. Therefore, this option of their disposal has always raised a question mark for decades. Figure 11 shows the process of tire production and recycling. However, in recent times, manufacturers are finding more and more uses for scrap tires such as in construction, retaining walls, creating highway barriers and lightweight construction materials in urban transport infrastructure projects. Companies are working to create biodegradable prototypes and sustainable tires [22].

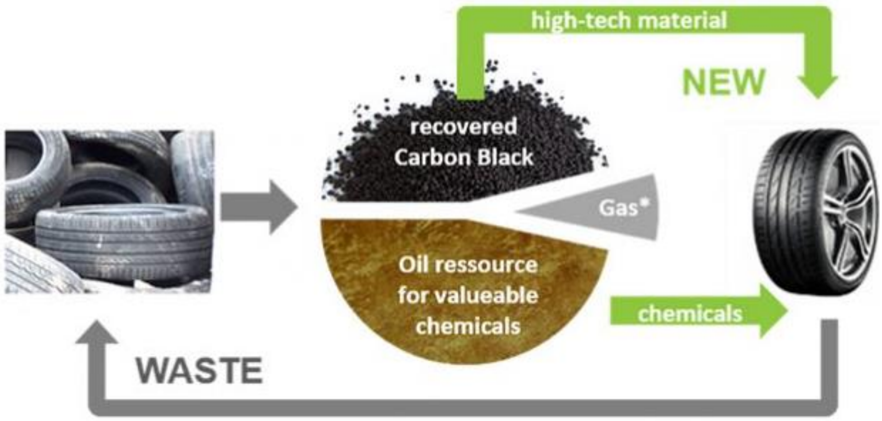

Figure 11 A simplified tire production and recycling process [22]

The phenomenon that leads to tires not having sufficient tread depth is tire wear. Tire wear is a process in which the pattern loss occurs due to the formation of small particles. That is, the worn material is thus released into the environment in the form of particles known as PM particles. Just like brakes, tires belong to non-exhaust sources of particles, i.e. environmental pollutants, which pollute the environment through wear. Figure 12 shows how particles are formed by tire wear. The particles produced by tire wear contain materials that are part of the tire, according to [23] the dominant materials in tire particles are Si, Zn, and S. Based on [24], it can be concluded that the composition of particles depends on the size of the particles, thus $PM_{2.5}$ particles contain Zn, Cu, S, Si and organic carbon, while PM_{10} particles contain Zn, Cu, Si, Mn. In the research [25], it was shown that the particles produced by tire wear are recognized as microplastics and that tire wear is the main factor that contributes to the emission of microplastics into the environment. According to a study [26] that analysed microplastics within the tributaries of the Charleston Harbor estuary, South Carolina (USA), tire wear particles were observed to be one of the most abundant types of microplastics. Based on [27], more than 0.5 million tons of particles are annually emitted in Europe, i.e. 6 million tons are broadcast worldwide. Tire particles are formed due to shear forces between the tread and the road. On average, tire particles contribute about 5% of atmospheric PM concentrations, and studies show values between 0.2% and 22% depending on different parameters [27]. According to the studies [28, 29], tires emit pollutants via atmospheric, water and land routes. Thus, tires represent a complex source of pollutants, including whole tires, particles, compounds and chemicals [28]. When it comes to the impact on human health, according to [30], it is stated that the impact on health is currently poorly researched or documented, but they represent a health and environmental risk [29].

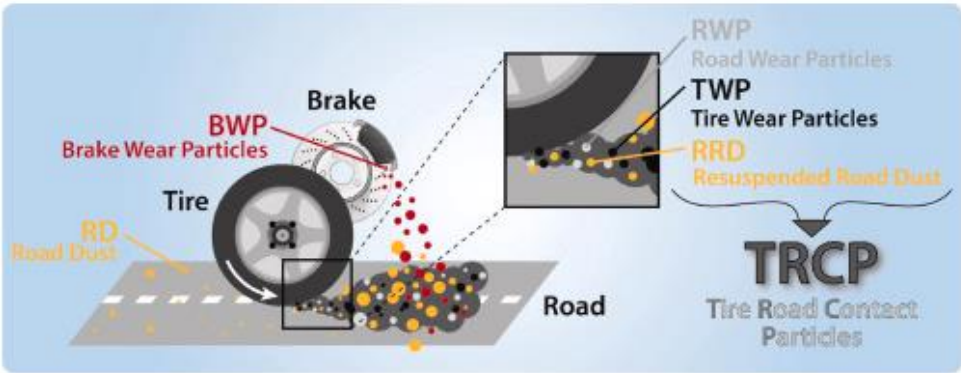

Figure 12 Tire wear and the formation of particles from various vehicle elements [27]

In addition to particle composition, size is also a significant factor that affects health and the environment. Smaller diameter particles can have a greater impact on the environment as well as on human health. According to research [31], it was determined that 94.80% of the particles produced by tire wear are 6 nm to 10 μm in size. In the research [32], trackers that attach to particles were monitored according to the source, i.e. brakes and tires. It was observed that the size of the particles in the composition of the tire wear trackers had a peak size of 10 μm to 18 μm. In the research [33], the sizes of the particles produced by tire wear on the side of the road were analysed, as shown in Figure 13. Particles with a larger diameter were analysed in one street and in three locations. Larger particle sizes were observed, while the concentration varied with respect to the measurement location. It has been shown that the emission of tires participates with 5% to 30% percent in the total emission, while the highest mass concentration is at the particle size in the case of 20 μm and 100 μm, as well as at sizes from 2 μm to 10 μm [34].

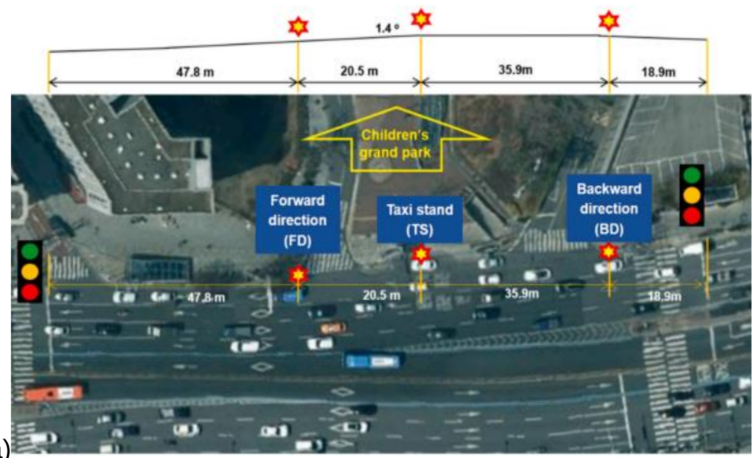

a)

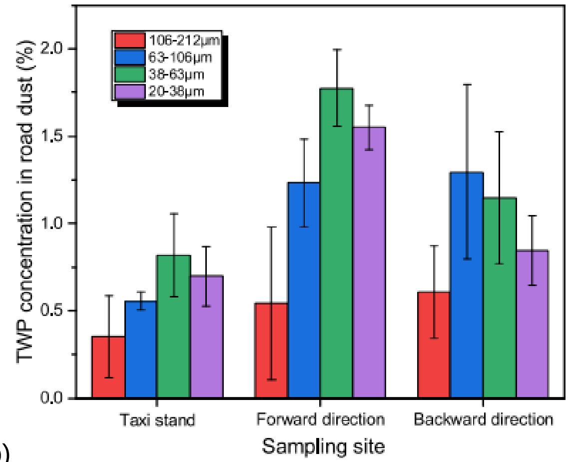

b)

Figure 13 Measurement of the emission of particles produced by tire wear, a) measurement locations, b) measurement results [33]

Research on the emission of particles caused by tire wear can be carried out in several ways, in the laboratory or on-road research. In the case of road research, it is more difficult to measure the emission of tire particles because it is difficult to separate them from particles that are not a product of tire wear or that are a product of tire wear but from other vehicles that were moving on the road [35]. When it comes to road tests, devices and equipment must generally be added to the vehicle that would collect particles or draw particles into a device for their measurement and analysis. Figure 14 shows some of the solutions that were used to measure and analyse particles that are produced by tire wear. As can be seen, near the contact between the wheel and the surface, i.e. at the exit from that contact on the rear side of the tire, a device is installed whose role is precisely to collect particles. Different researchers have used different but very similar solutions for the purpose of this measurement. Again, as a disadvantage, it is necessary to state that such measurements are very complicated, because when collecting or drawing in particles, other particles are also collected that were not formed during the wear of the used tire. In relation to brakes and measurements of the emission of brake particles, it is not possible here or the solutions are more complicated to ensure only the collection of particles that arise in the subject research. In the case of brake emissions, the aim is for the brake to be isolated by a special housing.

a)

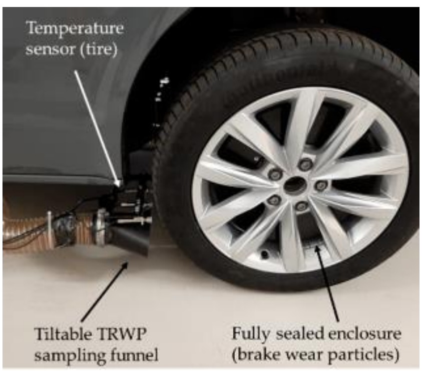

b)

c) d)

Figure 14 Variants of devices on vehicles for drawing in and measuring particles produced by tire wear in case of road tests, a) first variant, b) second variant, c) third variant [36, 37, 38]

Application of a real vehicle is also possible in laboratory conditions for testing the formation of particles during tire wear. In the case of the chassis dynamometer, where a real vehicle is applied, as shown in Figure 15. In this case, the vehicle moves on rollers that simulate the road, i.e. the movement of the vehicle on the road. In this case, the test is carried out in a laboratory, so it is easier to separate the tire wear particles from the particles that result from the wear of other elements. The Figure 15 shows a view of the test as well as the measuring installation and the setting of the measuring device in relation to the tire.

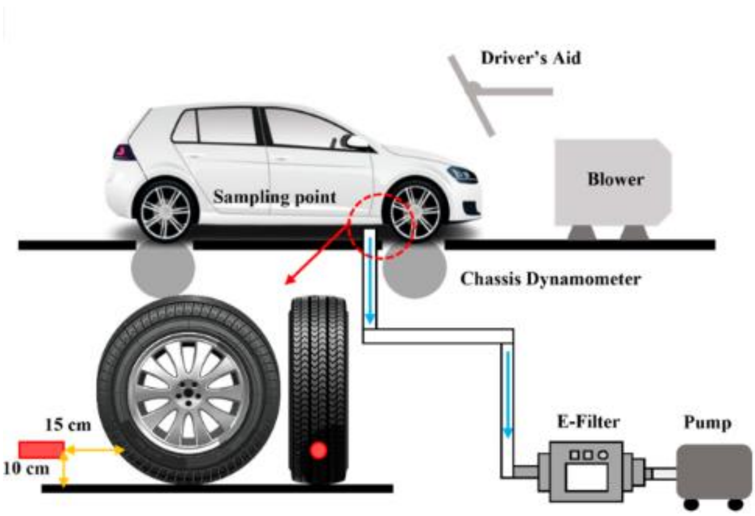

Figure 15 Examination of particle emissions caused by tire wear on a chassis dynamometer [39]

Application of a dynamometer and testing of tire wear without a real vehicle is also possible, as is the measurement of particle emissions caused by brake wear. Figure 16 shows different variants of tire wear tests using a dynamometer, where only the wheel is used and the movement of the vehicle on the road is simulated. It is noticeable that in each case, the tire load and its movement on the road are simulated. In this case, the road is simulated over a large-sized wheel that is coated with an asphalt surface or has asphalt characteristics. In some cases, as in brake emission testing, the wheel can be closed in the housing, where only the concentration of particles resulting from tire and road wear can be measured.

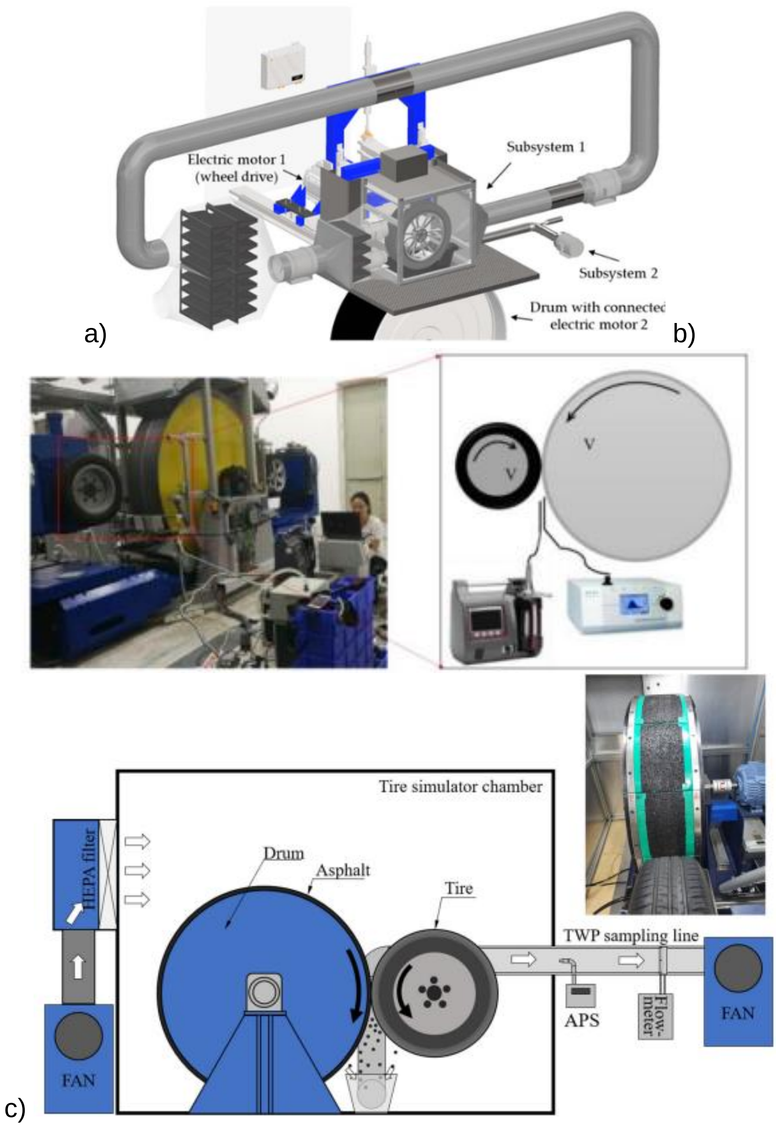

Figure 16 Examination of the emission of particles produced by tire wear in laboratory conditions [23, 35, 40]

CONCLUSIONS

Tires are an important element on a motor vehicle when it comes to vehicle safety. There are factors that can affect primarily the stopping distance of the vehicle and the turning of the vehicle when it comes to the characteristics of the tires. There are different tires that have different purposes when it comes to the conditions in which they are used. The use of tires in conditions for which they are not intended can extend the braking distance and endanger traffic safety. The characteristics of the tires change during the operation of the vehicle and in different time intervals. Thus, it is necessary to take care of the depth of the tread pattern, because tire wear can lead to a negative effect when it comes to braking distance. Over time, there are also changes in the characteristics of the material, so it is necessary to take into account the year of manufacture and the age of the tire, because the braking distance is also negatively correlated with the braking distance, so with the increase in the age of the tire, the braking distance also increases, or has an impact. Of course, such characteristics and the exact braking distance differ from manufacturer to manufacturer. When buying tires, it is necessary to pay attention to the categorization and characteristics of the tires based on the markings given by the manufacturer. First of all, when it comes to vehicle safety, it is necessary to take into account the class of tires according to the adhesion coefficient on wet pavement. The lowest classes have a worse braking distance on wet pavement compared to the classes of the higher category. Tire maintenance is also important at least when it comes to tire pressure. It is necessary to always maintain the pressure prescribed by the vehicle or tire manufacturer, otherwise the braking distance may be significantly longer.

Environmental pollution when it comes to tires is also a dominant problem. Tire wear leads not only to a reduction in vehicle safety, but also to environmental pollution. Tire wear occurs gradually because tire wear occurs when moving and braking. In the case of tire wear, there is the creation of particles that are micrometer in size and even smaller. These particles have a very small diameter, so they easily reach the environment and the human body. In addition to the size of the particles, the problem is also the composition of those particles. Tires consist not only of rubber but of a mixture of different materials in order to have satisfactory characteristics. Thus, these materials are also released into the environment in the form of particles, so these particles are also very small. With the increase in the number of vehicles and tires, the problem of pollution is getting bigger. Also a problem today are tires that are no longer usable due to the age of use or wear and tear, so in addition to particle pollution, they pollute when they leave.

Testing of particle emissions is carried out today using different methods, and most often it is the road tests or some variant of laboratory testing. Each methodology used for testing has its advantages and disadvantages. Real road tests and dynamometer tests, where the vehicle and wheel movement on the road are simulated, are most often used for tire emissions. Methodologies for testing the emission of particles resulting from tire wear will be the subject of subsequent research.

REFERENCES

[1] Li, T: "Literature review of tire-pavement interaction noise and reduction approaches", Journal of Vibroengineering, 20,6, 2018, 2424-2452.

[2] Tire Safety and Maintenance, https://michelinmedia.com/site/user/files/1/016---Unit-14-Tire-Safety.pdf, accessed 04.07.2024.

[3] Mitchel, L.: "Tyre Particle Health, Environment and Safety Report", Tyre Stewardship Australia, 2022.

[4] Jansen, S., Schmeitz, A., Akkermans, L.: "Study on some safety-related aspects of tyre use", European Commission, 2014, Brussels, Belgium, MOVE/C4/2013-270-1.

[5] SPRING 2016: When is the ideal time to remove winter tires?, https://georgetownvw.wordpress.com/2016/03/17/spring-2016-when-is-the-ideal-time-to-remove-winter-tires/, accessed 08.07.2024.

[6] Road Test Special – Winter Tires Vs. All-Season Tires. Is Your Car Ready For Winter?, https://roadtestdotorg.wordpress.com/2016/11/07/road-test-special-winter-tires-vs-all-season-tires-is-your-car-ready-for-winter/, accessed 08.07.2024.

[7] Comparation of temperature dependent brake distance, https://www.tyresafe.org/tyre-advice/all-season-tyres/winter-tyre-safety/, accessed 08.07.2024.

[8] Winter vs summer tyres – understand the differences, https://bestdrive.ie/news/winter-vs-summer-tyres-understand-differences/, accessed 08.07.2024.

[9] EU Tyre Label, https://www.goodyear.eu/en_za/consumer/learn/eu-tire-label-explained.html, accessed 20.07.2024.

[10] Tyre labels : Fuel efficiency, grip and rolling noise, https://www.tyreleader.co.uk/tyres-advices/car-tyres-label#wet, accessed 20.07.2024.

[11] Summer vs all-season vs winter tires, https://www.cjponyparts.com/resources/summer-all-season-winter-tires-infographic, accessed 20.07.2024.

[12] Our Pick of the Best 4WD Tyreshttps://www.fleetcrew.com.au/best-4wd-tyres/, accessed 23.07.2024.

[13] Tire performance over life time: Wet braking, https://toptirereview.com/tire-performance-over-life-time-wet-braking/, accessed 23.07.2024.

[14] Stoklosa, J., Bartnik, M.: „Influence of tire pressure on the vehicle braking distance“, The Archives of Automotive Engineering - Archiwum Motoryzacj, 97, 3, 2022, 60-73.

[15] Radu, A. I., Trusca, D., Toganel, G.: „Influence of tire pressure on the braking distance when driving on snow and asphalt“, IOP Conf. Series: Materials Science and Engineering, 444, 2018, 072013.

[16] Hadryś, D., Węgrzyn, T., Miros, M.: “The influence of various pressures in pneumatic tyre on braking process of car with anti-lock braking system“, Transport problems, 3, 1, 2008, 85-94.

[17] Tire Safety Practices, https://www.discounttire.com/learn/tire-safety, accessed 28.07.2024.

[18] Lorenčić, V.: “The Effect of Tire Age and Anti-Lock Braking System on the Coefficient of Friction and Braking Distance”, Sustainability, 15, 8, 2023, 6945.

[19] Kang, G.S., Lee, G., Cho, S. Y., Joh, H.I., Lee, D. C., Lee, S.: “Recycling of waste tires by synthesizing N-doped carbon-based catalysts for oxygen reduction reaction”, Applied Surface Science, 548, 2021, 149027.

[20] The current state of global tyre recycling: facts and figures, https://gradeall.com/the-current-state-of-global-tyre-recycling-facts-and-figures/#:~:text=Each%20year%2C%20over%20280%20million,million%20–%20are%20retreaded%20or%20reused, accessed 01.08.2024.

[21] Pavlović, A., Nikolić, D., Jovanović, S., Bošković, G., Skerlić, J.: „Life cycle assessment of the car tire with eco indicator 99 methodology“, Mobility & Vehicle Mechanics, 45, 3, 2019, 13-23.

[22] What Happens to Old Tyres After They Are Discarded, https://www.tyremarket.com/tyremantra/happens-old-tyres-discarded/, accessed 01.08.2024.

[23] Beji, A., Deboudt K., Muresan B., Khardi S., Flament, P., Fourmentin, M., Lumiere, L.: “Physical and chemical characteristics of particles emitted by a passenger vehicle at the tire-road contact”, Chemosphere, 340, 2023, 139874.

[24] Grechkin, A., V., and Kotliarenko, I. V.: “Assessment of the composition of solid particle emissions from tire and roadway wear that pollute the atmosphere of large cities”, IOP Conf. Series: Earth and Environmental Science, 867, 2021, 012095.

[25] Knight, L.J., Parker-Jurd, F.N.F., Al-Sid-Cheikh, M., Thompson, C. R.: “Tyre wear particles: an abundant yet widely unreported microplastic?”, Environmental Science and Pollution Research, 27, 2020, 18345–18354.

[26] Leads, R. R., Weinstein, J. E.: “Occurrence of tire wear particles and other microplastics within the tributaries of the Charleston Harbor Estuary, South Carolina, USA”, Marine Pollution Bulletin, 145, 2019, 569–582.

[27] Giechaskiel, B., Grigoratos, T., Mathissen, M., Quik, J., Tromp, P., Gustafsson, M., Franco, V., Dilara, P.: “Contribution of Road Vehicle Tyre Wear to Microplastics and Ambient Air Pollution”, Sustainability, 16, 2, 2024, 522.

[28] Mayer, P. M., Moran, K. D., Miller, E. L., Brander, S. M., Harper, S., Garcia-Jaramillo, M., Carrasco-Navarro, V., Ho, K. T., Burgess, R. M., Hampton, L. M. T., Granek, E. F., McCauley, M., McIntyre, J. K., Kolodziej, E. P., Hu, X., Williams, A. J., Beckingham, B. A., Jackson, M. E., Sanders-Smith, R. D., Fender, L. C., Mendez, M.: „Where the rubber meets the road: Emerging environmental impacts of Tire Wear particles and their chemical cocktails”, The Science of the Total Environment, 927, 2024, 171153.

[29] Parker-Jurd, F. N. F., Napper, I. E., Abbott, G. D., Hann, S., Thompson, R. C.: “Quantifying the release of tyre wear particles to the marine environment via multiple pathways”, Marine Pollution Bulletin, 172, 2021,112897.

[30] Bouredji, A., Pourchez, J., Forest, V.: “Biological effects of Tire and Road Wear Particles (TRWP) assessed by in vitro and in vivo studies – A systematic review” The Science of the Total Environment, 894, 2023, 164989.

[31] Zhong, C., Sun, J., Zhang, J., Liu, Z., Fang, T., Liang, X., Yin, J., Peng, J., Wu, L., Zhang, Q., Mao, H.: “Characteristics of Vehicle Tire and Road Wear Particles’ Size Distribution and Influencing Factors Examined via Laboratory Test”, Atmosphere, 15, 2024, 423.

[32] Lopez, B., Wang, X., Chen, L.-W. A., Ma, T., Mendez-Jimenez, D., Cobb, L. C., Frederickson, C., Fang, T., Hwang, B., Shiraiwa, M., Park, M., Park, K., Yao, Q., Yoon, S., Jung, H.: “Metal contents and size distributions of brake and tire wear particles dispersed in the near-road environment”, Science of The Total Environment, 883, 2023, 163561.

[33] Chae, E., Jung, U., Choi, S.S.: “Types and concentrations of tire wear particles (TWPs) in road dust generated in slow lanes”, Environmental Pollution, 346, 2024, 123670.

[34] Giechaskiel, B., Grigoratos, T., Mathissen, M., Quik, J., Tromp, P., Gustafsson, M., Franco, V., Dilara, P.: “Contribution of Road Vehicle Tyre Wear to Microplastics and Ambient Air Pollution”, Sustainability, 16, 2024, 522.

[35] Hesse, D., Feißel, T., Kunze, M., Bachmann, E., Bachmann, T., Gramstat, S.: “Comparison of Methods for Sampling Particulate Emissions from Tires under Different Test Environments”, Atmosphere, 13, 2022, 1262.

[36] Hesse, D.: “Beitrag zur Experimentellen und Analytischen Beschreibung Partikelförmiger Bremsenemissionen”, Ph.D. Thesis, Technische Universität Ilmenau, Ilmenau, Germany, 2020.

[37] Schmerwitz, F., Wieting, S., Aschenbrenner, N., Topp, A., Wies, B.: "Characterization of Tire Road Wear Particles in the Field and at Laboratory Scale", 12th International Munich Chassis Symposium 2021, 2022, 729-743.

[38] Andersson, J., Campbell, M., Marshall, L., Kramer, L., Norris, J.: "Measurement of emissions from brake and tyre wear", Final Report – Phase 1, Ricardo Energy & Environment, Report for Department for Transport, 2023, T0018 - TETI0037.

[39] Li, J., Zhang, M., Ge, Y., Wen, Y., Luo, J., Yin, D., Wang, C., Wang, C.: "Emission Characteristics of Tyre Wear Particles from Light-Duty Vehicles", Atmosphere, 14, 2023, 724.

[40] Zhang, X., Chen, P., Liu, F.: "Review of Tires Wear Particles Emission Research Status", IOP Conference Series: Earth and Environmental Science, 555, 2020, 012062.

NOTIFICATION TO AUTHORS

The Journal MVM publishes original papers which have not been previously published in other journals. This is responsibility of the author. The authors agree that the copyright for their article is transferred to the publisher when the article is accepted for publication.

The language of the Journal is English.

Journal ***Mobility & Vehicles Mechanics*** is at the SSCI list.

All submitted manuscripts will be reviewed. Entire correspondence will be performed with the first-named author.

Authors will be notified of acceptance of their manuscripts, if their manuscripts are adopted.

INSTRUCTIONS TO AUTHORS AS REGARDS THE TECHNICAL ARRANGEMENTS OF MANUSCRIPTS:

Abstract is a separate Word document, "*First author family name_ABSTRACT.doc*". Native authors should write the abstract in both languages (Serbian and English). The abstracts of foreign authors will be translated in Serbian.

This document should include the following: 1) author's name, affiliation and title, the first named author's address and e-mail – for correspondence, 2) working title of the paper, 3) abstract containing no more then 100 words, 4) abstract containing no more than 5 key words.

The manuscript is the separate file, „*First author family name_Paper.doc*" which includes appendices and figures involved within the text. At the end of the paper, a reference list and eventual acknowledgements should be given. References to published literature should be quoted in the text brackets and grouped together at the end of the paper in numerical order.

Paper size: Max 16 pages of B5 format, excluding abstract
Text processor: Microsoft Word
Margins: left/right: mirror margin, inside: 2.5 cm, outside: 2 cm, top: 2.5 cm, bottom: 2 cm
Font: Times New Roman, 10 pt
Paper title: Uppercase, bold, 11 pt
Chapter title: Uppercase, bold, 10 pt
Subchapter title: Lowercase, bold, 10 pt
Table and chart width: max 125 mm
Figure and table title: Figure _ (Table _): Times New Roman, italic 10 pt

Manuscript submission: application should be sent to the following e-mail:

mvm@kg.ac.rs ; lukicj@kg.ac.rs
or posted to address of the Journal:
University of Kragujevac – Faculty of Engineering
International Journal M V M
Sestre Janjić 6, 34000 Kragujevac, Serbia

The Journal editorial board will send to the first-named author a copy of the Journal offprint.

OBAVEŠTENJE AUTORIMA

Časopis MVM objavljuje orginalne radove koji nisu prethodno objavljivani u drugim časopisima, što je odgovornost autora. Za rad koji je prihvaćen za štampu, prava umnožavanja pripadaju izdavaču.

Časopis se izdaje na engleskom jeziku.

Časopis ***Mobility & Vehicles Mechanics*** se nalazi na SSCI listi.

Svi prispeli radovi se recenziraju. Sva komunikacija se obavlja sa prvim autorom.

UPUTSTVO AUTORIMA ZA TEHNIČKU PRIPREMU RADOVA

Rezime je poseban Word dokument, "*First author family name_ABSTRACT.doc*". Za domaće autore je dvojezičan (srpski i engleski). Inostranim autorima rezime se prevodi na srpski jezik. Ovaj dokument treba da sadrži: 1) ime autora, zanimanje i zvanje, adresu prvog autora preko koje se obavlja sva potrebna korespondencija; 2) naslov rada; 3) kratak sažetak, do 100 reči, 4) do 5 ključnih reči.

Rad je poseban fajl, „*First author family name_Paper.doc*" koji sadrži priloge i slike uključene u tekst. Na kraju rada nalazi se spisak literature i eventualno zahvalnost. Numeraciju korišćenih referenci treba navesti u srednjim zagradama i grupisati ih na kraju rada po rastućem redosledu.

Dužina rada: Najviše 16 stranica B5 formata, ne uključujući rezime
Tekst procesor: Microsoft Word
Margine: levo/desno: mirror margine; unurašnja: 2.5 cm; spoljna: 2 cm, gore: 2.5 cm, dole: 2 cm
Font: Times New Roman, 10 pt
Naslov rada: Velika slova, bold, 11 pt
Naslov poglavlja: Velika slova, bold, 10 pt
Naslov potpoglavlja: Mala slova, bold, 10 pt
Širina tabela,dijagrama: max 125 mm
Nazivi slika, tabela: Figure __ (Table _): Times New Roman, italic 10 pt

Dostavljanje rada elektronski na E-mail: **mvm@kg.ac.rs ; lukicj@kg.ac.rs**

ili poštom na adresu Časopisa
Redakcija časopisa M V M
Fakultet inženjerskih nauka
Sestre Janjić 6, 34000 Kragujevac, Srbija

Po objavljivanju rada, Redakcija časopisa šalje prvom autoru jedan primerak časopisa.

MVM *Editorial Board*
University of Kragujevac
Faculty of Engineering
Sestre Janjić 6, 34000 Kragujevac, Serbia
Tel.: +381/34/335990; Fax: + 381/34/333192
www.mvm.fink.rs